Imaging a life span

In vivo Magnetic Resonance Imaging of Development and Ageing

in Rat and Mouse Brain

Dissertation

zur Erlangung des Doktorgrades (Dr. rer. nat.)

der

Mathematisch-Naturwissenschaftlichen Fakultät

der

Rheinischen Friedrich-Wilhelms-Universität Bonn

vorgelegt von

Nicola Luam Kidane Hammelrath geb. Mengler

aus Bonn

Juni 2015

universitätbonn

Max Planck Institute
for Metabolism Research

Angefertigt mit Genehmigung der Mathemathisch-Naturwissenschaftlichen Fakultät der Rheinischen Friedrich-Wilhelms-Universität Bonn

Erster Gutacher: Prof. Dr. Mathias Hoehn

Zweiter Gutachter: Prof. Dr. Michael Hofmann

Tag der Promotion: 25. August 2015

Erscheinungsjahr: 2016

The great tragedy of science is the slaying of a beautiful hypothesis by an ugly fact.

T.H. Huxley

Table of contents

List of figures

Abstract

Rats and mice are the most abundantly used animal models in translational research. They are employed in the service of clinical research in the sense of establishing methods, testing therapeutic strategies and pharmacological interventions. Magnetic Resonance Imaging (MRI) has become the most important neuroimaging tool. It offers on the one hand absolute integrity of the tissue and thereby allowing multiple examinations of the same subject without confounding developmental processes and on the other hand effective exchange between bench and bedside, due to its high translational nature. Compared to the vastness of imaging studies in rodent models of neuropathological conditions, we know very little about the development of neuroimaging parameters over the life span of rats and mice. One of the major challenges in a longitudinal imaging study is the data handling and post-processing. In order to assure reliability and reproducibility of the results, the first goal of this thesis was to establish a post processing protocol and designed a graphical user interface. This allowed for robust analysis of the MRI data and for fast visual inspection of the registration success. In the second step, the presented studies established a time profile of the most widely used MRI parameters for cerebral development in mice and rats. This will help neuropathological studies to set a reasonable age threshold, avoiding maturation processes to potentially obliterate the therapeutical effect. Thirdly, a longitudinal study in rats was conducted, searching for translational biomarkers of cerebral ageing. A multimodal approach was chosen, employing not only structural MRI but also the most prevalent fMRI and PET markers. Calorie restriction and appropriate housing conditions led the rats to age healthy, without age-related diseases. The results demonstrate a rather heterogeneous ageing process across different parameters and cerebral GM regions. This is in strong contrast to the rather synchronized maturation processes but reflects the human situation during healthy ageing.

Our work created a baseline on structural MRI parameters, describing periods of life marked by immense structural reorganisation. The results will help future studies on pathologies in the adolescent or ageing brain and has helped defining the starting point of stable adulthood.

Zusammenfassung

In der präklinischen Forschung werden vornehmlich Ratten und Mäuse verwandt um neue Methoden zu etablieren und innovative therapeutische und pharmakologische Strategien zu testen. Mit Magnetresonanz Tomographie steht der Forschung eine Bildgebungsmethode zur Verfügung, die vollständig nicht-invasiv ist und auch bei wiederholter Anwendung keinerlei Einfluss auf die Entwicklungsbiologie zeigt. Zusätzlich zeichnet sich MRT durch ein besonders hohes translationales Potenzial aus. Ganz im Gegensatz zum Menschen ist über den Verlauf von neuroradiologischen Markern während der ontogenetischen Entwicklung und des Alterungsprozesses bei Ratten und Mäusen wenig bekannt. Diese Diskrepanz zu überbrücken war Ziel dieser Doktorarbeit.

Eine Langzeitstudie ist aufwendig und die entstehenden Datenmengen sind eine Herausforderung für effektive Auswertestrategien. Um die Reproduzierbarkeit der Ergebnisse zu garantieren, ist der erste Teil dieser Arbeit der Entwicklung von Strategien zur Datenverarbeitung und dem Design einer grafischen Benutzeroberfläche gewidmet. Dadurch konnte im Folgenden eine zuverlässige Datenverarbeitung und -analyse sowie eine schnelle und verlässliche Revision der Registrierung gewährleistet werden. Der zweite Teil beschreibt den zeitlichen Verlauf von MRT Parametern während der Gehirnreifung in Ratten und Mäusen. Die Entwicklungsprofile werden zukünftigen neuropathologischen Studien dabei helfen Tiere eines angemessenen Alters zu wählen, so dass potentielle therapeutische Erfolge nicht von inhärenten Reifungsprozessen überlagert werden. Der dritte Teil, eine multimodale Langzeitstudie in Ratten, sollte translationale Marker für Hirnalterung finden. Der multimodale Ansatz beinhaltete neben konventionellem, strukturellem MRT auch die gängigsten funktionellen MRT und PET-Paradigma. Eine kalorienreduzierte Ernährung sowie artgerechte Haltungsbedingungen ließen die Ratten gesund altern und reduzierten altersabhängige Krankheiten. Die Ergebnisse malen ein eher heterogenes Zeitprofil des Alterungsprozesses, sowohl im Vergleich der untersuchten Modalitäten als auch den verschiedenen Regionen der zerebralen grauen Substanz. Dieser parameter- und regionsspezifische Beginn des Alterns steht im Gegensatz zur zeitlich stark getakteten Entwicklung, spiegelt aber die klinische Erfahrung wider.

Die vorgelegte Doktorarbeit beschreibt die altersabhängige Entwicklung von strukturellen MRT Parameter und konzentriert sich dabei auf Lebensphasen, die durch besonders intensive strukturelle Reorganisation charakterisiert sind. Die Ergebnisse werden zukünftigen neuropathologischen Studien im adoleszenten oder alternden Gehirn als Messgrundlage dienen und definieren den zeitlichen Beginn des Erwachsenenalters.

Preface

“It is indeed remarkable that after a seemingly miraculous feat of morphogenesis a complex metazoan should be unable to perform the much simpler task of merely maintaining what is already formed.” Williams 1957

We now live longer than ever before; due to the benefit of good nurture, hygiene and modern medicine. However, living longer does not mean that the health span is prolonged as well. Now more than ever we have to tackle age-associated diseases, such as neurodegenerative diseases, diseases of the cardiovascular system or cancer. The challenge remains, and even increases for us to understand ageing processes.

Ageing is a peculiar thing. It can be observed everywhere in nature, whether in animals, plants, bacteria or funghi. It is omnipresent and yet difficult to define. Whether for egoistic or altruistic reasons, men were seeking to conquer ageing and death for thousands of years: While searching for the “Holy Grail”, alchemy and metaphysics all were hoping for eternal life. In the last century life sciences have postulated many theories, from a limited number of heartbeats in a lifetime, to an age-gene, to sexual reproduction or metabolic rate. In the following paragraphs the most important ageing theories and their history shall be explained.

Ageing is occurring on every level of an organism (systems, organs, cells, cell compartments, proteins and DNA) and everywhere with different time profiles and phenotypes. In the end the definition comes down to one rather unsatisfying sentence: The ageing phenotype reflects an accumulation of small changes, leading to functional decline. This accumulation can be due to environmental influences (nurture) or due to internal ageing programs (nature).

In 1889 August Weisman postulated his theory of immortal genes and a “perishable and vulnerable (…) soma”, believing in an ageing and death mechanism to reduce the fraction of old individuals in a population [1]. Finding such an allele, targeting and removing it should then lead to immortality. This was the first scientific theory of the evolution of ageing.

Longevity genes in *C. elegans*, fast ageing transgenic mouse models and even genetic heritance studies in humans imply on first sight that ageing is genetically programmed [2]. However, if genes were responsible for the ageing process, they regulate it only loosely. Life spans, ageing phenotypes and rates vary between individuals. This holds true even in *C. elegans*, a species showing a

development so completely synchronized that all adult individuals turn out to have the exact same number of cells [3]. It seems that a genetic ageing program can only be part of the story. What is more, an ageing gene contradicts our understanding of evolution. A phenomenon as ubiquitous and highly conserved as ageing would require strong selective forces, if it was genetically programmed. Evolution promotes genes that successfully increase the reproduction rate, whereas ageing manifests itself after the reproductive phase, in the selective shadow. This reasoning was the basis for another ageing theory, phrased in 1952 by Peter Medawar: The theory of mutation accumulation [4]. Medawar argued that because of that selective shadow, genes with detrimental effects late in life can accumulate in the genome. George Williams and his "antagonistic pleiotropy theory" (1957) followed a similar approach, hypothesising that a genes may differ between ages and somatic environments [5]. A gene that was beneficial during development may be harmful after the reproductive phase, in the selective shadow.

In the mean time a breathtaking discovery was made that slowly found its way into the ageing science: Clive McCay discovered that Wistar rats lived longer when kept on a strict calorie restricted diet (CR) [6; 7]. This was the first report of external factors determining the ageing process, of nurture being more important than nature. It led to a series of ageing theories, based on the assumptions that a metabolism is limited to a certain metabolic turnover or number of heartbeats. It seems that the reduced energy metabolism of CR animals has major beneficial effects [8-10]: The reduced metabolic rate leads to a chronic mild metabolic stress. Such mild chronic stress, whether energetic or thermic triggers the cellular stress resistance mechanisms and thereby increases the cell's resistance to insults. Both in mild chronic stress and in CR animals, cells show higher levels of heat shock protein and neurotrophic or neuroprotective factors. Furthermore, a reduction in metabolic rate reduces the formation of by-products, like reactive oxygen species (ROS) [11]. ROS challenge the somatic and mitochondrial metabolism, especially the DNA repair systems and are one of the major contributors to the cellular ageing process. Other theories highlight the role of aggregated proteins, a phenomenon found in many systems. Protein aggregations range from innocent lipofuscin in age spots, to detrimental amyloid plaques and Lewis' bodies in neurons of Alzheimer's and Parkinson's disease [12].

The question remains though, why cellular repair mechanisms cannot cope with these particular mistakes in folding and translation. Kirkwood hypothesized that the accumulation of damage can occur because the energetic priority is put into reproduction, rather than cellular and biochemical maintenance mechanisms (disposable soma theory, 1977) [13].

In recent years programmed ageing theories arose, based on changes observed in the endocrine system of the roundworm *C. elegans*. *C. elegans* larvae can stagnate in a specific developmental stage, when presented to unfavourable environmental conditions. This stage was termed *dauer*, according to the German word for duration and continuity. *Dauer* larvae are resistant to stress and do not feed and show a distinct physiology and morphology [14]. During this emergency state development, thus ageing is halted and can be continued when conditions change. The genes responsible for the *dauer* stage show strong homologies with components of the mammal insulin and insulin like growth factor (IGF) pathway. The main components of the insulin/IGF-1 pathway are highly conserved and can be found both in invertebrates (Drosphila and C. elegans) as well as in mammals [15]. It was found to interfere with the ageing process by altering the metabolism. The insulin/IGF-1 signalling cascade in mammals is closely linked to the growth hormone (GH) pathway and is part of the somatotropic axis, a key player in the regulation and control of metabolic processes [16]. As the signalling cascade is much more complex in mammals, the precise mechanisms are more difficult to unravel. However, mutant mice lacking components of the pathway show longevity and an altered insulin metabolism [17].

The somatotropic axis is a strong candidate to unite the opposing theories (nature vs nuture) to a combined theory of accumulated damage. In the fine equilibrium of a biological system (whether an organism or a cell) the smallest change can trigger a chain reaction and lead to major dysfunction. A major contributor to the homeostasis is the nutrition; the number of free radicals, fatty acids, vitamins, etc. is highly dependent on the diet. Changes can also be induced by external damage, like UV light and radiation or by intrinsic errors, like imperfect translation or protein misfolding. As somatic repair mechanisms are not perfect, low levels of damage accumulate with time, leading to the rather diffuse pathology of age. Depending on the environmental influences and the genetic predisposition, the ageing phenotype varies between individuals. This theory seems appealing. We can observe the proposed individuality in the ageing rate in daily life. However, there remain patterns and evolutions that are not purely random, but common within and between species. It seems that some systems are more prone to ageing than others. Are we witnessing an intrinsic ageing process?

Objectives

Demographic change is challenging economic and health systems as well as science. In a society with a growing proportion of elderly, understanding the ageing process and prolonging health span is no longer only a matter of philosophical discussion. Demographic prognoses for Germany and other Western countries foresee a decreasing population but an increase in the proportion of elderly. Along with this shift in the population pyramid, the incidence of age related diseases will rise. The *Institut für Gesundheits-System-Forschung* (Institute for research on health system; www.igsf.de) anticipates the morbidity rate of stroke to increase by as much as 94%, of dementia even by 144% by the year 2050. Neurological diseases are already attributed as the main reason for disability in elderly and one of the major challenges for effective translational research. Understanding the causes and pathologies of these diseases is crucial for prevention and treatment and needs appropriate animal models and the knowledge to discriminate between “normal” age-related and age-dependent, but disease-related, deterioration.

Despite major progress in the translational ageing research, studies often miss the link between bench and bedside, whether it is in the choice of animal models or the tests used to evaluate the intervention [18]. Animal models should represent the patient population in critical characteristics and be combined with the advantages, such as reproduction rate, genetic manipulations, convenient handling and housing. Neuroscientists have created a large variety of animal models displaying the main symptoms of age-related diseases, for example artery occlusion to induce an ischemic stroke [19], injection of 6-OHDA to deplete dopaminergic neurons similar to the pathology of Parkinson’s disease [20] and transgenic mice showing Alzheimer’s pathology [21]. These animal models provide mechanistic insight into disease pathology and evolution, as well as a platform to test potential therapies. However, most pre-clinical research employs young animals, which are not necessarily representative of the natural disease state. That age of an animal affects the outcome of an intervention was shown for several disease models, e.g. the recovery after stroke [22]. Even more, age is considered rather a disease itself and is examined and treated separately with its own transgenic animals, than an important influence upon diseases. Without doubt, young animals are convenient in terms of breeding cycle, animal handling and training and they are easy to purchase. Aged animals in contrast are expensive and spent already much time in breeding facilities before arriving in the laboratories, making it difficult to control housing environment as well as habituating them to the specific setup and staff within the lab, a situation that is particularly important for

behavioural and cognitive tests. Although information assessed with young animals is informative, the findings cannot necessarily be extrapolated to aged subjects, making it essential to investigate in aged animals. Comparing the few studies that did focus upon aged animals so far, it becomes obvious that a common definition of “old” age is lacking. The range of ages for animals referred to as “old” spans from twelve to 28 months [23-25]. While we have a fairly good time scale of developmental phases in humans (from infancy to old age), we know little about the distinct phases in rats, making it difficult to model human age stages. This holds true not only for ageing but also for development and maturation processes. Many animal models, like rodents or the zebrafish were chosen for their fast development, neglecting that not only genetic background but also developmental stages matter. Comparison between the late-developing human brain and the fast rodent brain are especially difficult for brain maturation processes, like myelination, synaptogenesis and neuronal arborisation. Not all systems develop in the same pace across species. An open database is now available which compares different cerebral processes, like myelination or neurogenesis across different mammalian strains for the first weeks, in rats and mice for example until weaning is terminated and with proclaimed adulthood (www.translatingtime.net). In fact, there is evidence that the brain continues to mature well beyond the adult age [26; 27].

Paediatricians have a clear understanding of neurological, psychological and sensorimotor stages and the pace of human development. Standardized and regular examination have created a standard to which individuals can be compared. Meanwhile, gerontologists have implemented a battery of tests, examining the neurological and sensorimotor function of older patients in order to establish function-based biomarkers of ageing. These biomarkers help to predict the anticipated life span and the probability of a later disability [28; 29]. Many of those markers could be adapted to rodent studies, allowing judgement of intervention success. However, potential therapies are tested in rodent models for ageing and age-associated diseases and evaluated with rodent specific tests. Standard tests in rodent models do not necessarily find an equivalent in clinical trials, raising the question if treatment, which is considered successful in preclinical research, actually targets clinically relevant parameters.

Whether preclinical research outcomes affect parameters used as a standard read-out in medical research is often unknown. Common biomarkers for clinic and animal models are worthwhile. Putative biomarkers for brain development and ageing should be non-invasive and comparable both in animal models and in humans. It is conceivable that the benefits such as those attained by blood pressure analysis in cardiovascular diseases, could be achieved by measuring glucose and insulin levels for glucose intolerance gait analysis [28] and using non-invasive imaging for neurological

disorders. While stroke and Parkinson's disease affect mostly the motor system, Alzheimer's disease has the strongest impact on the cognitive function. All neurodegenerative diseases, and ageing itself, are associated with changes in neuronal activity, that are reflected not only in the functional but even more so in the metabolic profile of the whole brain or specific brain regions.

Neuroimaging techniques have evolved to be the most important clinical and pre-clinical tool for diagnostics and follow-up. Magnetic Resonance Imaging (MRI) reveals macro- as well as microstructural changes completely non-invasively, Positron Emisson Tomography (PET) visualizes molecular and metabolic alterations and functional MRI reflects the neuronal or neurovascular response to a given task. MRI ageing studies in humans have shown a variety of structural changes throughout life, among them volume ratios of grey and white matter as well as changes in the integrity of the white matter tracts [30-33].

We conducted a multimodal longitudinal study in rats, monitoring the functional state as well as the structural integrity of the brain *in vivo*. A detailed description of brain maturation and ageing processes will create a baseline for imaging parameters and help finding biomarkers that can be translated into the clinic. Monitoring the complete lifespan can furthermore contribute to define age stages in the rat. A second study was assigned to describe postnatal maturation of the neocortex in mice, and to establish a protocol that allows comparison of histological and imaging findings. As data handling and post-processing are rather challenging in such a large-scale study, the first goal was to establish protocols for data analysis and a platform facilitating the control of the registration success.

Theoretical background of imaging methods

MRI – Magnetic Resonance Imaging

MAGNETIC

Conventional Magnetic Resonance Imaging (MRI) employs the magnetic properties of the hydrogen nucleus. Hydrogen is the element with the least complex nucleus, consisting only of one positively charged proton. The hydrogen nucleus has a quantum mechanical property, the nuclear spin: it is rotating about an axis. The rotation or spin of any charged particle generates a small magnetic field (characterized by a magnetic momentum) and produces magnetic dipoles. Hydrogen is not the only nucleus, bringing the prerequisite for MRI. All isotopes with an odd number of protons or neutrons have a total spin that is not zero, but instead equal ½ and therefore provide a magnetic momentum. This is exploited for example in fluorine (19F), phosphorous (31P) and carbon (13C) MRI.

When a nucleus with spin=½ is brought into an external magnetic field, quantum mechanics anticipates two characteristics:

1- Spins align with the magnetic field either parallel or anti-parallel. In other words, they take one of two energy states: spin down (high energy level) and spin up (low energy level). The ratio between the two states is not 50:50, but is slightly in favour of the low energy state/parallel.

2- Spins precess around an axis parallel to the magnetic field. The frequency of the spin precession is unique for different nuclei in different field strengths and is termed *Larmor* frequency.

For MRI a powerful and static magnetic field is applied. The strength of a magnetic field is given in the unit Tesla (T). Field strengths differ between scanners and between applications. In clinical diagnostics, field strengths of 1.5T are common, in preclinical research field strengths with 11T and higher are in use.

Nevertheless, MRI is not sensitive enough to visualize individual spins. Instead, MR images are resolved into voxels (volume elements), and all spins within one voxel are treated as an entity. This spin ensemble is not uniform in energy state (up/down) or phase orientation, having a slight excess on “up spins” and a random phase location. The excess of “up spins” is creating a constant magnetization parallel to the magnetic field, termed the “thermal equilibrium of the spins”. After any

kind of disturbance, the spins will restore this low energy state: net magnetization parallel to the magnetic field B_0 and random phase orientation.

RESONANCE

The net magnetization and the spatial orientation can be represented by a vector: The vector length represents the magnitude of magnetization, its direction codes the spatial orientation of the spins. Just like a vector, the magnetization can be decomposed into a longitudinal and a transversal component, the magnetization parallel and perpendicular to B_0, respectively. In the equilibrium state, the longitudinal component is making 100% of the net magnetization, the transversal one zero. The equilibrium state can be disturbed when applying a radiofrequency (RF) pulse. This pulse creates a supplementary, magnetic field (B_1) perpendicular to B_0. The additional B1 field leads to a nutation of the magnetization. For a short time the spin equilibrium is lost: they are reoriented towards B_1 and are synchronized in their precession. The amplitude and the duration of the pulse are responsible for the degree of reorientation: the more energy the pulse renders, the stronger the spatial orientation of the spins will be deflected. In our vector representation this means: the longitudinal magnetization is decreasing as the transversal magnetization is growing. As a consequence our magnetization vector is tilted towards the transversal plane; the achieved angle is called flip angle. A 90° pulse will flip the magnetization vector into the transversal plane, in which case the transversal component of the magnetization will grow to 100% and the longitudinal component will be zero. The frequency of the RF pulse must match the Lamor frequency. Only then will the oscillation of the applied pulse be in resonance with the spins, synchronizing their precession. This state is called phase coherence. The transversal magnetization that is in phase coherence can be detected with a coil and is the basis of the MR image.

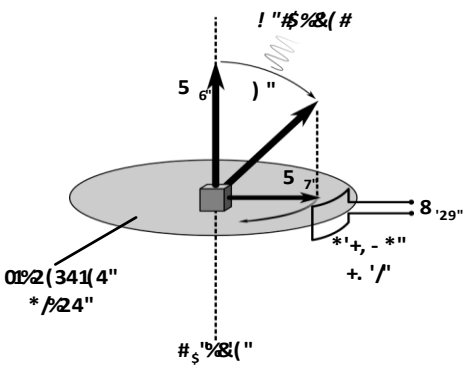

Figure 1: MR signal
Spins behave like bar magnets and can be aligned by an external magnetic field ($\mathbf{B_0}$); creating a net magnetization vector $\mathbf{M_z}$ parallel to $\mathbf{B_0}$. A radiofrequency (**RF**) pulse flips this vector towards the transverse plane with a flip angle of α. Precession of the spins in the **transverse plane** is reflected in the transverse vector component $\mathbf{M_T}$ and induces a voltage (U_{MR}) in **a pickup coil**.
Adapted with permission from Kalthoff [34]

IMAGING

After excitation, the spins lose their phase coherence and restore the thermal equilibrium. These relaxation processes are modulated by the interaction between spins and their surroundings (spin-lattice relaxation), between the individual spins (spin-spin relaxation), and by inhomogeneities of the magnetic field. The different components are described by three principle time constants: the spin-lattice relaxation time (T1), the spin-spin relaxation time (T2) and by a time constant T2*. As different biological tissues differ in their composition of macromolecules and water content, they generate an intrinsic MRI-contrast based on their relaxation times.

The duration and strength of the excitation pulse, the number of applied pulses, the time between consecutive scans (repetition time) and the time between excitation and data acquisition (echo time) are characterized by the MRI sequence and determine the image contrast. Spatial localization in the brain is achieved by supplementary non-static magnetic fields, so called gradients. The strength, direction and timing of the gradients can be controlled by the MRI sequence.

T1 is dependent on the thermodynamic interactions between the spins and the surrounding tissue. It is affected by the distinct macromolecular environment of the tissue. The spins absorb energy during excitation with the RF pulse. In tissue with many large molecules (like fatty tissue) the energy is quickly assimilated by the surrounding molecules; the spins restore their thermal equilibrium in a short amount of time. In tissue with fewer macromolecules the exchange takes longer. T1 is defined as the time when 67% of longitudinal magnetization is restored.

T2 is defined as the time when the transversal relaxation is decreased to 37% of the initial signal intensity. T2 reflects mainly the local water content in biological tissue. In tissue with high water content, the spins keep their phase coherence longer than in tissue with high fat content, thus showing a higher T2 value (e.g.: ventricles vs. white matter).

T2* reflects transversal relaxation due to interactions between spins (spin-spin relaxation) and additionally due to field inhomogeneities. Imperfections of the static magnetic field, poor adjustment to the sample (insufficient shim) or different tissue susceptibilities (especially between air and tissue) create constant inhomogeneities in the local magnetic field, leading to a faster decay of the signal than anticipated in the pure spin-spin relaxation model.

While conventional, structural MRI contrasts (T1, T2, T2*) rely on the chemical and molecular differences between tissues, Diffusion Weighted Imaging (DWI) employs another molecular characteristic: Brownian motion. Water movement in biological tissue is not completely free

(isotropic) but is limited by cell membranes (anisotropic). While DWI can visualize differences in diffusion rate, Diffusion Tensor Imaging is sensitive to differences in diffusion directionality, eg. between white matter (with a preferred diffusion direction along the axons) and grey matter.

In a DWI sequence two successively applied, pulsed gradient fields are used to detect movement. The sensitivity of the sequence is determined by the length, strength and spacing of these gradient pulses and is stated in the b-value. Most DWI sequences are based on the Stejskal-Tanner sequence from 1965 [35]. As previously stated, the precession (Lamor) frequency is dependent on the field strength. After a 90° RF pulse the first strong gradient changes the precession frequency of the spins, as a function of their spatial localization: the affected spins will loose their phase coherence causing the signal to be attenuated. A refocusing RF pulse (180°) and a second gradient pulse (of identical orientation and strength) restore the signal. However, if spins are moving along the gradient direction, the experienced second gradient field will differ from the first one. In this case, the signal will not be restored completely: the higher the diffusion rate the more attenuated the signal.

In Diffusion Tensor Imaging (DTI) the gradients are employed not only for spatial localization, but also for encoding the directionality of motion. A DTI dataset consists of at least six gradient directions and an A0 image without diffusion weighting, based on these images three eigenvectors are calculated for every individual voxel. Different diffusion associated parameters can be retrieved from such a dataset: the main diffusion direction, the degree of anisotropy (fractional anisotropy), the rate of diffusion (mean diffusivity), the degree of diffusion along the main direction (axial diffusivity) and perpendicular to it (radial diffusivity).

fMRI – functional Magnetic Resonance Imaging

Functional magnetic resonance imaging is based on three premises: (1) Neurons consume more energy during active firing than in resting state; (2) the increased demand of oxygen and nutrients is met by a haemodynamic response of the local blood vessels; and (3) the difference in the haemodynamic parameters can be visualized by MRI.

An active, firing neuron has a higher cerebral metabolic rate (CMR) compared to its resting state. The increased glucose and oxygen consumption causes the local blood levels to drop. This is compensated by vasodilation of the arterioles and arteries. The consequence is a regional increase of cerebral blood flow and volume (CBF and CBV). The mechanism matching the haemodynamic response to the metabolic need of the neuronal tissue is called neurovascular coupling. The cellular and molecular constituents of this mechanism have long remained elusive. As vessels in an area broader than the actual electrophysiological activation are recruited, neurovascular coupling must not rely on local feedback systems alone (e.g. higher local CO_2 levels acting upon smooth musculature of arterioles). A major advance has been the discovery that astrocytes play a key role in neurovascular coupling [36]. Astrocytes are the most numerous cells in the CNS and are very heterogeneous in morphology and function. Here we refer to the protoplasmic astrocytes in the grey matter of the brain. The distinct, star-like morphology reveals the key role of protoplasmic astrocytes in neurovascular coupling: Their fine processes are very elaborate and build endfeet contacting neurons, synapses and blood vessels alike. The current understanding of the neurovascular coupling mechanism is centered on the trinity of neuron, astrocyte and vessel, the so-called neurovascular unit (Figure 2). The neurotransmitters released by firing neurons are detected not only by the postsynaptic neurons, but also by astrocytes. The astrocytes integrate the signal and modulate the vascular reaction by various vasoactive mediators, among them potassium [37], nitric oxide [38], glutamate and other neurotransmitters.

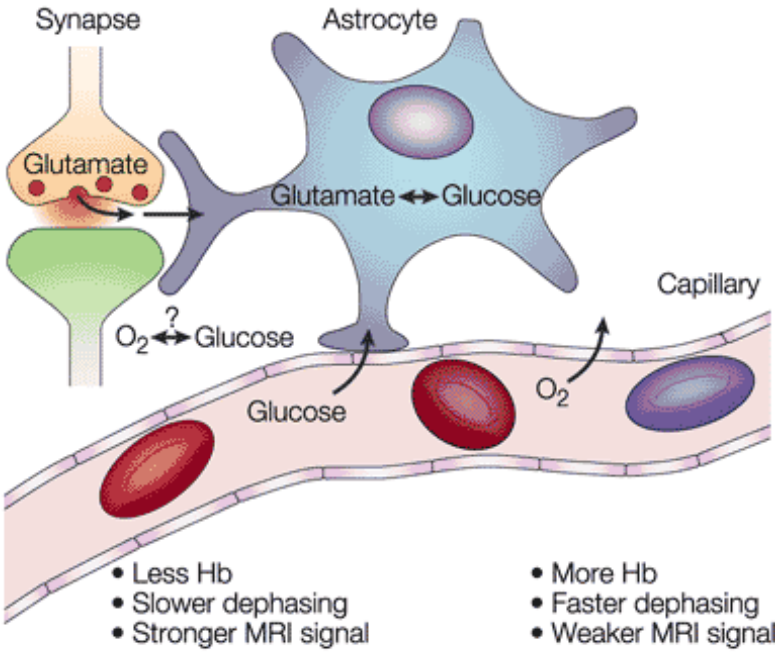

Figure 2: Neurovascular coupling
The neurovascular unit consists of neuron, astrocyte and vessel. Upon neuronal activation, synapses release glutamate. Neuronal activity requires energy, supplied by the blood vessels. Astrocytes detect the released transmitter and modulate the haemodynamic response.
Printed with permission from Nature Publishing Group [39].

Functional MRI aims to visualize the neuronal representation of a stimulus. Several indirect approaches are possible, relying on different aspects of the haemodynamic response: Imaging the change in cerebral blood volume, cerebral blood flow or in the blood oxygen level. The most commonly used, both in clinics and in research, is the blood oxygen level dependent (BOLD) fMRI. BOLD fMRI employs the magnetic properties of haemoglobin, the carrier protein for oxygen in the blood.

Haemoglobin consists of four protein complexes, each associated with a haem group with high affinity to oxygen. Two different states exist simultaneously in the blood: oxygenated haemoglobin (OHb), with oxygen bound to the haem group and deoxygenated haemoglobin (DHb), without oxygen. The ratio between the two is the basis for the fMRI contrast.

The central ion of the deoxygenated haem group is a Fe^{2+} ion, assigning paramagnetic properties to haemoglobin. A paramagnetic particle influences the behaviour of surrounding spins in a magnetic field. In this case: Haemoglobin is surrounded by water in the blood, reducing the phase coherence of the hydrogen nuclei and causing field distortions. With binding of oxygen, the iron ion becomes diamagnetic, reducing its influence on the surrounding protons. The reduced inhomogeneity in the blood shows up as a signal increase on T_2* weighted MR images. As the signal intensity is dependent on the binding of oxygen molecules on haemoglobin in the blood, the signal difference between more and less oxygenated blood is called blood oxygenation level dependent (BOLD) signal.

The increased cerebral metabolic rate of oxygen ($CMRO_2$) upon activation first leads to a reduction of oxygenated haemoglobin followed by a decreased signal, the initial dip. With a delay of about two seconds the vessels dilate and the blood volume and flow increase; the wave of fresh, oxygen-rich blood overcompensates the oxygen consumption of the neurons. As a consequence the percentage of oxygenated haemoglobin and thus the BOLD signal rises above the resting state level.

Functional magnetic resonance imaging in rodents encounters some difficulties, as the rat has to be anaesthetised or at least immobilised without lowering brain re-/ activity or influencing the haemodynamic response to the stimulus. To enable longitudinal measurement of the BOLD response, animals can be sedated with an α2-adrenoreceptor agonist (medetomidine) [40]. A well established stimulation paradigm for fMRI in rats uses electrical forepaw stimulation to activate the contralateral somatosensory cortex of the forepaw [41].

PET – Positron Emission Tomography

Positron emission tomography can visualize biochemical processes by using radioactive nuclides that coupled to a biochemically active compound and administered to the subject. The radioactivity can be detected by scintillation crystals inside a PET scanner and the spatial distribution of the radioactive tracer can be calculated, based on the positron annihilation that follows positron/ +β-decay.

Emitted positrons travel only short distance (approx. 1mm) in tissue before they lose their velocity and interact with an electron. A collision of the two antagonistic particles leads to their annihilation and the resultant energy is transferred into two γ-photons of each 511 keV. The two rays created are at an angle of 180° and travel into opposite directions (line of response) (Figure 3). The γ-photons are detected by the main part of the PET scanner, a ring of crystals. When two photons arrive in a given time, the coincidence window, they are considered simultaneously. If such a pair is found, the point of annihilation can be localized on the line of response. The exact position along this line cannot be given, but is assessed statistically. The vast number of simultaneous events during a PET measurement allows computing a probability histogram for every voxel, giving the number of annihilation incidences.

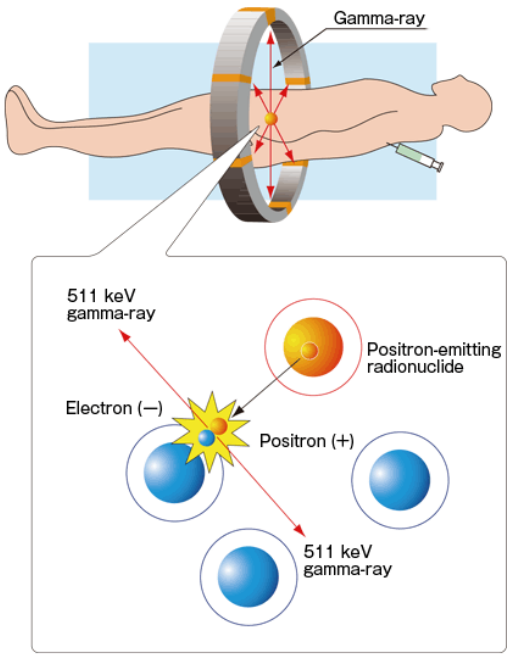

Figure 3: Positron annihilation after β-decay.
The radioisotopes used in PET undergo a positron or β-decay. The positrons move only a short distance in tissue before colliding with an electron. The two particles annihilate each other and the energy left is transferred into two γ-rays. The two γ-rays travel in an angle of 180° in opposite direction along the line of response [42].

The spatial resolution of the PET image is determined by the coincidence window of a PET scanner and the number and quality of crystals. The smaller the coincidence window, i.e. the shorter the allowed delay between a pair of photons, the less false positive annihilations are registered. PET raw data has to be corrected for several other factors: different efficiency of the individual crystals (normalizing to standard emitter), dead time (time after signal detection until a crystal is able to detect the next one), attenuation (tissue absorption) and scattered or random counts. The correction steps decrease the number of false positive counts but also the signal to noise ratio (SNR). The low SNR and the fact that the origin of annihilation is about 1mm away from the actual site of activity, explain the relatively poor spatial resolution of μPET.

The most frequently used radioactive tracer is certainly ^{18}Fluoro-deoxy-D-glucose (^{18}FDG). ^{18}FDG is a glucose derivative, which has radioactive Fluor instead of one of the hydroxyl groups. ^{18}FDG PET is based on one assumption: firing neurons take up and consume more glucose than “resting” neurons. ^{18}FDG is, like regular glucose, actively transported across the blood brain barrier and taken up by cells. It also passes in the first step of normal glucose metabolism, the phosphorylation by a hexokinase to glucose-6-Phosphate. The second metabolic step, the transformation to fructose-6-P by glucose-6-P-isomerase, is hindered by the missing hydroxygroup in the ^{18}FDG molecule. Reversing the phosphorylation is a rather slow process in all organs, apart from the liver. Until this can be accomplished, the radioactive ^{18}FDG-6-P molecules accumulate inside the cells.

The characteristic tracer kinetics of ^{18}FDG offer two scan paradigms, differing in the timing of tracer administration and data acquisition: static and dynamic measurements. The nomenclature may be misleading on first sight, as it does not refer to the brain activity that is imaged, but to the tracer kinetics that can be observed.

In static PET the administration of the tracer is separated in time from the acquisition period. During the incubation time, subjects can be engaged in different tasks, like memory tests, conditioning or sensorimotor tasks. Brain regions involved in solving them will consume and take up more ^{18}FDG. This paradigm asks for a control measurement, to which the task-driven data can be compared. Furthermore, it only yields relative measures for glucose consumption, being dependent on within-subject normalization.

In a dynamic PET paradigm, data acquisition starts simultaneously with tracer injection. The resulting image represents a resting state of the brain that is not modulated by behaviour. The first frames of such a dataset deliver information on tracer dynamics and input function which form the basis of the modelling calculations for absolute glucose consumption of the brain [43].

In order to identify regions of interest PET data has to be coregistered with either a CT (computed tomography) or an MR image. Coregistration is easy in combined scanners, supplying a fixed relation of the coordinate systems. Alternatively a manually or semi-automatically registration can be used when using a broadly distributed tracer, like ^{18}FDG.

Registration

Longitudinal imaging studies are challenging in terms of data postprocessing and handling. For the sake of processing time and standardization, a (semi-) automated processing strategy is necessary. Manual postprocessing, such as ROI selection or registration, is highly dependent on the individual rater's personal experience. Intra-rater variability is an issue especially in long-term studies, as the evaluation strategy will change with time and experience.

A crucial step for an effective and standardized evaluation of large-scale datasets is a reproducible and precise registration procedure. Registration is the process of transforming different volumes into a common space, i.e. one source into a target dataset. The main result is a matrix, encoding the spatial deformation of the source file. Normalization to a common space like a template brain allows comparison of corresponding structures, the use of standardized volumes/regions of interest and unbiased morphometry.

Several registration procedures exist, differing in numerous aspects [44; 45]:

(1) image dimensionality (2D/ 3D)

(2) registration basis (intensity/ landmarks)

(3) modalities (intra- /intermodal)

(4) degree of rater interaction

(5) optimization procedure (cost function)

(6) geometrical transformation

(7) object (organ/region of interest)

(8) subject (intra-/ intersubject/ subject-atlas)

In the following section, the specific aspects relevant for this study shall be explained. For a more detailed review of different methods of image registration see Sotiras et al. [46], Lester and Arridge [47] or Fitzgerald et al. [44].

(1) MRI and PET imaging produce a set of distinct, successive 2D images; combined they can be considered as one 3D volume. In special cases, however, the volume should not be considered as a consecutive volume, but rather be treated slice-wise. In fMRI where dimensions in z-direction (voxel depth) are considerably higher than in-plane, a slice-wise approach is advisable so not to lose information by interpolation.

(2-5) Registration can be based on different features of a volume (registration basis). Most common in medical imaging is an intensity-based transformation, independent of a rater to define features of

interest or landmarks. The transformation algorithm will align the source image to the target, based on the intensity of the voxel alone. The transformation is determined by iteratively running an algorithm, trying to maximize the similarity between the datasets. The voxel similarity is measured by a cost-function, which is lowest when similarity is best. Different optimization procedures can be iteratively employed to minimize the cost function/ maximize the similarity. Images of the same modality show similar contrast and can be aligned using a normalized cross correlation. Intermodal registration most often uses mutual information.

(6) The geometrical transformation of the source can be limited with various degrees of freedom (DOF), depending on the registration paradigm. The most restricted form of transformation is rigid-body registration with six DOF, allowing three rotations and translations, respectively. Affine registration allows the source to be sheared and scaled with three supplementary scaling factors (DOF=12). These two methods are called linear, because they treat the volume uniformly. They are sufficient for most intra-subject registrations. In cases where the datasets vary strongly, e.g. subjects of different ages and genetic backgrounds, a more complex approach is suitable. The brain of young animals is not only smaller, but shows different proportions than of older subjects. Non-linear registration takes such local differences into consideration, resulting in a precise match between the source and target file. Non-linear registration defines more than twelve DOF. Neuroimaging data comes with a high resolution and many structural details. When the algorithm weighs all structures equally, it might find a similarity on a detail first and iterate the transformation based on this local minimum/maximum. Introducing a structural hierarchy reduces the incidence of these local minima traps and increases the accuracy. In a hierarchical scheme the image resolution is artificially reduced (by downsampling or a Gaussian filter) so that the strong contrasts of the most global features are registered first. Step-wise the resolution is increased, allowing the finer details to be considered in the transformation. This approach is also called coarse-to-fine manner.

(7-8) The target of a registration can either be another subject, the same subject under different conditions or a standardized template. Intraindividual registration is interesting for longitudinal studies and helps visualizing processes of development, age or pharmaceutical intervention. Registration to a template brain or atlas allows the evaluation of standardized regions or volumes of interes (ROI/VOI). It is always advisable to decrease the extent of the transformation necessary, in order to minimize the incidence of registration mistakes. A template brain should thus represent a population mean, bring high resolution of the same modality and be matched in respect to age and strain.

Automated registration procedures are beneficial as they reduce rater variability as well as time. However, they lack any external control mechanism. All registration paradigms can fail, especially upon fluctuations in raw image quality and preprocessing. A review process must be done manually/visually by an expert and includes comparing the alignment based on landmarks and features of interest. A graphical interface is needed that allows screening large scale data quickly and reliably.

Original research articles

I. A visualization platform for high-throughput, follow-up, co-registered multi-contrast MRI rat brain data
Artem Khmelinskii, Luam Mengler, Pieter Kitslaar, Marius Staring, Mathias Hoehn, Boudewijn P. F. Lelieveldt
Proc. of SPIE Vol. 8672 (2013) 86721W-7

II. Brain maturation of the adolescent rat cortex and striatum: Changes in volume and myelination
Luam Mengler, Artem Khmelinskii, Michael Diedenhofen, Chrystelle Po, Marius Staring, Boudewijn P.F. Lelieveldt, Mathias Hoehn
NeuroImage 84 (2014) 35–44

III. Morphological maturation of the mouse brain: An in vivo MRI and histology investigation
Luam Hammelrath, Siniša Škokić, Artem Khmelinskii, Andreas Hess, Noortje van der Knaap, Marius Staring, Boudewijn P. F. Lelieveldt, Dirk Wiedermann, Mathias Hoehn
NeuroImage 125 (2016) 144-152

IV. Healthy ageing: a functional and structural profile of the rat brain
Luam Hammelrath, Chrystelle Po, Artem Khmelinskii, Eberhardt Pracht, Dirk Wiedermann, Heike Endepols, Cordula Schäfer, Marius Staring, Boudewijn P.F. Lelieveldt, Mathias Hoehn
in preparation

Publication I – Graphical User Interface

A visualization platform for high-throughput, follow-up, co-registered multi-contrast MRI rat brain data

Artem Khmelinskii, Luam Mengler, Pieter Kitslaar, Marius Staring, Mathias Hoehn, Boudewijn P. F. Lelieveldt

Proc. of SPIE Vol. 8672 (2013) 86721W-7

A visualization platform for high-throughput, follow-up, co-registered multi-contrast MRI rat brain data

A. Khmelinskii[a], L. Mengler[b], P. Kitslaar[a], M. Staring[a], M. Hoehn[b], B. P. F. Lelieveldt[*a,c]
[a]Division of Image Processing, Department of Radiology, Leiden University Medical Center, Leiden, the Netherlands;
[b]In-vivo-NMR Laboratory, Max Planck Institute for Neurological Research, Cologne, Germany;
[c]Department of Intelligent Systems, Delft University of Technology, Delft, the Netherlands

ABSTRACT

Multi-contrast MRI is a frequently used imaging technique in preclinical brain imaging. In longitudinal cross-sectional studies exploring and browsing through this high-throughput, heterogeneous data can become a very demanding task. The goal of this work was to build an intuitive and easy to use, dedicated visualization and side-by-side exploration tool for heterogeneous, co-registered multi-contrast, follow-up cross-sectional MRI data. The deformation field, which results from the registration step, was used to automatically link the same voxel in the displayed datasets of interest. Its determinant of the Jacobian (detJac) was used for a faster and more accurate visual assessment and comparison of brain deformation between the follow-up scans. This was combined with an efficient data management scheme. We investigated the functionality and the utility of our tool in the neuroimaging research field by means of a case study evaluation with three experienced domain scientists, using longitudinal, cross-sectional multi-contrast MRI rat brain data. Based on the performed case study evaluation we can conclude that the proposed tool improves the visual assessment of high-throughput cross-sectional, multi-contrast, follow-up data and can further assist in guiding quantitative studies.

Keywords: Visualization, Exploration, Side-by-side, Multi-contrast MRI, Follow-up, Cross-sectional, High throughput, Rat, Brain, Image Processing, Image Registration

1. INTRODUCTION

Preclinical neuroimaging uses the combination of various imaging techniques to help understand the brain and treat brain disorders. One of the imaging techniques most frequently used to characterize the brain is multi-contrast MRI. Combined, this heterogeneous data allows overcoming the limitations of the individual imaging techniques by providing the researcher with complementary information. However, in studies with several subjects and multiple time-points, exploring and browsing through the multi-contrast, cross-sectional, longitudinal heterogeneous data becomes a very demanding task.

One way to combine heterogeneous data is to use image registration, which allows t o find the spatial relation between the cross-sectional, longitudinal or multi-modal images, thus combining them into a common reference frame [1-7]. In this work we focus on lifespan multi-contrast neuroimaging, where detection of local deformations over the lifespan is essential. Though several registration and brain analysis toolkits are publicly available [8-10], there are currently no simple, dedicated and easy to use applications that allow quick inspection of such life-span MR data in an integrated and intuitive way.

The main contributions of this work are:

i. We provide an intuitive platform to integrate and visualize high-throughput co-registered multi-modal, cross-sectional follow-up data
ii. Our approach allows for an efficient data management and improves side-by-side exploration of high-throughput data by automatically linking the same region of interest(ROI)/voxel in the datasets using the deformation field obtained during the registration. Combining the latter with a determinant of the Jacobian visualization [7, 11-18] allows for a more accurate and faster visual assessment of brain change/deformation with time
iii. The presented tool was evaluated by means of an end-user case study evaluation [19] with three experienced domain scientists and made publicly available. Life span, cross-sectional, multi-contrast MRI rat brain data was used

*b.p.f.lelieveldt@lumc.nl; phone +31 71 526 1882; fax +31 (0)71 526 6801; www.lkeb.nl

Medical Imaging 2013: Biomedical Applications in Molecular, Structural, and Functional Imaging,
edited by John B. Weaver, Robert C. Molthen, Proc. of SPIE Vol. 8672, 86721W

2. METHODS

2.1 A visualization platform for high-throughput, follow-up, co-registered multi-contrast MRI brain data

To model local deformation in different regions of the brain over an individual's life-cycle, non-rigid B-spline registration is used [1-7, 11-18]. After a registration is performed, the deformation field and its determinant of Jacobian (detJac) are calculated. The deformation field is a vector image, where each voxel contains the information about its displacement (in physical coordinates) during the registration. The detJac extracts local expansion/compression information from the deformation field. In the construction of the data visualization application proposed in this work we explore the combination of displaying the images of interest (as originally acquired) with the information provided by the deformation field and its detJac.

When comparing 2 different datasets (e.g.: same subject, 2 time-points) the information provided by the deformation field is used to link the same ROI in the displayed datasets of interest: without distorting the original data one can automatically pin-point the exact same region/voxel in both datasets and understand what deformation the brain underwent from one time-point to another in all directions.

The detJac is used to inspect that deformation field: values between 0 and 1 indicate local compression, values above 1 indicate local expansion, and 1 indicates volume preservation [7, 11-18]. Identifying areas of local compression or expansion can facilitate the detection of areas of interest (brain change/deformation) in longitudinal studies and allows for a faster screening of the brain data before further proceeding to quantitative studies.

To handle high throughput co-registered data and to allow quick selection and switching between the hundreds of datasets a logical data management approach was devised. The final application consists of a two-step wizard: after the user defined the main data directory, a list of all the available co-registered data is presented, which can be sorted by subject name, age, modality or type of experiment; in the second step, the user performs the data analysis/exploration, selecting and switching between any dataset of interest. Figure 1 shows and describes in more detail the main components of the application.

2.2 Experimental set-up

To demonstrate and evaluate the application potential of the proposed visualization and exploration tool from an end-user point of view, a case-study with three experienced domain scientists was performed. Multi-contrast longitudinal MRI rat brain data from an existing life span study, exploring juvenile development and ageing processes of the brain was chosen to test the application.

2.3 Rat brain data

From postnatal day 21, two groups of four male Wistar rats (Harlan-Winkelmann GmbH, Borchen, Germany) were housed pairwise under standardized environmental conditions. Food restriction (80% of *ad libitum* consumption) started at an age of about 3 months in order to minimize obesity, a risk factor for age-related diseases [20]. The different groups were introduced into the study with different ages: Group 1 was followed from the age of three weeks with data available up to 14 months at the time of co-registration; Group 2 from ten until 24 months.

Animals were employed in MRI experiments on a bimonthly basis, with supplementary scans in the first 3 months to account for the fast cerebral growth. MRI experiments were conducted on an 11.7 T Bruker BioSpec™ horizontal bore scanner (Bruker Biospin, Ettlingen, Germany). Animals were anaesthetized using 2% Isoflurane (Forane, Baxter, Deerfield, IL, USA) in 70:30 N_2O:O_2, and vital functions were monitored continuously.

This study design shows traits of both a longitudinal and a cross-sectional approach. This beneficial combination allows monitoring the development of the same individuals over time, and at the same time excluding, or identifying possible long-term effects created by repeated measurement and anaesthesia.

T2 weighted images were chosen for their anatomical detail, diffusion tensor imaging (DTI) for the information on tissue anisotropy and myelination. T2 maps were calculated from an MSME (multi slice multi echo) sequence (10 echoes) with TE = 10 ms, TR = 5000 ms (IDL version 6.4, Boulder, CO, USA). The DTI datasets were used to calculate fractional anisotropy (FA), mean diffusivity (MD) and eigenvalue maps (DTI studio version 3.0.3, Baltimore, MD, USA). Both datasets were acquired with identical geometry, slice positioning and spatial resolution (FOV = 28 x 28 mm, resolution 0.146 x 0.146 mm inplane and 0.5 mm slice thickness; without gaps). Multiplying the number of subjects by the number of time-points and by the numbers of different MRI maps the total number of datasets exceeds 500.

2.4 Image registration

Image registration was performed between every two consecutive time-points and between each time-point and the baseline. In Group 1, the 3m old brain served as the baseline, for Group 2, the 10m old brain served as baseline. All registrations were performed using the first echo of the MSME data, chosen for its high anatomical detail and high SNR. The resultant transforms were propagated to the T2 maps and the DTI data. To compensate for any rotation, translation and scaling that exists between different datasets, rigid and affine transformations were applied. These are linear global transformations. To model local differences that allow detecting changes in different regions of the brain over the life-cycle (deformation, volume change, eventual tumor development, etc.), non-rigid B-spline registration was performed after the global initialization. For this data the following parameters were chosen: normalized correlation coefficient as a similarity measure, a four-level Gaussian image pyramid with downsampling and the B-spline with an eight point spacing transformation model. For all images a binary mask was available, made by an expert using the BET tool of the FSL package [9]. The image registration was performed using the publicly available `elastix` toolbox [7, 21].

With the registration results for any possible combination of data at hand, one can easily choose what to visualize and compare side-by-side: same subject-same modality-different time-points, different subjects-same modality-same time-points, same subject-different modalities-different time-points, different subjects-different modalities-same time-point, etc. The presented tool was developed in MeVisLab™ [22], is cross-platform and does not require any other software to be installed.

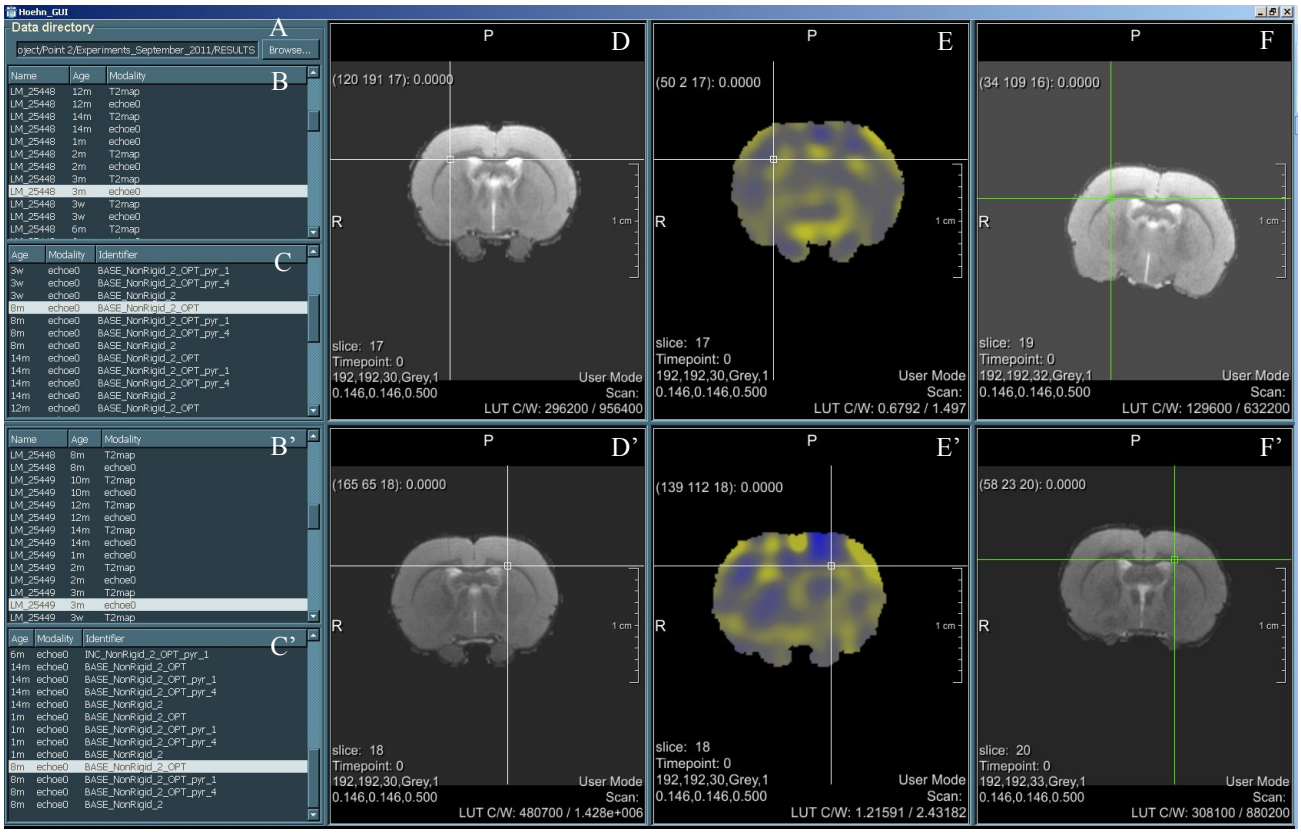

Figure 1. A screenshot of the proposed visualization platform for co-registered high-throughput multi-contrast, follow-up, cross-sectional MRI brain data exploration. Once the main directory is defined in (A), (B) presents a list with all the available data: different subjects acquired using different modalities in different time-points. This list can be sorted according to subject name, age or modality. After a baseline dataset of interest is selected in (B) a list of all the datasets co-registered to it (other subjects, time-points, modalities, types of experiment) is presented in (C). This way a quick overview of the co-registered data is available. The view panel (D) shows the selected baseline from (B), and panel (F) shows the dataset of interest that was previously co-registered to the selected baseline. These 2 datasets of interest are now

automatically linked using the deformation field obtained in the registration. This way, the anatomical location of a voxel in the baseline dataset on the left (white cursor), is pinpointed on the right (green cursor) allowing for an intuitive side-by-side exploration of the original, non-distorted data. The view panel in the middle (E) shows the detJac, allowing for a quick visual assessment of brain change/deformation that occurred between the time-point in (D) and the time-point in (F). Values above 1 (bright yellow) indicate local expansion, values between 0 and 1 (bright blue) indicate local compression and values equal or very close to 1 (grey) indicate volume preservation. The bottom row – (B'), (C'), (D'), (E') and (F') duplicates the functionality of the top row – (B), (C), (D), (E) and (F). This allows making different types of comparisons as described in the paragraph above. The images displayed are an example of the co-registered rat brain data: on the top row two time-points for subject S1 are shown and compared to the bottom row where the same time-points for subject S2 are presented

2.5 End-user evaluation and results

The proposed visualization and exploration tool was evaluated based on the principles and terminology set out by Yin for case study research [19]. The main study question was formulated as: *"How can the visualization platform assist neuroimaging researchers in studying changes over time in multi-modal rat brain data?"* and the case was defined as *"use of the tool by three domain and widely published scientists, referred to as DW, a clinical and experimental MRI expert, CB, a medical and pre-clinical visualization expert and LvdW, a neuroimaging, pre-clinical MRI expert"*. None of the users was involved in any stage of the development of the application before taking part in the evaluation presented here. Together with each of the domain scientists, in three separate, independent sessions, we used the application to analyze the multi-contrast, follow-up cross-sectional rat brain MRI data. That data was acquired to study juvenile development and ageing processes of the brain. During the evaluation sessions, feedback on the application was gathered and structured according to the following study propositions. Following, each proposition is stated, together with its related feedback, after which general comments and preliminary conclusions are presented.

Easy to use, does not have a steep learning curve

All three users confirmed this statement. CB added that all basic functions were straight-forward and indeed after a few minutes of explanation one could start using the application and that one of the positive aspects of the application was that since all files in the user-defined directory followed a naming convention all the data could be easily read by application. He also pointed out that it was positive that selecting a baseline automatically showed all registered datasets to ease selection of the follow-up datasets. LvdW also confirmed that the application was straightforward and intuitive to use. Both CB and LvdW suggested that auto-adjust the window-level for each selected dataset would be an improvement and that it should also be linked between the datasets being compared side-by-side.

The proposed platform allows for a fast selection and switching between the datasets of interest, efficiently handling the high-throughput data (more than 500 datasets).

DW confirmed this statement. CB commented that the tool indeed allows for fast selection from large sets, without having to waste time with orthodox file opening dialogs. However, there is room for improvement in terms of assisting the user in their progress, for example keeping track of comparisons they've made, perhaps even suggesting interesting comparisons based on image metrics. CB found the proposition a bit too broadly defined: he fully agreed that it facilitates selection and comparison, but there is more to be done in terms of integrated efficient handling of high-throughput data. LvdW noticed that the application is indeed convenient to load registered/linked data and suggested an improvement: make it possible to sort the data based on modality, subject, age, etc.

Automatically linking the same ROI/voxel in the displayed datasets, by using the deformation field of the previously performed registration improves side-by-side exploration of follow-up data.

DW confirmed that the linked cursor improved side-by-side exploration. CB noted that indeed this is an effective way that helps one to relate the registered parts of the two datasets being compared, adding that an interesting possibility would be extending the cursor's region of influence, so that local deformation could be better investigated. LvdW commented that automatic linking contributed to a considerable time saving.

The proposed platform allows for an intuitive exploration of cross-sectional and multi-modal data.

DW and LvdW agreed with the statement, the latter one adding that one really gets to know their data well with this application. CB stated that he was not sure what intuitive meant in this context. He added that slice-views were important in any application based on tomographic data and this tool enables basic comparison with slice-views, and so can form a basic part of any comparison toolbox. He expects that it will be useful for the visual inspection of cross-sectional and multi-modal data.

Combining the display of the two time-points of interest together with a detJac visualization allows for a more accurate and faster visual assessment of brain change/deformation.

DW agreed with this statement. CB stated that the detJac visualization is definitely useful for the quick location of areas of significant shrinkage and expansion, which is important in many small animal follow-up studies. He added that side-by-side visualization of time-points is a basic but reliable way to compare data and in the case of this tool, one could also consider putting the baseline and follow-up views directly adjacent to ease comparison. LvdW said that the assessment of brain change/deformation was definitely faster also because of the linked cursor.

The above also holds true in the detection of asymmetries in brain deformation.

All three users agreed with this statement. CB added, that indeed it seemed easy to spot (as)symmetries in the colour coded detJac and that it would help to have a detJac threshold operator to filter out small changes.

All three also suggested that a colorbar showing color scale of the detJac would be helpful.

The tool can be also used for a fast, qualitative assessment of the registration accuracy, since one can quickly check if the clicked points in image-time-point 1 have the correct correspondence in the image-time-point 2.

All three users agreed that the tool could be in principle used to qualitatively assess the registration accuracy. DW commented that one could recognize misregistration, but for a routine quality check he prefers an overlay image. CB stated that he was not convinced, because one has to probe the positions. He agreed that one can spot-check easily for registration accuracy, but this is not the best way to check for whole slices or even the whole volume. In the case of slices, he would prefer also having alpha-blended slices or even red-green blended slices. LvdW stated that it required some expertise for someone to notice that something is wrong with the registration accuracy and that this was not the most obvious tool for that; if we want to make it visual, she'd rather look at a difference image.

The tool can help guide the quantitative study of age-related brain deformation, in that, areas of interest can be localized and qualitatively assessed before further studied

DW agreed with the statement and added that it had indeed potential. CB also confirmed this statement, adding that this kind of explorative tool should be part of any quantitative analysis pipeline, both for quality checking the data and for finding areas of interest that deserve further quantification. LvdW stated what this tool is something that she'd certainly use for getting a feel for the data, since often, one starts by looking through the data to see what quantification use in the experiment. She concluded by adding that a possibility to draw a region of interest and propagate through all the time-points would also be advantageous.

Regarding the execution times of the implemented tool, once the user defined the main data directory, the elaboration of the list of all co-registered datasets organized by subject name, age and modality (more than 500) takes no more than10 seconds on a 2.40GHz Intel Quad Core™ with 4GB of RAM, normal Windows™ desktop PC. Once the list is ready, the selection and switching between different datasets of interest takes around one tenth of a second.

3. DISCUSSION, CONCLUSION AND FUTURE WORK

In this paper we presented a tool that allows to visualize and explore high-throughput multi-contrast, cross-sectional follow-up co-registered MRI data of rat brain. It is independent of the used registration toolkit and does not distort the original data. Using the proposed tool, one can automatically link the same ROI in the displayed datasets by using the deformation field of the previously performed registration, thus improving side-by-side exploration of follow-up data and quickly visually assess brain change/deformation by combining the display of the two time-points of interest together with a detJac visualization.

The proposed visualization and exploration platform was evaluated by three domain experts based on the methods set out by Yin [19] for case study research. All three were enthusiastic with the application. CB commented that he expects it to be useful for the visual inspection of cross-sectional, follow-up and multi-contrast data and form the basis of any comparison toolbox. LvdW commented on the possibility of using the tool in future studies in her research group once the tool becomes publicly available. All three domain experts commented that to assess the registration accuracy they would prefer either a difference or an overlay or and alpha-blended image. The authors agree with this comment, but since the evaluation of the registration accuracy was not the main concern while implementing this tool, it is definitely a

feature that one can add in the future versions together with the option to draw ROIs and propagate their deformation through all the time-points.

Since the performing of the case study evaluation with the domain experts, we implemented several essential suggestions made by the users: auto-adjustment of the window-level and its linkage between the datasets that are being compared; make it possible to sort the listed data (based on modality, subject, age, etc.); add a threshold operator to filter out changes and a colorbar showing the color scale of the detJac. Based on the analysis of the performed case study we can conclude that the proposed application can improve the visual assessment of high-throughput multi-contrast follow-up data and further assist in guiding the quantitative studies. The proposed tool was tested and evaluated using longitudinal MR rat brain data. However, it can be applied to any type of co-registered pre-clinical or clinical follow-up, cross-sectional multi-modal data.

Besides the input from the interviewed domain experts, we must add that from our own experience, the side-by-side visualization tool combined with the detJac map was successfully used to identify and follow in time a spontaneous brain tumor growth, later confirmed *ex vivo* and identified as melingeoma [23]; and to detect changes in cortical thickness during juvenile development allowing the creation of physiologically meaningful ROIs for quantitative analysis of imaging parameters [24].

To add new options and features, the presented tool, together with the correspondent source code and a user-manual will be made publicly available for download via www.lkeb.nl

4. ACKNOWLEDGMENTS

We would like to acknowledge Dirk Wiedermann, Charl Botha, and Louise van der Weerd for their time and willingness to serve as external domain experts for our evaluation. Financial support from Medical Delta is gratefully acknowledged.

Financial support for the data acquisition was obtained from the German Ministry of Education and Research (BMBF-0314104 / Biomarkers of Brain Ageing) and from the EU FP7 program TargetBraIn (HEALTH-F2-2012-279017).

REFERENCES

[1] Maintz, J.B.A. and Viergever, M.A., ,"A survey of medical image registration," Med Image Anal, 2, 1-36 (1998)
[2] Zitova, B. and Flusser, J., "Image registration methods: a survey," Image Vision Comput 21, 977-1000 (2003)
[3] Lester, H. and Arridge, S.R., "A survey of hierarchical non-linear medical image registration," Pattern Recognit 32(1), 129–149
[4] Hill, D.L.G., Batchelor, P.G., Holden, M. and Hawkes, D.J., "Medical image registration," Phys Med Biol 46(3), R1–R45 (2001)
[5] Hajnal, J.V., Hill, D.L.G. and Hawkes, D.J. editors [Medical image registration], CRC Press, (2001)
[6] Modersitzki, J., [Numerical methods for image registration], Oxford University Press, (2004)
[7] Klein, S., Staring, M., Murphy, K., Viergever, M.A. and Pluim J.P.W., "elastix: a toolbox for intensity based medical image registration," IEEE T Med Imaging, 29(1), 196-205 (2010)
[8] Gouws, A., Woods, W., Millman, R., Morland, A. and Green, G., "DataViewer3D: An Open-Source, Cross-Platform Multi-Modal Neuroimaging Data Visualization Tool," Front Neuroinformatics, 3: 9 (2009)
[9] http://www.fmrib.ox.ac.uk/fsl/index.html (Version 4.1.7, 15 October 2012)
[10] http://www.freesurfer.net/ (15 October 2012)
[11] Rohlfing, T., Maurer, Jr.C.R., Bluemke, D.A. and Jacobs, M.A., "Volume-preserving nonrigid registration of MR breast images using free-form deformation with an incompressibility constraint," IEEE T Med Imaging, 22(6), 730-741, (2003)
[12] Lorenzi, M., Ayache, N. and Pennec, X., "Alzheimer's Disease Neuroimaging Initiative, Schild's Ladder for the Parallel Transport of Deformations in Time Series of Images," Inf Process Med Imaging, 22, 463-74, (2011)
[13] Maheswaran, S., Barjat, H., Rueckert, D., Batec, S.T., Howlett, D.R., Tilling, L., *et al.,* "Longitudinal regional brain volume changes quantified in normal aging and Alzheimer's APP×PS1 mice using MRI," Brain Res, 1270, 19-32 (2009)
[14] Lau, J.C., Lerch, J.P., Sled, J.G., Henkelman, R.M., Evans, A.C., and Bedell. B.J., "Longitudinal neuroanatomical changes determined by deformation-based morphometry in a mouse model of Alzheimer's disease," Neuroimage, 42(1), 19-27 (2008)
[15] Zamyadi, M., Baghdadi, L., Lerch, J.P., Bhattacharya, S., Schneider, J.E., Henkelman, R.M., *et al.,* "Mouse embryonic phenotyping by morphometric analysis of MR images," Physiol Genomics, 42A(2), 89-95 (2010)

[16] Spring, S., Lerch, J.P. and Henkelman, R.M., "Sexual dimorphism revealed in the structure of the mouse brain using three-dimensional magnetic resonance imaging," Neuroimage, 35(4), 1424-33 (2007)
[17] Falangola, M.F., Ardekani, B.A., Lee, S.P., Babb, J.S., Bogart, A., Dyakin, V.V., *et al.,* "Application of a non-linear image registration algorithm to quantitative analysis of T2 relaxation time in transgenic mouse models of AD pathology," J Neurosci Methods, 144(1), 91-7 (2005)
[18] Lerch, J.P., Carroll, J.B., Spring, S., Bertram, L.N., Schwab, C., Hayden, M.R., *et al.,* "Automated deformation analysis in the YAC128 Huntington disease mouse model," Neuroimage, 39(1): 32–9 (2008)
[19] Yin, R. K., [Case study research: design and methods], 4th edn. Sage (2009)
[20] Mattson, M. P., and Wan, R. Q., "Beneficial effect of intermittent fasting and caloric restriction on the cardiovascular and cerebrovascular systems," J Nutr Biochem 16, 129-137 (2005)
[21] http://elastix.isi.uu.nl (15 October 2012)
[22] http://www.mevislab.de/ (Version 2.1(VC8), 15 October 2012)
[23] Khmelinskii, A., Mengler, L., Kitslaar, P., Staring, M., Po, C., Reiber, J.H.C., Hoehn, M. and Lelieveldt, B.P.F., "Interactive system for exploration of multi-modal rat brain data," Proc EMIM (2011)
[24] Mengler, L., Khmelinskii, A., Po, C., Staring, M., Reiber, J.H.C., Lelieveldt, B.P.F., and Hoehn, M., "Juvenile development and ageing mediated changes in cortical structure and volume in the rat brain," Proc EMIM (2011)

Publication II – Brain Maturation in Rat

Brain maturation of the adolescent rat cortex and striatum: Changes in volume and myelination

Luam Mengler, Artem Khmelinskii, Michael Diedenhofen, Chrystelle Po, Marius Staring, Boudewijn P.F. Lelieveldt, Mathias Hoehn

NeuroImage 84 (2014) 35–44

NeuroImage 84 (2014) 35–44

Contents lists available at ScienceDirect

NeuroImage

journal homepage: www.elsevier.com/locate/ynimg

Brain maturation of the adolescent rat cortex and striatum: Changes in volume and myelination ☆

Luam Mengler [a], Artem Khmelinskii [b], Michael Diedenhofen [a], Chrystelle Po [a], Marius Staring [b], Boudewijn P.F. Lelieveldt [b,c], Mathias Hoehn [a,*]

[a] In-vivo-NMR Laboratory, Max Planck Institute for Neurological Research, Cologne, Germany
[b] Division of Image Processing, Dept. of Radiology, LUMC, Leiden, The Netherlands
[c] Dept. of Intelligent Systems, Delft University of Technology, Delft, The Netherlands

ARTICLE INFO

Article history:
Accepted 16 August 2013
Available online 27 August 2013

Keywords:
Brain development
Age-dependent T2 relaxation changes
Age-dependent diffusion changes
Myelination maturation
Tissue restructuring during cerebral development
Volume changes of cerebral structures during development

ABSTRACT

Longitudinal studies on brain pathology and assessment of therapeutic strategies rely on a fully mature adult brain to exclude confounds of cerebral developmental changes. Thus, knowledge about onset of adulthood is indispensable for discrimination of developmental phase and adulthood. We have performed a high-resolution longitudinal MRI study at 11.7 T of male Wistar rats between 21 days and six months of age, characterizing cerebral volume changes and tissue-specific myelination as a function of age. Cortical thickness reaches final value at 1 month, while volume increases of cortex, striatum and whole brain end only after two months. Myelin accretion is pronounced until the end of the third postnatal month. After this time, continuing myelination increases in cortex are still seen on histological analysis but are no longer reliably detectable with diffusion-weighted MRI due to parallel tissue restructuring processes. In conclusion, cerebral development continues over the first three months of age. This is of relevance for future studies on brain disease models which should not start before the end of month 3 to exclude serious confounds of continuing tissue development.

Introduction

Brain development is a continuous process, which proceeds well after birth and even adolescence. Most studies employing rats claim to use "young adults", implying a fully matured brain parenchyma. However, the definition for "young adults" is diverse and ranges between two and four months old and body weight of 200 to 350 g.

For longitudinal studies it is particularly important to be able to discriminate between natural, development-dependent tissue changes and those alterations due to induced diseases or lesions. As individual organs, tissues and microstructures mature at different paces, great care must be taken in choosing the age and observation period for the animal model of interest.

Adolescence is understood as the time of transition between infancy and adulthood, despite a lack of clear and unambiguous boundaries between those stadiums. In some cases, adulthood is used equivalent to full sexual maturity. Depending on the research interest, adolescence is described by changes not only in social (Meaney and Stewart, 1981), cognitive or risk-taking behavior (Spear and Brake, 1983), but also in the neurotransmitter system (Andersen, 2003). The onset and extent of this phase may differ for different strains/breeds, between the sexes and for further different parameters, and conservative age range includes postnatal days 28 to 42 (Spear, 2000). This time window starts about a week after rat's weaning age and ends shortly after sexual maturity.

As many of these characterizations were based on group comparisons at different ages, they describe mere group averaged values, while inter-individual variability in the temporal profile of development may be completely lost. We hypothesized that intra-individual longitudinal studies using noninvasive imaging modalities may allow the identification of biomarkers of developmental phases of the brain which will distinguish between an early, adolescent period of pronounced cerebral development and a later, matured, "steady state" cerebral adulthood. We further hypothesized that such biomarkers could be reflected either in anatomical, structural and volume changes over time or in quantitative tissue characterization through physiology-based imaging parameters. For this purpose, we have followed male Wistar rats from 21 days until 6 months. We measured whole brain, cortical and striatal volume changes with high-resolution T_2-weighted MRI to look for structure-related biomarkers. For developmental tissue changes, T_2 relaxometric

* Corresponding author at: In-vivo-NMR Laboratory, Max Planck Institute for Neurological Research, Gleuelerstrasse 50, D-50931 Köln, Germany. Fax: +49 221 4726 337.
E-mail address: mathias@nf.mpg.de (M. Hoehn).

1053-8119/$ – see front matter © 2013 The Authors. Published by Elsevier Inc. All rights reserved.
http://dx.doi.org/10.1016/j.neuroimage.2013.08.034

imaging and diffusion imaging were recorded to investigate the microstructure of the tissue and the myelination, respectively.

Materials and methods

Animals

All animal experiments were conducted in accordance with the German Animal Welfare Act and approved by the local authorities (Landesamt für Naturschutz, Umwelt und Verbraucherschutz NRW). From postnatal day 21 on (weaning age) twelve male Wistar rats (Harlan-Winkelmann GmbH, Borchen, Germany, and Janvier, Le Genest Saint Isle, Cedex, France) were held in an environment with controlled temperature (21 +/− 1 °C), humidity (55%+/− 10%), and light (12/12 h dark/light cycle). Animals were housed in groups of four until the age of two months, and in pairs afterwards, and were given access to food and water *ad libitum*.

Study design

Animals were subdivided into three survival groups: three weeks (n = 4), three months (n = 4) and six months (n = 4) to obtain histological specimens of all those ages. MRI experiments were conducted at the age of three weeks (3W), one (1M), two (2M), three (3M) and six (6M) months, until sacrifice, depending on group. Hereafter, we will refer to these time points using the above-introduced abbreviations.

MRI

MRI experiments were conducted on an 11.7 T Bruker BioSpec horizontal bore, dedicated animal scanner (Bruker Biospin, Ettlingen, Germany). RF transmission was achieved with a quadrature volume resonator (inner diameter 72 mm), while a quadrature rat brain surface coil (~30 mm × 30 mm) was used for signal reception. After induction of anesthesia with 3% isoflurane, rats were placed in an MRI compatible cradle, and the head was fixed with ear bars and a support ring for the upper incisors in order to reduce movement artifacts. Animals were anesthetized with 2% isoflurane (Forane, Baxter, Deerfield, IL, USA) in a 70/30 mixture of N_20 and O_2, and vital functions were monitored during the whole anesthesia period using DASYLab (version 9.0, Measurement Computing Cooperation, Norton, MA, USA). The breathing rate was assessed *via* a breathing pillow, placed under the thorax, and kept at 70–80 breaths/minute by adjusting the isoflurane concentration. Body temperature was recorded with a rectal temperature probe, and regulated by a feedback system (set value: 37 °C) controlling a heating blanket with warm circulating water (Medres, Cologne, Germany).

T_2-weighted imaging (T2WI) was chosen for the anatomical detail of the images (first TE) and the information on tissue microstructure. Diffusion tensor imaging (DTI) was acquired for information on tissue anisotropy and myelination. Both scan protocols, T2WI and DTI, were set to cover the volume between olfactory bulb and cerebellum and were acquired with identical geometry (field of view: 28 mm × 28 mm, matrix 192 × 192, 0.5 mm slice thickness, no interslice gaps). The number of slices was adjusted individually in every session in order to account for brain growth.

T2WI was acquired using a Multi Slice Multi Echo sequence (MSME; TR/TE = 5000 ms/10 ms; 10 echoes with 10 ms inter-echo spacing). DTI was recorded with an 8-shot spin echo EPI sequence (30 directions; b-value = 630 s/mm^2, and five supplementary A_0 images) using a Stejskal–Tanner sequence.

The TurboRARE sequence, used for the generation of the rat brain template, used a TR/TE_{eff} = 4000 ms/32.5 ms and a RARE factor of 8. Two averages were recorded with a field of view 28 mm × 28 mm (matrix 192 × 192) and 0.5 mm slice thickness.

Postprocessing

Quantitative T_2 maps were calculated from the MSME multi-echo trains assuming mono-exponential decays, using IDL (IDL version 6.4, Boulder, CO, USA).

Raw diffusion data was first eddy current corrected (FSL version 4.1.7, FMRIB Centre, Oxford, UK). Then, eigenvalues (λ_1, λ_2, λ_3) and mean diffusivity (MD) maps were calculated using DTI Studio (DTI studio version 3.0.3, Baltimore, MD, USA). As the tensor elements have been reported to be more sensitive than the fractional anisotropy (FA) alone which is a mathematical expression of the combination of the tensor elements (Bockhorst et al., 2008; Deo et al., 2006; Song et al., 2002), we have focused our analysis on $\lambda_{\parallel}$and $\lambda_{\perp}$. The three eigenvalues stand for the length of the three principal axes (directions) measured in diffusion tensor imaging. The first, largest eigenvalue (λ_1) represents the axial or parallel diffusivity ($\lambda_{\parallel}$), while the perpendicular or radial diffusivity ($\lambda_{\perp}$) is the average of the two minor axes, the second (λ_2) and third eigenvalue (λ_3). The average of all three eigenvalues is the mean diffusivity (MD) (Basser et al., 1994).

Registration and VOIs

The registration paradigm included registration to a template brain. This template was generated by registering separate data sets of 35 three month-old male Wistar rats to each other. Then one average brain template was generated from these 35 registered data sets. Additionally, volumes of interest (VOIs) for several anatomical structures were manually created based on a rat brain atlas (Paxinos and Watson, 1998). In the following, the VOIs of the cortex and the striatum are analyzed. All analysis used the brain volume represented by the series of coronal sections shown in Fig. 1, where the volumes were conservatively selected to avoid errors at the boundaries of the acquired maps and thus in order to avoid an error in volume determination. The ROI "*whole brain*" was defined as the brain tissue limited caudally by the cerebellum and rostrally by the rhinal fissure, as demonstrated in the sagittal section scheme in Fig. 2.

First, the 3M MRI dataset was registered to the template brain, then, the 2M and 6M data sets were registered to the 3M data set of each subject, the 1M MRI data was registered to the 2M and the 3W data to that at 1M. Thus, data sets of all time points of each individual were registered step-by-step to the template brain starting with the data sets of the 3 month old animals and propagating to the next-closest time point. Using the information provided by the deformation field (see below for details) for each registration step, the template VOIs were propagated from one time point to the next, thereby enabling quantitative comparison of corresponding areas. Subsequently, the VOIs were evaluated quantitatively for MRI parameter changes and for volume change.

All registration steps were carried out with the first echo (TE1) image of the MSME sequence (TR/TE = 5000 ms/10 ms), chosen for its high anatomical details and high signal-to-noise ratio (SNR). Individual brain masks were created (brain extraction tool in FSL) and applied during all steps of the registration process. The masks of all, the reference data set and the deforming data set, were used to crop the images to sections merely larger than the masks themselves to facilitate the registration steps of the brain. The quality and success of the registration process was controlled by visual inspection using a custom-made graphic user interface (GUI) (Khmelinskii et al., 2013).

Registration was performed in a coarse-to-fine process. Initial registration was accomplished with a rigid transformation for rough global alignment. Subsequently, an affine registration was conducted to compensate for brain size scaling during the animal's developmental growth. Finally, a non-rigid B-spline registration was applied to follow regional changes. A Gaussian image pyramid was employed in all registration steps, applying four resolutions for the rigid and affine and two for the B-spline part. Normalized correlation was used as a similarity

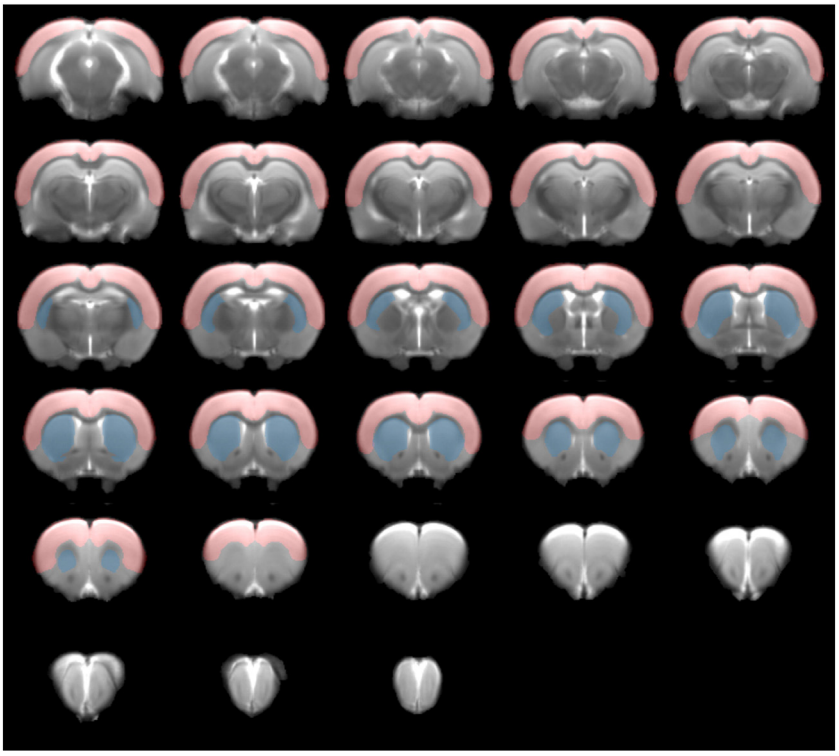

Fig. 1. Template brain with regions of interest (ROIs). The template brain is an average MR image stack (TurboRARE) of a three month old rat brain (n = 35 male Wistar rats). The extent shown here from the onset of the cerebellum caudally (top left) to the rhinal fissure rostrally (right bottom) was defined as the *whole brain* ROI. Superimposed are the structural ROIs for cortex (red) and striatum (blue), both based on Paxinos and Watson rat brain atlas (Paxinos and Watson, 1998).

metric. The registration was implemented using the open source image registration toolbox Elastix (Klein et al., 2010). Detailed information on the registration parameters can be found at the Elastix website (http://elastix.bigr.nl/wiki/index.php/Par0020).

The absolute three-dimensional deformation, necessary for the registration of two data sets, is contained in the deformation matrix. The identical geometry of the DTI and MSME (thus also the TE1) data sets allowed us to apply these deformation matrices of the TE1 images in a second step to the parameter maps. The VOIs are then available for all parameter maps of all time points, thereby enabling not only the quantitative evaluation of the T_2 and diffusivity changes, but also the computation of brain structure volumes.

Cortical thickness determination

The mean cortical thickness was assessed by measuring the distance between external capsule/corpus callosum and dorsal brain surface. For this purpose, a semi-automated macro was implemented in ImageJ (version 1.46, NIH, Bethesda, MD; USA) measuring the cortex thickness perpendicular to a manually generated outline of the white matter. In this procedure the most medial part of the corpus callosum was excluded, because the assumption of a parallel cortex is not met in this region.

In detail, in a first step a "profile image" is created: A manually generated outline ("Segmented Line" tool in ImageJ) is used to fit a curve to the center of the corpus callosum using Gaussian combined with Heaviside

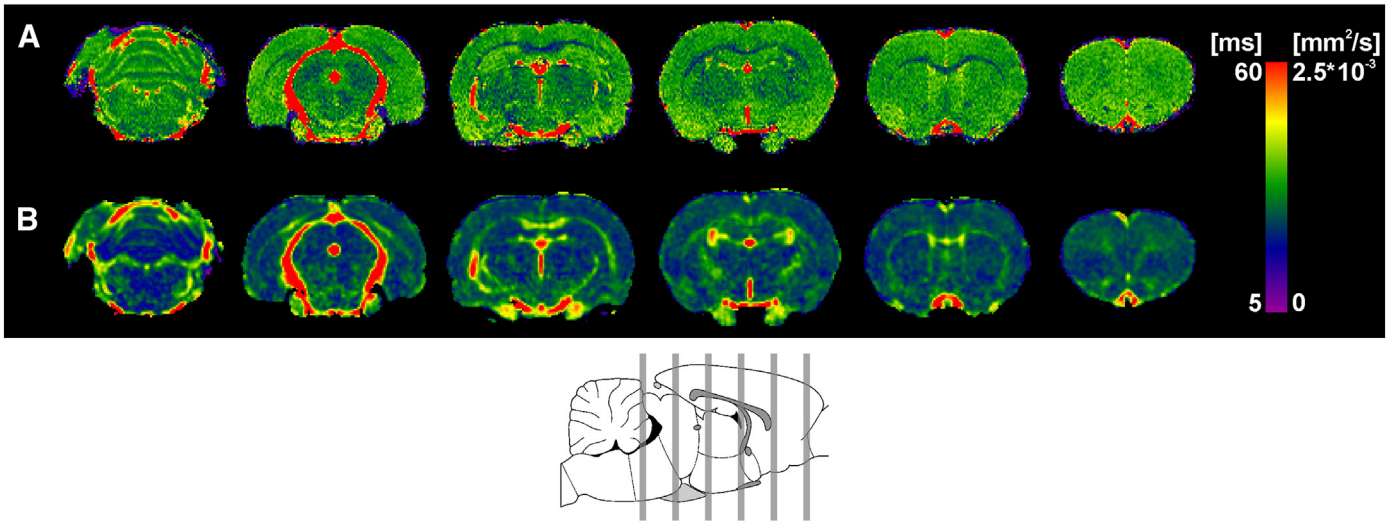

Fig. 2. Magnetic resonance data. Representative T_2 (A) and $\lambda_{\parallel}$ (B) map of a 3M old animal, before registration to the template brain. Depicted is every 5th MR image of an acquired 30 slice-stack, gray lines in the rat brain sketch (Paxinos and Watson, 1998) below indicate their anatomical position.

step function fits. Straight lines, perpendicular to this curve and reaching the cortical surface, form the "profile image", *i.e.* the curve is straightened. In a second step, the cortex thickness is measured in the profile image by determining the length of the straight lines perpendicular to the curve crossing the cortex only. This distinction is achieved by submitting the gray scales in the profile image to a Rodbard fitting function. This procedure of cortex thickness determination was performed for the somatosensory cortex in 5–6 slices.

Histology

At 3W, 3M and 6M, animals were sacrificed by transcardial perfusion with phosphate buffered solution (PBS) and 4% paraformaldehyde (PFA). Brains were postfixed overnight in 4% PFA before treatment with 30% sucrose. Tissue sections of 40 μm thickness were cut (Microtome, Leica Microsystems, Wetzlar, Germany) and preserved at −20 °C for histological staining. Sections at six selected levels were stained for both myelin and for cell nuclei, using Black-Gold II (BGII) (Schmued et al., 2008), and cresyl violet (CV), respectively (both: EMD Millipore, Billerica, MA, USA).

In order to assess the cell and myelin density in the brain, image acquisition and evaluation was conducted with a Keyence BZ9000 fluorescence microscope (Keyence, Neu-Isenburg, Germany) with a cell count analysis tool (Keyence). Quantification was based on contrast and color intensity in full-focus projections of images with 20× magnification (focal planes of 3 μm). ROIs were chosen in multiple areas: four cortical ROIs per hemisphere, each, in 6 sections (48 in total) and three striatal ROIs per hemisphere, each, in three sections (18 in total). Relative myelin content was defined as the relative area covered by BGII stained processes; cell density was determined as the number of CV stained cell nuclei per area.

Statistics

Longitudinal MRI data was evaluated using repeated measures ANOVA (SPSS version 18, IBM Corp. Armonk, NY, USA) with a repeated within-subject design. Where Mauchly's test indicated that the assumption of sphericity was violated ($p < 0.05$), we report the results with Greenhouse–Geisser corrected (ε) degrees of freedom and significance levels. Post-hoc pairwise comparisons with Bonferroni test are reported for consecutive time points only, unless interpretation of supplementary comparisons was useful.

Histological data was checked upon homogeneity of variances using Levene's test and analyzed with a one-way ANOVA with subsequent Bonferroni correction (SPSS).

All data were expressed as standard error of the mean (SEM) unless otherwise stated.

Results

Volume changes during development

The brain undergoes a strong growth during the first postnatal months. This growth curve was found to be quite homogeneous across the eight animals examined in this study. The volume change is significant for all three VOIs (whole brain: $\chi^2(5) = 16.7$ $p < 0.05$, $\varepsilon = 0.46$; $F(1.37,9.6) = 68.86$, $p < 0.001$; cortex: $F(3,21) = 65.48$, $p < 0.001$; striatum $\chi^2(5) = 18.3$ $p < 0.05$, $\varepsilon = 0.4$; $F(1.2, 8.4) = 33.5$, $p < 0.001$). Whole brain volume (excluding cerebellum and olfactory bulb) increases from $1202.9 +/- 18.9$ mm^3 (SEM) to $1585.5 +/- 43.9$ mm^3 (SEM) (Fig. 3A), thus gaining about 30% during the five weeks between postnatal week three and end of month two ($p < 0.001$). After 2M, brain volume is no longer changing significantly. Analyzing the cortical and striatal volumes separately, their volumetric plots (Figs. 3B and C), both show a highly significant increase ($p < 0.001$) from 3W to 1M, a continuous growth from 1M to 2M ($p < 0.05$), and no significant change from 2M to 3M.

Separate to the strong volume growth of whole brain, cortex and striatum, the cortical thickness shows a different developmental growth pattern. The cortical thickness grows substantially and significantly between 3W and 1M ($p < 0.05$), at which time it stabilizes already (Fig. 3D) ($\chi^2(5) = 14.96$ $p < 0.05$, $\varepsilon = 0.43$; $F(1.29,9) = 6.86$, $p < 0.05$).

Quantitative MRI parameter changes during development

Simultaneous with the dramatic volume changes, the quantitative MRI variables are changing. T_2 relaxation time of the whole brain, the cortex and the striatum decreases substantially and continuously in the time window between 3W and 2M ($p < 0.05$ between 3W/1M and 1M/2M) with a statistically significant effect over time (whole brain: $F(3,21) = 28.84$, $p < 0.001$; cortex: $F(3,21) = 36.4$, $p < 0.001$; striatum: $F(3,21) = 30.6$, $p < 0.001$). After 2M, the T_2 decrease in the striatum levels out, while the T_2 values of cortex and whole brain are still decreasing until the age of six months (Fig. 4A). Note that the T_2 decrease of the whole brain contains a contribution from shrinking relative ventricle volume, while the cortical and striatal T_2 decrease is primarily due to tissue reorganization processes.

The diffusion parameters axial ($\lambda_{\parallel}$), mean (MD), and radial diffusivity ($\lambda_{\perp}$) show a decrease during the first six months of cerebral development with a statistical effect over time (repeated measures ANOVA) in all three structures analyzed (Figs. 4B–D). However, not all parameters show differences between subsequent time points (*T*-test).

$\lambda_{\parallel}$ evolves similarly in cortex and striatum, both in respect to the absolute values and the relative change over time. In both areas, $\lambda_{\parallel}$ shows a light but steady decrease during the first three months (cortex: $F(3,21) = 6.72$, $p < 0.01$; striatum: $F(3,21) = 9.33$, $p < 0.001$) followed by stagnation thereafter. Mean $\lambda_{\parallel}$ of the whole brain is slightly higher compared to the absolute values of cortex and striatum, but follows the same qualitative developmental pattern ($F(3,21) = 6.86$, $p < 0.01$). None of the three structures shows a significant difference in $\lambda_{\parallel}$ between sequential time points, but they all show a difference between 3W and 3M ($p < 0.05$).

MD values of the three VOIs tend to increase from striatum to cortex to whole brain (Fig. 4C), though their qualitative development over time is alike and statistically significant in all three cases (whole brain: $F(3,21) = 13.29$, $p < 0.001$; cortex: $F(3,21) = 9.1$, $p < 0.001$, striatum: $F(3,21) = 19.13$, $p < 0.001$). The first three time points until 2M show a slowly decreasing trend followed by a steep decline between 2M and 3M and a rather stable phase thereafter (*i.e.* 3M to 6M). Despite the qualitative similarity in the development, the cortical ROI did not show any significant changes between sequential time points.

$\lambda_{\perp}$ development with time is similar to MD, but here the cortical values are equal to or even higher than those of the whole brain. In all three VOIs, an effect of time was observed (whole brain: $F(3,21) = 11.69$, $p < 0.001$; cortex: $F(3,21) = 6.72$, $p < 0.01$; striatum: $F(3,21) = 21.23$, $p < 0.001$) with a particularly strong $\lambda_{\perp}$ decrease between 2M and 3M. This difference was found to be significant in whole brain and striatum ($p < 0.05$), while in the cortex, the $\lambda_{\perp}$ values at 3M significantly differ only from 3W and 1M ($p < 0.01$) but not from 2M.

Histological analysis of developmental changes

Histological evaluation of the brains at different developmental stages revealed a pronounced increase in myelinated fibers on Black-Gold II staining during the first six months. This development was analyzed both qualitatively (Fig. 5) and quantitatively (Fig. 7A). The three-week young brains show positive staining only in the white matter structures, such as the corpus callosum, the anterior commissure, or fornix (Fig. 5). At 3W, myelinated fibers are barely detectable in the cortex, their contribution to the tissue is as low as 1% (Fig. 7A). By 3M, the radially oriented fibers of the cortex become myelinated to a high degree and cover about 15% of the cortex. At six months of age, the cortical

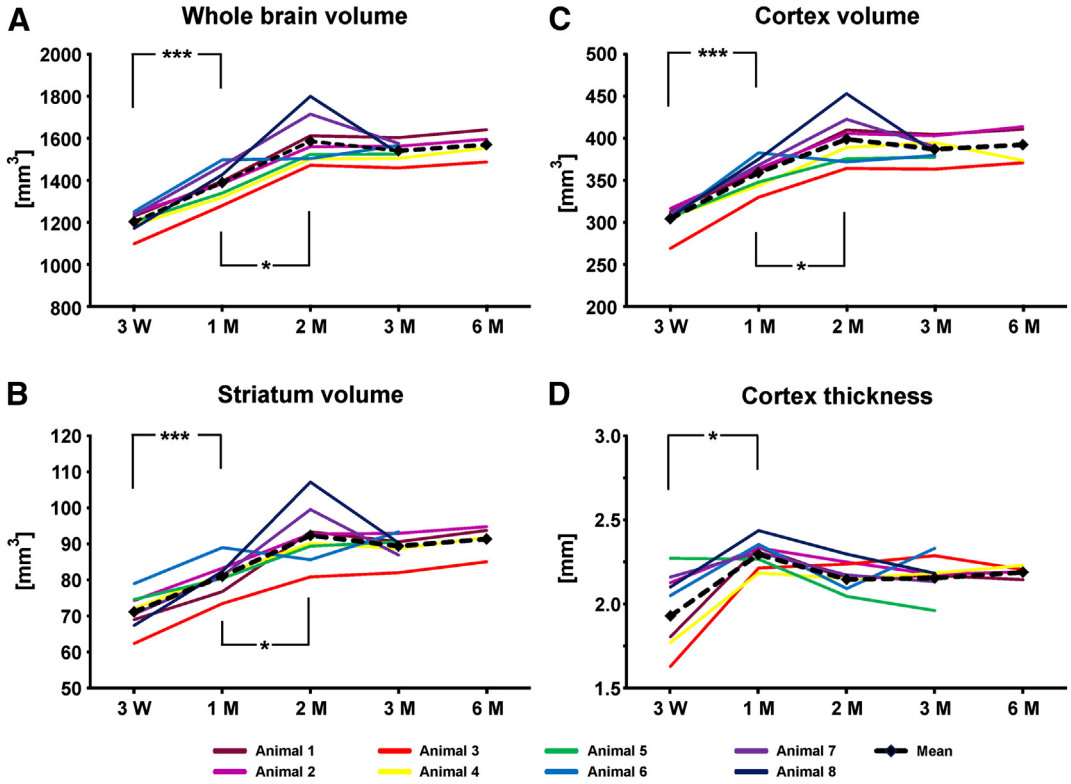

Fig. 3. Individual volume changes of developing brain regions. The graphs show the absolute volume of the whole brain (A), the striatum (B) and cortex (C) and the cortical thickness (D) plotted against the age for each individual animal. Here and in subsequent figures, ages are given as follows: three weeks, one, two, three and six months: 3W, 1M, 2M, 3M and 6M respectively. Red/yellow lines represent animals #1–4, which were followed from 3W to 6M, blue/green lines indicate animals #5–8, followed from 3W to 3M of age; the broken black line indicates the mean value. Note, for this and subsequent figures statistical significance is indicated for consecutive time points only; significance levels are Bonferroni corrected and represented by * $p < 0.05$, ** $p < 0.01$ and *** $p < 0.001$ and correspond in color to the respective data line.

layers can be recognized and at this time, 70% of the cortex is $BGII^+$. The increase of cortical $BGII^+$ area is apparent over time and found to be highly significant ($F(2,6) = 32,3$, $p < 0.001$).

In the striatum changes are not as pronounced upon visual inspection. Quantitative analysis, however, reveals a strong increase in relative area covered with myelin ($F(2,6) = 33,4$, $p < 0.001$). The white matter bundles of the striatum are already distinguishable at three weeks but make up only 5% of the area; with time they become more intensively stained and increase in numbers until, at three months, they represent about 28% of the striatal area. Here, in contrast to the cortical maturation, a further increase from 3M to 6M was not observed.

No maturation change is noticeable by visual inspection of CV staining of animals of different ages (Fig. 6). Quantitative analysis of cell density confirms this impression for the cortical but not for the striatal ROIs (Fig. 7B). Cell density in the cortex remains stable over the course of the first six months of maturation, with no distinct differences between the single time points. In the striatum, however, cell density is decreasing between 3W and 3M, reaching a constant level thereafter ($F(2,6) = 25.3$, $p < 0.01$).

Discussion

This study combined a longitudinal and cross-sectional approach to monitor postnatal development in Wistar rats by noninvasive *in vivo* MRI and conventional histology. We have assessed the noninvasive *in vivo* biomarkers cerebral growth, tissue water and tissue structure by MRI relaxation time measurements, and tissue diffusion parameters together with *ex vivo* tissue myelination state and cell density. With these parameters, we have been able to characterize and define the time window of brain maturation in the male Wistar rat. This novel definition is of paramount importance for longitudinal studies of the rat brain when it is important to discriminate in which phase of development or maturation the subject under investigation is at the start of the study or during its runtime. We have shown in this study that the rat brain and especially the rat brain cortex are indeed not yet fully developed at 3 months of age. Furthermore, individual brain regions and processes have been shown to have individual time scales for maturation. Based on these observations, we recommend careful examination of the brain structures under investigation before investigating functional topics or disease models in longitudinal examinations.

In vivo MRI parameter patterns of brain maturation

When inspecting the *in vivo* data alone, different maturation time profiles become apparent. Changing MR parameters alone, however, do not allow conclusions about single microstructural processes. Yet, the combination of the different *in vivo* measurements in this study suggested cell density and myelination to be strongly responsible for changes in T_2 and diffusion, respectively. Additional histological tissue characterization can reveal such changes in microstructure with high sensitivity, thus permitting unambiguous interpretation of the MRI parameters. In the present study, two tissue properties were analyzed: the development of myelinated fibers was visualized with the well characterized Black-Gold II staining (Schmued et al., 2008), while cell density was evaluated with cresyl violet, in order to detect neuronal as well as glial cell types.

Independent of ROI selection (whole brain, cortex or striatum), the first two months show continuous volume changes, accompanied by a dramatic T_2 decrease. This result of decreasing T_2 relaxation time with early growth is supported by an earlier study on postnatal rats in our group (Kallur et al., 2011). Judging from the T2WI-based volume data alone, one is tempted to believe that brain growth is completed by the end of two months. Interestingly enough, we have found that the quantitative parameter, T_2 relaxation time, continues to decrease beyond 2M,

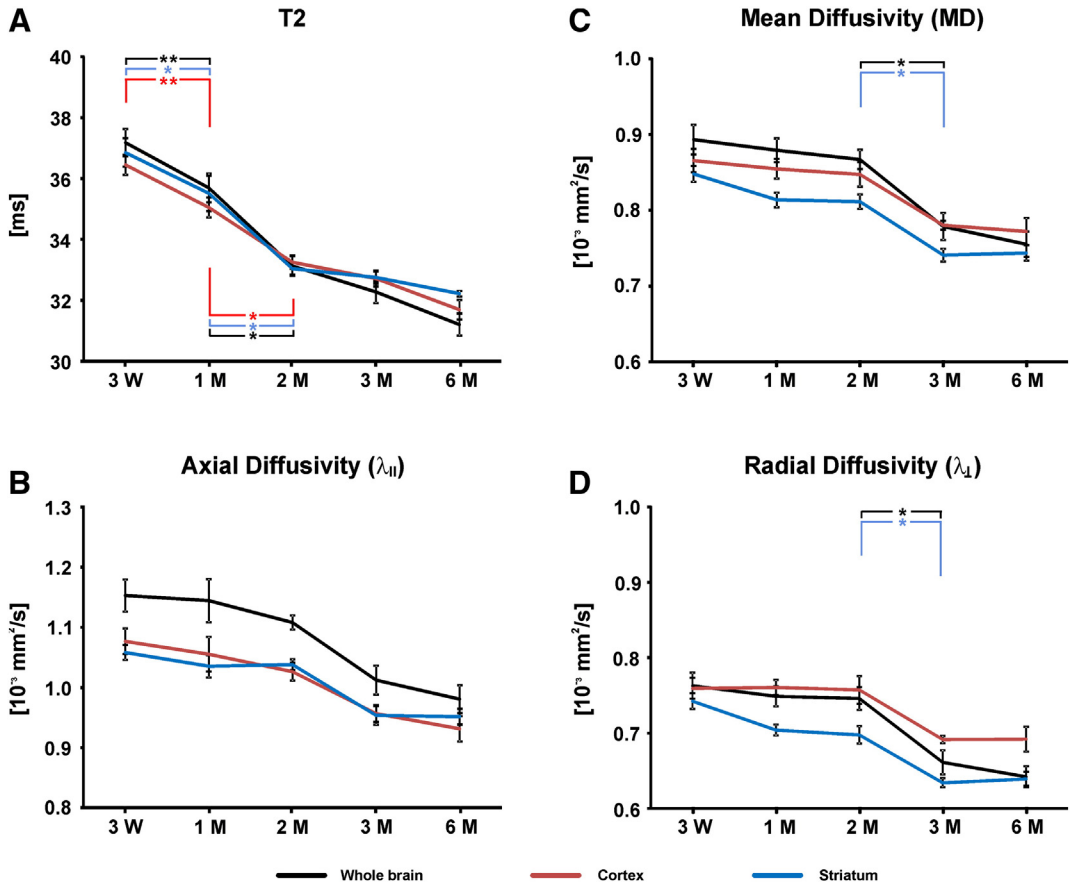

Fig. 4. Quantitative MR parameters. Evolution of the mean T_2 (A), axial (B), mean (C) and radial diffusivity (D) over time is shown for the three regions of interest: whole brain (black), cortex (red) and striatum (blue). The data shown is an average of n = 8 rats until 3M and n = 4 rats at 6M of age with error bars indicating the standard error of the mean (SEM).

indicative that water content and/or tissue reorganization processes continue to change at a time when the brain volume has reached a mature state. This is in agreement with reports on dramatic decrease of brain water content with increasing gestational age in humans (Hüppi and Dubois, 2006), while it continues to further decrease substantially during early development for many species, including rodents (Samorajski and Rosten, 1973). This T_2 decrease (as an indicator of brain water content decrease) may well be related to increasing myelination as a growing tissue compartment, consequently resulting in decrease of the extracellular space available for brain water.

Myelination as well as increased cell density, both decrease the amount of free water in the brain in favor of intracellular water compartmentation (Anderson et al., 2000; Chabert and Scifo, 2007). This is in agreement with early neurochemical studies (Fuller et al., 1982; Lancaster et al., 1984; Norton and Poduslo, 1973) which had reported that brain development is accompanied by a decreasing water content of the tissue and a constant increase of the myelin fraction. Indeed, our diffusion data show that the myelination process is not yet finished at 2M, again in agreement with the early reports describing ongoing myelination increases in healthy rats during their observation period of 52 days (Lancaster et al., 1984) and 70 days (Fuller et al., 1982), respectively. Previous studies reported that during adolescence changes in DTI parameters reflect myelination, but during the neonatal period, they rather reflect changes in general water content and structure (Wozniak and Lim, 2006). In our study, a pronounced decrease in the DTI parameters MD and $\lambda_\perp$ was found between 2M and 3M and reflects the dramatic change of the myelination status, confirmed by histology across the whole brain *ex vivo* between 3W and 3M (Figs. 5 and 7). As discussed earlier in model systems, diffusion anisotropy integrates information on myelination state and on axonal structure (Deo et al., 2006; Song et al., 2002). According to these authors, myelination changes are best represented by the radial diffusion tensor eigenvalue $\lambda_\perp$, while these changes have relatively little effect on the maximal eigenvalue $\lambda_\parallel$. Myelination acts like a restriction on radial free water mobility and, in consequence, leads to a reduced mean diffusivity, most clearly seen in a strong reduction in $\lambda_\perp$. This is in line with our MRI and histology results, showing that in the striatum with its strongly myelinated, big fiber bundles, MD as well as $\lambda_\perp$ are reduced more strongly than in the cortex. The drop in $\lambda_\parallel$ observed here is probably a result of the general diffusivity reduction, rather than actual reduced axial weighting. Though the *ex vivo* data is available only for 3W and 3M, the high temporal resolution of the DWI data suggests that the major period of myelination is between 2M and 3M.

When interpreting myelination, as assessed here by BGII staining, one must consider that staining intensity is not taken into account for the present quantification approach, thus denser packing in bundles is not represented in the evaluation. The strong myelination of the first three months is followed by rather subtle changes, observed both in staining intensity and stained area. In contrast to the DWI results, this is indicative that the brain is not completely developed at three months, thereby revealing the sensitivity limit of diffusion MRI.

In the following we discuss *in vivo* as well as *ex vivo* data of the different cerebral structures, followed by a recommendation for age-relevant brain studies.

Whole brain

The whole brain ROI shows higher MD and $\lambda_\parallel$ values and a stronger decrease over time, when compared to cortical and striatal ROIs. As the whole brain ROI includes all cerebral structures between olfactory bulb and cerebellum, it consists to a better part of white matter rich structures such as the hippocampus, the striatum, and the actual

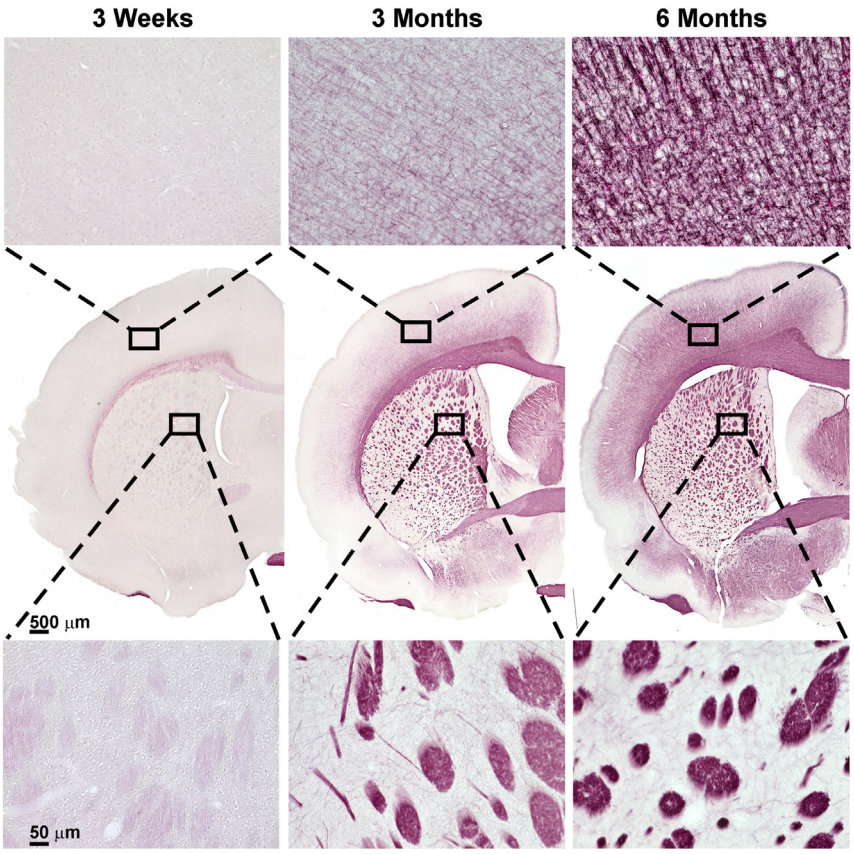

Fig. 5. Histological evaluation of myelin content. Black-Gold II staining was used to visualize cerebral myelin content, representative brain sections of differently aged animals are pictured here from left to right: 3W, 3M, 6M. The middle row shows an overview (4× magnification) of one hemisphere with the position of the two close-ups indicated by the black squares: the upper row shows a ROI (20×) in the cortex, the lower row in the striatum.

white matter. Thus, when interpreting the strong drop in diffusivity values with age, the major cause probably is myelination. As fluid compartments have the highest diffusivity, reduction in the relative size of the ventricles will further lower the mean diffusivity in the whole brain.

Cortex

The *ex vivo* and *in vivo* results for the cortical ROI suggest a rather complex maturation process. Most prominent is the apparent discrepancy between the evolution of cortical volume and of cortical thickness and of MRI diffusivity parameters and myelin content. These apparently contradicting findings reflect only different aspects of the same processes.

The cortical volume was found to increase until 2M, yet the cortex thickness has reached maximum already after 1M. These findings are in full accordance with *ex vivo* examination by Romand and colleagues, reporting a significant cortex increase along the long body axis between postnatal day 36 and 60 while thickness development already ended with postnatal day 36 (Romand et al., 2011). Thus, the cortex reaches its final thickness after one month while rostral/caudal expansion of the brain continues until at 2M.

Interestingly, the cortical growth phase is not accompanied by changes in cell density; according to Mortera et al. (Mortera and Herculano-Houzel, 2012), mainly neurogenesis rather than gliagenesis accounts for the volume increase. With the volume increase, the T_2 is reducing strongly until 2M, showing a decreasing trend afterwards. Apparently this T_2 change is not due to a changing density of cells, but must emerge from other maturation processes. A reduced T_2, as well as MD can indicate a reduction of free water in the tissue (Whittall et al., 1997), thus, decreasing the random movement of free water molecules and resulting in altered spin–spin interaction, the physical mechanism of T_2. Apart from myelination and higher cell density, the observed T_2 decrease may have several additional reasons coming from neuronal ramification and synaptogenesis, to simple compression and fine changes such as changing protein composition of the extracellular matrix. Especially the T_2 change beyond 3M, during growth stagnation and with major myelination processes terminated, reflects the high sensitivity of T_2 for tissue composition changes.

Our histological evaluation does not account for such processes of microscopic tissue composition alterations, so that *ex vivo* explanations for cortical T_2 changes are limited to the aspect of myelination. The BGII staining revealed a continued cortical myelination at least until 6M, contributing to reduction of extracellular space because of constant cell density. Although the radial organization increases pronouncedly on the BGII staining between 3M and 6M, this is not reflected on diffusion parameters. No decrease in either $\lambda_\perp$ or MD could be detected between these time points, indicating that further myelination after 3M was accompanied by other processes diminishing the radial diffusivity sensitivity. This diminishing diffusion sensitivity parallel to the ongoing myelination process may, at least in part, account for the apparent discrepancy between our results and earlier reports by Bockhorst and colleagues, reporting a decrease between postnatal day eight and 28, but no further change in cortical $\lambda_\parallel$, $\lambda_\perp$ or MD after postnatal day 28 (Bockhorst et al., 2008). Those earlier data may suffer from technical reduction of diffusion sensitivity: while we recorded our diffusion data at 11.7 T, data by Bockhorst et al. were collected at 7 T and needed more signal averaging, thus resulting in longer scan time, and, in consequence, making the images prone to movement artifacts which may lead to some blurring of the diffusion strength in the reconstructed quantitative parameter images. Support for such explanation comes from those authors reporting that the diffusion-weighted images needed to be

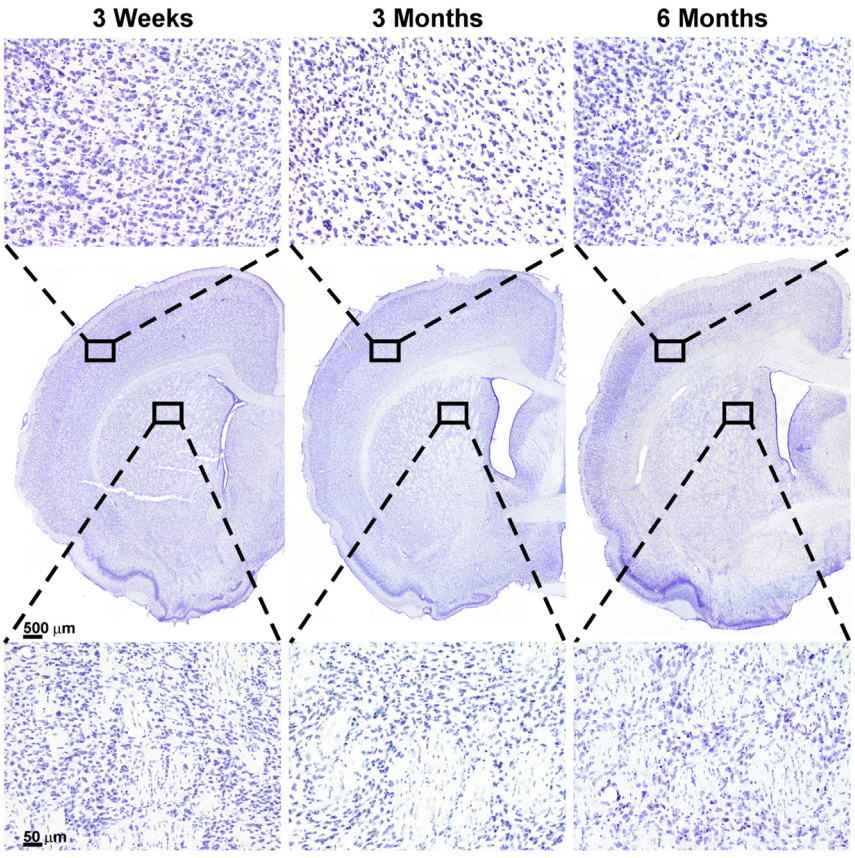

Fig. 6. Histological evaluation of cell density. Cell density was assessed *via* cell counting in cresyl violet stained sections. Representative brain sections of differently aged animals are pictured here from left to right: 3W, 3M, 6M. The middle row shows an overview (4× magnification) of one hemisphere, the upper and lower row show the close-ups indicated by the black squares: the upper row a ROI (20×) in the cortex, the lower row in the striatum.

warped to minimize image distortions induced by eddy currents. We therefore believe that our observations of diffusion changes persisting until 3M are based on more robust and more sensitive raw data recording.

The cortical architecture features radial compartments, like the pyramidal axons and functional columns, and layers perpendicular to the radial compartments. From such well characterized cortices as the primary visual cortex, it is known that the radial organization of the pyramidal neurons is established prenatally, and that their processes mature within the first postnatal weeks (Miller, 1986). This columnar/radial organization is not yet reflected in the histological staining, as the axons are not yet myelinated, but can be found in the DWI when inspecting the direction of the first eigenvector, $\lambda_{\parallel}$(Hoehn-Berlage et al., 1999). With the maturation of the cortical layers and the branching of the neurons within, the distinct and homogeneous pattern of the eigenvector dissolves, becoming less regular with increasing age. Though the radial structure appears dominant in the BGII staining, the layering structure of the cortex seems to modulate the major λ values seen in the DWI data afterwards. Cell-dense layers like layer IV, rich on interneurons, branches and cross connections, will have a more

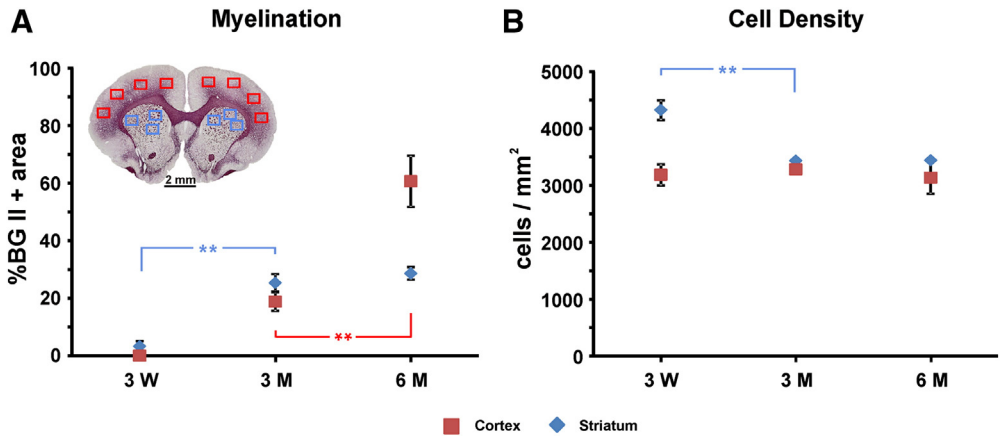

Fig. 7. *Ex vivo* histological quantification. Quantification of the histological sections was performed on eight cortical and six striatal close ups with 20× magnification per section. A representative overview section (4×) is inserted in the upper left, with the 14 ROIs indicated by red (cortex) and blue (striatum) boxes. The relative $BGII^{+}$ area reflects the extent of myelination (A), while cell density is assessed by the mean number of cells per mm^2 (B). Both graphs give the mean value for cortex (red) and striatum (blue) with error bars representing SEM ($n = 3$).

restricted and less directed diffusion than layers with fewer cell bodies. Though the spatial resolution is not sufficient to illustrate these differences within the cortex, diffusion of water molecules could be deflected between layers rather than along the myelinated axons in some parts of the cortex and be generally reduced during the maturation of the cortical parenchyma.

Striatum

In the striatum the developmental time scale observed in DWI appears to be consistent with the myelination process visualized in histology, showing big fiber bundles on CV and BGII stained tissue sections. The significant volume growth until 2M and the increasing trend until 6M are accompanied by an antiparallel development of the T_2 values equivalent to those in the cortex and whole brain ROIs. The changes in diffusivity are manifested quite strongly until 3M, as the striatum is rich in white matter bundles stretching toward the internal capsule. Histological assessment shows that in the same time frame, until 3M, cell number and myelin content of the striatum are changing remarkably and stabilize thereafter. Cell density is decreasing between 3W and 3M, maybe due to both, the striatal growth (until 2M) and the volume demanding myelination process. The strong myelination is reflected in the decrease of radial and mean diffusivity between 2M and 3M. At three months, however, all processes seem to be terminated and the striatal tissue has completely matured.

Consequences for investigations on cerebral disease models

Many studies on cerebral diseases are based on the assumption of inducing the disease or lesion on healthy and adult animals. There is, however, a wide body of literature on such disease model investigations using rats of body weight ranging between 270 and 320 g. According to standard weight-age diagrams provided by the animal suppliers for the strain of Wistar rats used in the present study, this weight range makes the animals typically around two months old, at any rate clearly younger than 3 months of age. In this case, volume change and cortical thickness have already stabilized, cell density in the striatum has also stabilized but myelination in both, striatum and cortex, continues up to 3M for striatum, for cortex even up to 6M. Based on the diffusion changes alone, myelination changes are very pronounced between months two and three. Taken these new observations together, it must be cautioned that lesion studies during this age period may be influenced by ongoing developmental brain maturation processes. This situation may be even more complex in the case of studies dealing with evaluation of therapeutic strategies. In light of our new observations, it would therefore be preferable to perform such disease model investigations (including those on therapeutic evaluations) on Wistar rats being at least three months of age at the beginning of the investigations.

Future studies will increase the temporal resolution of the maturation and growth changes to even better define the end of the developmental phase. Improvement of spatial resolution of the MRI will permit detailed analysis of structures prone to contain partial volume effects, such as corpus callosum or ventricular spaces, and will extend the whole volume to include hindbrain and olfactory bulb.

Conclusions

Combining longitudinal MRI measurements with histological tissue characterization, we have derived a temporal profile of postnatal rat brain maturation. Different cerebral structures show an individual timeline for postnatal development. While the striatum seems to be fully matured by three months, the cortex is still changing until at least six months. Our present results convincingly demonstrate that brain volume is a reliable variable of having reached a steady state situation concerning organ expansion while measurement of cortical thickness will be misleading for two to three month old rats. Clear indications of ongoing developmental changes in the rat brain point to the time window until three months of age; in particular persistent myelination aspects in cortex and striatum make it advisable to speak of “adult animals” only from three months of age on. Future investigations on disease models or lesions may have to consider this age of three months as a safer threshold to avoid ongoing developmental changes in the brain opposing the study of the patho-mechanisms of interest.

Acknowledgment

We gratefully acknowledge the support of Dr. Daniel Kalthoff for the development of the rat brain template based on MRI and his help with setting up ImageJ based macros for analysis of cortical thickness. We furthermore thank Melanie Nelles and Ulla Uhlenküken for their technical support. Financial support was obtained from the German Ministry of Education and Research (BMBF-0314104/Biomarkers of Brain Ageing) and from the EU FP7 program TargetBraIn (HEALTH-F2-2012-279017).

Conflict of interest

The authors have no conflict of interest. The funding agencies had no influence on study design, performance or analysis.

References

Andersen, S.L., 2003. Trajectories of brain development: point of vulnerability or window of opportunity? Neurosci. Biobehav. Rev. 27, 3–18.
Anderson, A.W., Xie, J., Pizzonia, J., Bronen, R.A., Spencer, D.D., Gore, J.C., 2000. Effects of cell volume fraction changes on apparent diffusion in human cells. Magn. Reson. Imaging 18, 689–695.
Basser, P.J., Mattiello, J., Lebihan, D., 1994. Estimation of the effective self-diffusion tensor from the NMR spin-echo. J. Magn. Reson. B 103, 247–254.
Bockhorst, K.H., Narayana, P.A., Liu, R., Vijjula, P.A., Ramu, J., Kamel, M., Wosik, J., Bockhorst, T., Hahn, K., Hasan, K.M., Perez-Polo, J.R., 2008. Early postnatal development of rat brain: *in vivo* diffusion tensor imaging. J. Neurosci. Res. 86, 1520–1528.
Chabert, S., Scifo, P., 2007. Diffusion signal in magnetic resonance imaging: origin and interpretation in neurosciences. Biol. Res. 40, 385–400.
Deo, A.A., Grill, R.J., Hasan, K.M., Narayama, P.A., 2006. *In vivo* serial diffusion tensor imaging of experimental spinal cord injury. J. Neurosci. Res. 83, 801–810.
Fuller, G.N., Divakaran, P., Wiggins, R.C., 1982. The effect of postnatal caffeine administration on brain myelination. Brain Res. 249, 189–191.
Hoehn-Berlage, M., Eis, M., Schmitz, B., 1999. Regional and directional anisotropy of apparent diffusion coefficient in rat brain. NMR Biomed. 12, 45–50.
Hüppi, P.S., Dubois, J., 2006. Diffusion tensor imaging of brain development. Semin. Fetal Neonatal Med. 11, 489–497.
Kallur, T., Farr, T.D., Boehm-Sturm, P., Kokaia, Z., Hoehn, M., 2011. Spatio-temporal dynamics, differentiation and viability of human neural stem cells after implantation into neonatal rat brain. Eur. J. Neurosci. 34, 382–393.
Khmelinskii, A., Mengler, L., Kitslaar, P., Staring, M., Hoehn, M., Lelieveldt, B.P.F., 2013. A visualization platform for high-throughput, follow-up, coregistered multicontrast MRI rat brain data. Proc. SPIE 8672, 86721W-86721W-7.
Klein, S., Staring, M., Murphy, K., Viergever, M.A., Pluim, J.P.W., 2010. elastix: a toolbox for intensity-based medical image registration. IEEE Trans. Med. Imaging 29, 196–205.
Lancaster, F.E., Philipps, S.M., Patsalos, P.N., Wiggins, R.C., 1984. Brain myelination in the offspring of ethanol-treated rats: *in utero versus* lactational exposure by cross-fostering offspring of control, pairfed and ethanol-treated dams. Brain Res. 309, 209–216.
Meaney, M.J., Stewart, J., 1981. A descriptive study of social development in the rat (Rattus norvegicus). Anim. Behav. 29, 34–45.
Miller, M.W., 1986. Maturation of rat visual cortex. III. Postnatal morphogenesis and synaptogenesis of local circuit neurons. Dev. Brain Res. 25, 271–285.
Mortera, P., Herculano-Houzel, S., 2012. Age-related neuronal loss in the rat brain starts at the end of adolescence. Front. Neuroanat. 6 (45). http://dx.doi.org/10.3389/fnana 2012.00045.
Norton, W.T., Poduslo, S.E., 1973. Myelination in rat brain: changes in myelin composition during brain maturation. J. Neurochem. 21, 759–773.
Paxinos, G., Watson, C., 1998. The Rat Brain in Stereotaxic Coordinates, 4 ed. Academic Press, San Diego, CA.
Romand, S., Wang, Y., Toledo-Rodriguez, M., Markram, H., 2011. Morphological development of thick-tufted layer V pyramidal cells in the rat somatosensory cortex. Front. Neuroanat. 5.5. http://dx.doi.org/10.3389/fnana 2011.00005.
Samorajski, T., Rosten, C., 1973. Age and regional differences in the chemical composition of brains of mice. Monkeys and Humans. Progress in Brain Research: Neurobiological Aspects of Maturation and Aging.Elsevier 253–265.

Schmued, L., Bowyer, J., Cozart, M., Heard, D., Binienda, Z., Paule, M., 2008. Introducing Black-Gold II, a highly soluble gold phosphate complex with several unique advantages for the histochemical localization of myelin. Brain Res. 1229, 210–217.

Song, S.K., Sun, S.W., Ramsbottom, M.J., Chang, C., Russell, J., Cross, A.H., 2002. Dysmyelination revealed through MRI as increased radial (but unchanged axial) diffusion of water. Neuroimage 17, 1429–1436.

Spear, L.P., 2000. The adolescent brain and age-related behavioral manifestations. Neurosci. Biobehav. Rev. 24, 417–463.

Spear, L.P., Brake, S.C., 1983. Periadolescence: age-dependent behavior and psychopharmacological responsivity in rats. Dev. Psychobiol. 16, 83–109.

Whittall, K.P., Mackay, A.L., Graeb, D.A., Nugent, R.A., Li, D.K.B., Paty, D.W., 1997. *In vivo* measurement of T2 distributions and water contents in normal human brain. Magn. Reson. Med. 37, 34–43.

Wozniak, J.R., Lim, K.O., 2006. Advances in white matter imaging: a review of *in vivo* magnetic resonance methodologies and their applicability to the study of development and aging. Neurosci. Biobehav. Rev. 30, 762–774.

Publication III – Brain Maturation in Mouse

Morphological maturation of the mouse brain: An in vivo MRI and histology investigation

Luam Hammelrath, Siniša Škokić, Artem Khmelinskii, Andreas Hess, Noortje van der Knaap, Marius Staring, Boudewijn P. F. Lelieveldt, Dirk Wiedermann, Mathias Hoehn

NeuroImage 125 (2016): 144-152

NeuroImage 125 (2016) 144–152

Contents lists available at ScienceDirect

NeuroImage

journal homepage: www.elsevier.com/locate/ynimg

Morphological maturation of the mouse brain: An in vivo MRI and histology investigation

Luam Hammelrath [a], Siniša Škokić [a,b], Artem Khmelinskii [c,d], Andreas Hess [e], Noortje van der Knaap [a,f], Marius Staring [c], Boudewijn P.F. Lelieveldt [c,g], Dirk Wiedermann [a], Mathias Hoehn [a,c,d,*]

[a] Max Planck Institute for Metabolism Research, In-vivo-NMR Laboratory, Gleuelerstraße 50, Cologne, Germany
[b] Croatian Institute for Brain Research, University of Zagreb School of Medicine, Šalata 12, Zagreb 10000, Croatia
[c] Division of Image Processing, Dept. of Radiology, Leiden University Medical Center, PO Box 9600, 2300 RC Leiden, The Netherlands
[d] Percuros B.V., Drienerlolaan 5-Zuidhorst, 7522 Enschede, NB, The Netherlands
[e] Institute of Experimental and Clinical Pharmacology and Toxicology, University of Erlangen-Nürnberg, Fahrstr. 17, 91054 Erlangen, Germany
[f] Donders Institute for Brain, Cognition and Behaviour, Dept. of Cognitive Neuroscience, Radboud University Nijmegen, P.O. Box 9010, 6500 GL Nijmegen, The Netherlands
[g] Dept. of Intelligent Systems, Delft University of Technology, Mekelweg 4, 2628 CD Delft, The Netherlands

ARTICLE INFO

Article history:
Received 31 July 2015
Accepted 5 October 2015
Available online 14 October 2015

Keywords:
MRI
Mouse brain
Brain development
Cortex
Myelination
DTI

ABSTRACT

With the wide access to studies of selected gene expressions in transgenic animals, mice have become the dominant species as cerebral disease models. Many of these studies are performed on animals of not more than eight weeks, declared as adult animals. Based on the earlier reports that full brain maturation requires at least three months in rats, there is a clear need to discern the corresponding minimal animal age to provide an "adult brain" in mice in order to avoid modulation of disease progression/therapy studies by ongoing developmental changes. For this purpose, we have studied anatomical brain alterations of mice during their first six months of age. Using T2-weighted and diffusion-weighted MRI, structural and volume changes of the brain were identified and compared with histological analysis of myelination. Mouse brain volume was found to be almost stable already at three weeks, but cortex thickness kept decreasing continuously with maximal changes during the first three months. Myelination is still increasing between three and six months, although most dramatic changes are over by three months. While our results emphasize that mice should be at least three months old when adult animals are needed for brain studies, preferred choice of one particular metric for future investigation goals will result in somewhat varying age windows of stabilization.

Introduction

The development of the brain continues well beyond birth and goes through various phases of adolescent changes (Andersen, 2003; Meaney and Stewart, 1981; Spear and Brake, 1983) before it reaches a state in adulthood which is considered a steady state condition. Such steady state is usually assumed when adult animals are studied, be it in the course of neurodevelopmental studies (Tissir and Goffinet, 2003) or for the investigation into cerebral disease evolutions (Adamczak et al., 2014; van Dorsten et al., 1999) and development of corresponding therapeutic strategies (Bockhorst et al., 2008). This requires the definition of a time window in early age when this cerebral maturation has been reached as well as the definition of a time window in progressed age when aging processes start to disturb this steady state. The definition of the onset of adulthood and the end of maturation is the goal of the present study. Often, adulthood of experimental animals was used equivalent to full sexual maturity or to body weight indications only. However, in an earlier study on rat brain maturation we have been able to point out a wide temporal discrepancy of sexual maturity to full brain maturation (Mengler et al., 2014).

With the wide access to studies of selected gene expressions in transgenic animals, mice have become the dominant species for experimental investigations on cerebral diseases, including stroke (Adamczak et al., 2014), neurodegenerative diseases such as Alzheimer's disease (Zempel and Mandelkow, 2014), trauma (Webster et al., 2015) and many more. Many of these studies are performed on animals of not more than eight weeks, declared as adult animals. Based on the earlier reported situation on rats that full brain maturation requires animals with an age of at least three months (Mengler et al., 2014), there is a clear need to discern the corresponding minimal animal age to provide an "adult brain" in mice.

* Corresponding author at: In-vivo-NMR Laboratory, Max Planck Institute for Metabolism Research, Gleuelerstrasse 50, D-50931 Köln, Germany.
E-mail addresses: Luam.Mengler@sf.mpg.de (L. Hammelrath), sskokic@hiim.hr (S. Škokić), A.Khmelinskii@lumc.nl (A. Khmelinskii), andreas.hess@fau.de (A. Hess), Noortje.vanderKnaap@radboudumc.nl (N. van der Knaap), M.Staring@lumc.nl (M. Staring), B.P.F.Lelieveldt@lumc.nl (B.P.F. Lelieveldt), dirk.wiedermann@sf.mpg.de (D. Wiedermann), mathias@sf.mpg.de (M. Hoehn).

http://dx.doi.org/10.1016/j.neuroimage.2015.10.009
1053-8119/

Magnetic resonance imaging (MRI) has become an indispensible tool in neuroanatomy. MRI provides information on macrostructural as well as microstructural changes in the intact tissue, without suffering from shrinkage or other preparation artifacts, like shearing or cutting artifacts. The non-invasive character of MRI allows a longitudinal investigation of subjects and can complement histology when studying development, aging or disease models. Especially in postnatal development, MRI has proven useful for the detection and measurement of region specific growth and myelination (Wozniak and Lim, 2006). The relative water content of a tissue contributes greatly to contrast based on the spin–spin relaxation time contrast T2. Additionally, the different water diffusion characteristics in tissues are captured in diffusion tensor imaging (DTI); the structural complexity of a tissue not only changes the degree of diffusion, but also the directionality of the water movement. In recent years, postnatal development in rodent brains was frequently studied using DTI of ex vivo specimen (Mori et al., 2001; Zhang et al., 2003, 2005). These studies have built a fair basis for DTI-based morphometry of white matter. However, they lack detailed gray matter characterization and only few studies were performed with true in vivo measurements.

Neurodevelopmental studies of cerebral and in particular of cortical morphology can help identify structural, anatomic changes and reorganizations. Here, we have employed T2 relaxivity and DTI MRI in order to visualize microscopic as well as morphometric changes of the mouse brain and to unravel the time profile of the development and maturation of cortical structures.

Methods

Animals

All experiments were performed on C57Bl/6J mice (Janvier, Le Genest Saint Isle, Cedex, France) of four different postnatal ages: three, eight, twelve and twenty-four weeks.

Animals were allowed two weeks of habituation upon arrival. Weaning mice (P21) were born in the facility. They were housed in groups of four and were given access to food and water ad libitum, in an environment with controlled temperature (21 +/− 1 °C), humidity (55 +/− 10%), and light (12/12 h dark/light cycle). All animal experiments were conducted in accordance with the German Animal Welfare Act and approved by the local authorities (Landesamt für Naturschutz, Umwelt und Verbraucherschutz NRW).

MRI acquisition and data processing

MRI experiments were conducted on a 9.4 T Bruker BioSpec horizontal bore, dedicated animal scanner (Bruker Biospin, Ettlingen, Germany), equipped with a gradient system of 660 mT/m at 110 μs ramp time. For RF excitation a quadrature volume resonator (inner diameter 72 mm; Bruker Biospin) was used, for signal reception a quadrature mouse brain surface coil (Bruker Biospin) was applied. MRI data was acquired using Paravision 5.1 software. After induction of anesthesia, mice were placed in an MRI compatible cradle (Bruker Biospin), and the head was fixed with ear bars and a support ring for the upper incisors in order to reduce movement artifacts. Animals were anesthetized with 2% isoflurane (Forane, Baxter, Deerfield, IL, USA) in a 70/30 mixture of N_20 and O_2; vital functions were monitored during the whole anesthesia period using DASYLab (version 9.0, Measurement Computing Cooperation, Norton, MA, USA). The breathing rate was assessed via a breathing pillow, placed under the thorax, and kept at 100–120 breaths/min by adjusting the isoflurane concentration. Body temperature was recorded with a rectal temperature probe, and regulated by adjusting the temperature of a warm water circulation system (Medres, Cologne, Germany), feeding a heating blanket and the MR cradle.

T2WI and DTI protocols were set to cover the volume between the rhinal fissure and the anterior part of the cerebellum, and imaging data was acquired with identical geometry for both scans (field of view: 28 mm × 28 mm, matrix 192 × 192, 0.5 mm slice thickness, no inter-slice gaps). The number of slices was adjusted individually in every session according to age dependent brain size.

T2W images were acquired with a multi slice multi echo sequence (MSME TR/TE = 5000 ms/10 ms; 10 echoes, with 10 ms inter-echo spacing). For every voxel a monoexponential decay curve was determined from the ten echoes of the MSME (IDL version 6.4, Boulder, CO, USA) and the resulting spin–spin relaxation time was calculated pixelwise to obtain quantitative T2 maps.

Diffusion tensor imaging was recorded with an 8-shot spin echo EPI sequence (30 directions; b-value = 670 s/mm^2, and five supplementary A0 images), with a gradient scheme according to Jones 30 (Jones et al., 1999; Skare et al., 2000). DTI data is prone to distortions due to eddy currents, induced when strong gradient pulses are switched on and off, and to motion artifacts originating from the subject. Prior to tensor calculation, we therefore applied an eddy current correction (FSL version 4.1.7, FMRIB Centre, Oxford, UK) and visually inspected the single frames, discarding the corrupted ones. The occurrence of other distortions and artifacts was limited during image acquisition by applying an automatic ghost correction, the use of a fat suppression module (1.9 ms Gaussian pulse, 1,400 Hz bandwidth, 2 ms spoiler) and navigator echoes. The total acquisition time added up to 50 min, including adjustment scans and a full brain RARE sequence. The RARE data set was used for co-registration of measurements at separate time points.

From the diffusion tensor, three eigenvectors and the corresponding eigenvalues (λ_1, λ_2, λ_3) can be determined, representing in each voxel the main diffusion directions and the magnitude of diffusivity in all three directions. The largest eigenvalue (λ_1) represents the axial or parallel diffusivity ($\lambda_\parallel$), while the perpendicular or radial diffusivity ($\lambda_\perp$) is the average of the two minor values, the second (λ_2) and third eigenvalue (λ_3). The average of all three eigenvalues is a measure for the mean diffusivity (MD) (Basser et al., 1994). Based on the three eigenvalues, the fractional anisotropy (FA) is calculated, giving a measure for the anisotropy of diffusion within the voxel ($0 < FA < 1$, where 0 = isotropic condition).

Registration procedure and deformation-based morphometry (DBM)

The first echo of the MSME yields the best anatomical contrast and a high SNR, thus best qualifying for co-registration of individual image data sets. The images were stripped of external tissue (Smith, 2002) and normalized to a template brain compiled of n = 24 nine week old C57/Bl6 mice. The registration followed a hierarchical scheme (Mengler et al., 2014) and was implemented using Elastix (Klein et al., 2010). Detailed information on registration parameters can be found here (http://elastix.bigr.nl/wiki/index.php/Par0025). Two independent raters controlled the quality and success of the registration process using a custom-made graphic user-interface (Khmelinskii et al., 2013). Subsequently, the displacement field, containing the local deformations relative to the template, was applied to re-orient the calculated maps derived from the T2WI and DTI datasets.

The template was manually labeled with anatomical brain regions of interest (see below), and the corresponding volumes of interests (VOIs) were mapped in the native space of the individual datasets.

The displacement field encodes the anatomical differences between two ages of a brain, such that each voxel describes the transformation vector to the homologous position. A measure derived from the deformation matrix is the determinant of the Jacobian (detJac), representing the local volumetric changes. The detJac ranges from 0 (100% shrinkage) over 1 (no volume change) without upper boundary (volume increase). A logarithmic transform makes the Jacobian distribution symmetric, setting aside every a priori assumption on volume growth (Leow et al., 2006; Yanovsky et al., 2008). Volume changes were evaluated based on this log detJac using MATLAB 2011b (MathWorks Inc., Natick, MA, USA).

ROI analysis

Quantitative MRI parameters were evaluated for specific regions focussing on key structures, both in white and gray matter. Gray matter structures were manually segmented within the template brain, covering the cerebral cortex, thalamus, hippocampus and striatum (Inline Supplementary Fig. S1). The corresponding regions of interest (ROIs) were transformed to the individual datasets, using the inverse displacement fields generated during the registration process, and evaluated for volume of the tissue structure and its quantitative MRI parameters. As white matter structures are rather small, their boundaries are blurred on MRI data, due to partial volume effects, making transformation delicate. In order to avoid transformation errors, particularly when adjusting for local tissue expansion and brain growth, ROIs were created on averaged age maps generated of the respective age group data, acting as age-specific "templates". The following white matter structures were analyzed: corpus callosum, fimbrium, external and internal capsule.

Inline Supplementary Fig. S1 can be found online at http://dx.doi.org/10.1016/j.neuroimage.2015.10.009.

Using the same strategy, the cortex was segmented into cortical layers (upper, middle and lower cortex) on the first echo image of the multi-echo spin echo sequence. This was executed for different cortex areas: motor cortex (M1), primary somatosensory cortex of the forelimbs (S1), whisker barrel field of the somatosensory cortex (BF) and secondary somatosensory cortex (S2).

Cortical thickness determination

Cortical thickness measurements were performed on the individual datasets as well as on the age group average datasets. For the former the original MRI datasets per age were affine registered. In all cases the cortex was manually segmented. This resulted in a surface representation of the cortex with outer and inner boundaries. For each surface element (triangle) of the cortical outer boundary the surface normal was calculated. This surface normal is perpendicular to the surface therefore running from the outer to the inner boundary of the cortex. The length of this surface normal from the outer to the inner boundaries corresponds to the thickness of the cortex at that position. The thickness and position for every surface element were stored in a so called surface lattice. This surface lattice was mapped onto the outer cortex and color coded (cf. Fig. 3)

Next, in order to determine the most anterior and posterior coordinates for M1 and S1 a 3D mouse brain atlas, derived from Franklin & Paxinos (Franklin, 2007) was affine registered to every dataset. From the most anterior to the most posterior landmark for M1 and S1 a path was interpolated along the outer cortex surface. Additionally, a supplementary path along the lateral aspect of the cortex was created, stretching from the most anterior to the most posterior part of the segmented cortex. The cortical thickness at each coordinate of the different paths was obtained as the thickness value from the nearest element of the surface lattice.

From the individual datasets of these thickness profiles (Inline Supplementary Fig. S3) the averaged values across all animals of a given age are also presented (cf. Fig. 3).

Inline Supplementary Fig. S3 can be found online at http://dx.doi.org/10.1016/j.neuroimage.2015.10.009.

Histological examination

After the MRI session, mice were deeply anesthetized with isoflurane and perfused transcardially with saline, followed by 4% PFA. Brains were extracted, postfixed overnight and kept in sucrose solution until they sank. Specimens were serially sectioned at 30 μm on a freezing microtome (Leica Microsystems, Wetzlar, Germany) and kept at −20 °C in cryo-protective solution. After mounting on glass slides, sections were washed, heated, and stained for myelin before dehydrating in alcohol, clearing, and coverslipping. Myelin staining was achieved with the black-gold technique (Schmued et al., 2008) until fine fibers of the molecular layer appeared in the 24 week specimen. At selected levels, overview images of the sections were taken with 4× magnification (Keyence BZ-9000, Keyence Corp., Neu-Isenburg, Germany). ROIs in the upper, central and lower part of the S1 and M1 were chosen and corresponding images acquired with 40× magnification. ROI images were transformed into binary images using the "make binary" tool implemented into ImageJ software (version 1.46r, NIH, Bethesda, MD, USA) without applying supplementary thresholds. Black areas were defined as "stained for myelin". All postprocessing and analysis was performed using ImageJ software.

Statistical analysis

As MRI parameters of the same subject cannot be considered independent data, MANOVAs for the different parameters were performed to find differences between the age groups. Significant MANOVAs were followed up by separate ANOVAs for the individual ROIs. A Tukey HSD test, for post hoc pair-wise comparisons, revealed differences within a variable and ROI and between ages (all in SPSS version 22, IBM Corp. Armonk, NY, USA).

Results

Tissue selective ROI analysis of MRI parameters during developmental changes

ROI-based analysis of the T2 relaxation time values showed an initial decrease of T2 both in white and in gray matter from three to eight weeks of age. From eight weeks on, the T2 values were increasing slightly and continuously, continuing even till 24 weeks of age (Fig. 1). Using Pillai's trace there was a detectable effect of age on T2 values ($V = 2.49$, $F(27, 18) = 3.275$, $p < 0.01$). Separate ANOVAs for the different ROIs supported this effect to be highly significant for every ROI, except for the fimbrium. Results of the post hoc pairwise comparisons (Tukey HSD test) between the ages are illustrated in Fig. 1.

The DTI derived parameters revealed a more differentiated time profile. Fractional anisotropy (FA) was increasing in all white matter structures, except the internal capsule (ic). In gray matter, FA values went through a maximum at eight weeks of age in the hippocampus and caudate putamen but there was no clear age pattern in the thalamus. In the cortex, the FA value was continuously decreasing from three weeks of age on (Fig. 1). According to Pillai's trace there was an effect of age on fractional anisotropy values ($V = 2.46, F(27, 15) = 2.53, p < 0.05$). However, separate univariate ANOVAs on the individual ROIs revealed significant effects for the FA in the external capsule only ($F(3,11) = 10.869$, $p \leq 0.001$). This effect did not reach statistical relevance in the pairwise comparison. Corresponding behavior of axial diffusivity, proton density and of radial diffusivity did not show any significant effect of age in multivariate or univariate ANOVAs.

When analyzing volumes of defined tissue areas over time, it is noted that for all gray matter regions analyzed the final volume is reached within the first eight postnatal weeks, with no further global or local volume changes observable after this time point (Fig. 2A). A strong effect of age is supported by a multivariate ANOVA, $F(15, 51) = 4.843$, $p < 0.001$, post hoc pairwise comparison revealed that significant differences occur only until week eight. The volume increase, however, is not substantial enough to be clearly revealed in the deformation-based morphometry, showing mostly volume reduction of ventricular cavities and only slight volume increases in the deep gray matter of the thalamus (Fig. 2B).

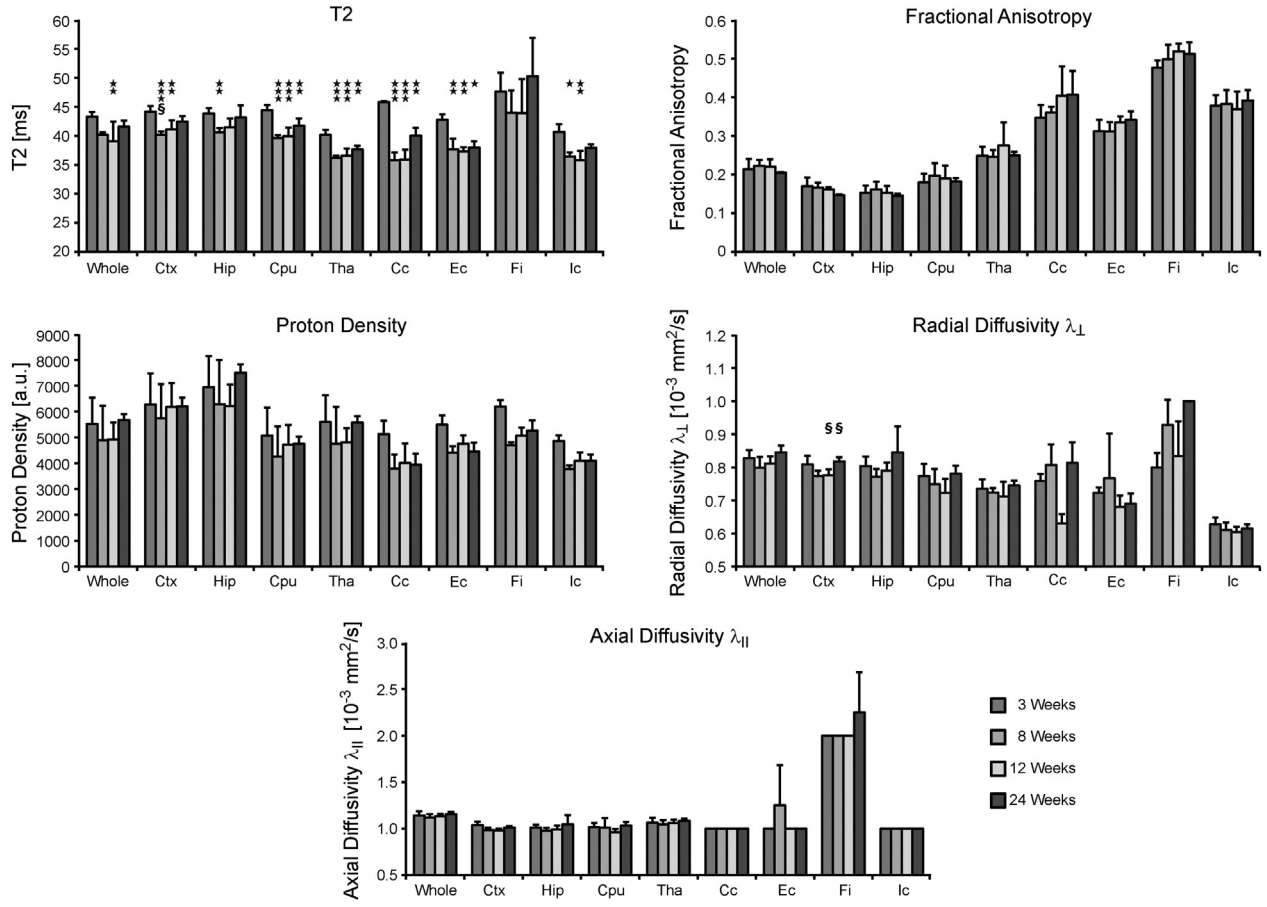

Fig. 1. Quantitative MRI parameters in different ROIs. The data shown is the group average of the different ages for T2, fractional anisotropy (FA), proton density, radial (RD) and axial diffusivity. Nine different ROIs in gray and white matter were analyzed: whole brain (whole), cortex (ctx), hippocampus (hip), striatum (Cpu), thalamus (Tha), corpus callosum (Cc), external capsule (Ec), fimbrium (Fi), internal capsule (Ic). The error bars indicate the standard error of the mean (SEM). Significance levels of post hoc pair-wise comparisons are indicated by the following symbols: significantly different from three weeks with $p < 0.05$ *; $p < 0.01$ **; $p < 0.001$ ***/significantly different from twelve weeks with $p < 0.05$ ♦; $p < 0.01$ ♦♦; $p < 0.001$ ♦♦♦/ significantly different from 24 weeks with $p < 0.05$ §; $p < 0.01$ §§; $p < 0.001$ §§§.

Age dependent changes in the cortex

The cortex thickness is decreasing from rostral to caudal direction. This pattern is preserved during all stages in the observation period (3–24 weeks) as depicted in the 3-dimensional color-coded cortex thickness maps in Fig. 3. The most caudal part (visual cortex) is thinnest while the rostro-medial cortex area around the motor cortex showed the largest thickness. Focusing on individual anatomical regions, their local absolute values also decrease with increasing age, indicating a continuing flattening of the cortex over time. This effect was found most pronounced in the most rostral end of the motor and somatosensory cortex regions, selected here for visualization (Fig. 3). As the whole brain still expands during the observation period, this cortical flattening largely counteracts the expected volume increase of the cortex.

T2- and DTI-derived contrast did not permit to discriminate the histologically defined cortical layer structure. Nevertheless, robust radial variation of fractional anisotropy contrast permitted a subdivision of the cortex into upper, central and lower cortical sections, as outlined in Fig. 4. Analysis of these three sections was performed for both FA and T2 parameters in the primary somatosensory cortex S1 and the motor cortex M1 as the anatomical regions of utmost interest (the results for S2 somatosensory cortex and barrel field cortex are presented in Inline Supplementary Fig. S2). A clear cortical depth dependent variation is observed for fractional anisotropy (Fig. 4 top diagrams), which was lost in the earlier analysis of the whole cortex as a single ROI (Fig. 1). This cortical depth dependent variation was noted irrespective of age within the first six months. The T2 values on the other hand did not reflect a section dependent variation (Fig. 4, bottom diagrams).

Inline Supplementary Fig. S2 can be found online at http://dx.doi.org/10.1016/j.neuroimage.2015.10.009.

Investigating T2 in the different cortical sections, using a multivariate ANOVA showed a significant effect of age in S1 and M1 ($V = 0.78$, $F(6,64) = 6.77$, $p < 0.001$). Post hoc pairwise comparisons (Tukey HSD) revealed highly significant differences between all age groups in the upper and central layers of M1 ($p < 0.01$) and between three weeks and the other ages in the lower layer. In S1, T2 was significantly decreasing after three weeks, followed by a gradual increase from eight weeks on. Despite this increase, T2 values did not reach the T2 values at weaning age at three weeks but stayed significantly below this three week value in the lower and central sections.

Fractional anisotropy (FA) seems to be more layer dependent than T2. While FA was decreasing in the upper and central layers over time, both in S1 and in M1, it remained unchanged in the lower layer for S1, but was even slightly increasing with age in M1. However, these observations did not reach statistical significance in a multivariate ANOVA (Pillai's trace: $V = 0.3$, $F(6, 62) = 1.82$, $p > 0.1$).

Myelin stained tissue sections showed an increase in the quantified staining intensity after the age of three weeks (Fig. 5). Further, a clear radial increase of staining intensity was noted from cortex surface towards the corpus callosum, independent of age group. ROIs corresponding to the cortical sections defined in the in vivo MRI were used to estimate the myelination intensity in these cortical sections as a

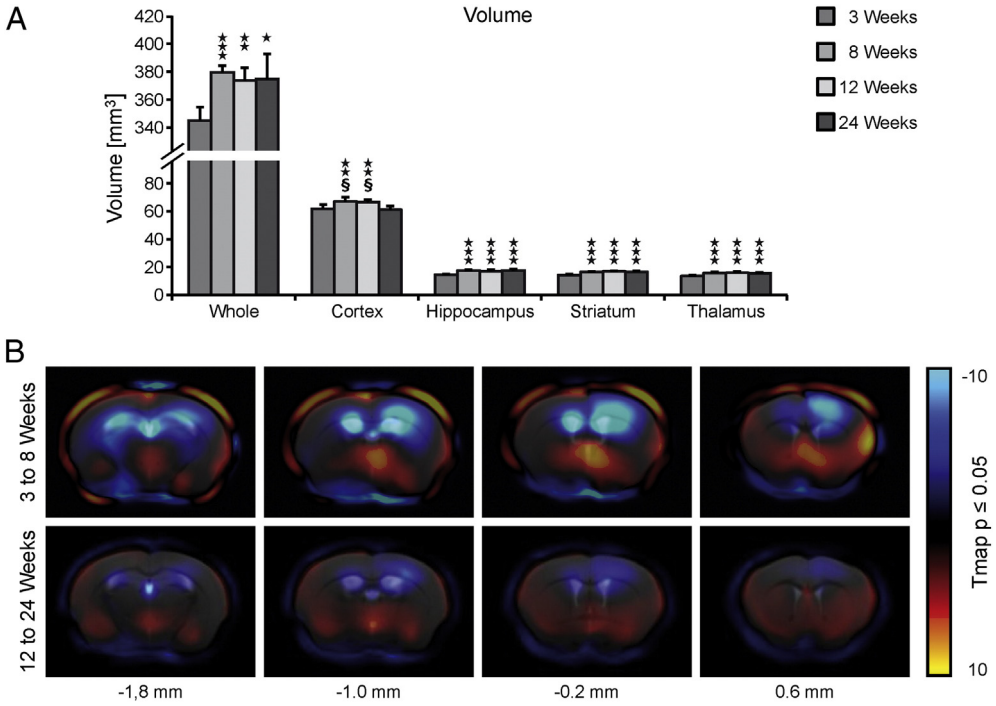

Fig. 2. Volume changes. Two different approaches to determine volume changes are shown here: ROI analysis (A) and deformation based morphometry (B). A: The mean volume of the different age groups is given for whole brain (as defined from cerebellum to olfactory bulb), cortex, hippocampus, striatum and thalamus (all four as defined by the ROIs in Inline Supplementary Fig. S1). Error bars show the standard error of the mean (SEM), significance levels are given corresponding to Fig. 1, here: difference to three weeks ($p < 0.05$ *; $p < 0.01$ **; $p < 0.001$ ***). B: T-maps superimposed onto the template brain. The T-maps depict the volume changes that are found significant in a t-test (with a p-value < 0.05) from three to eight weeks (upper row) and from twelve to twenty-four weeks (lower row). The T-values are color coded, with blue shades indicating a shrinkage in tissue and red shades representing a tissue expansion between the ages. Below, the position of the selected sections is given, relative to bregma.

function of age. This analysis revealed an effect of age for all three cortical sections (Pillai's trace: $V = 1.9$ $F(6,4) = 18.24$ $p < 0.01$). After three and again after eight weeks, the myelin content of the cortical layers increased substantially across all cortical layers. This observation holds for both S1 and M1.

Discussion

We have investigated the anatomic changes of the mouse brain during the first six months of age with the aim to discern developmental and maturation phases, thus identifying criteria of adult mouse brain. As we had reported in an earlier study on rat brain, maturation to a steady state "adult" situation of the brain takes much longer than sexual maturation. This distinction between developing/adolescent and adult brain is even more important in mice as they have become the most widely used species for a broad range of neuroscientific and neurological investigations, partly due to the easy access to transgenic animals. We realize that there are many aspects and corresponding variables to shape a complex picture of maturation. Among others there are neurotransmitter levels, receptor expressions or other molecular and cellular factors to be considered in further studies. Here, we have analyzed volume changes and structural alterations of the mouse brain using in vivo MRI. The use of different MRI modalities at high spatial resolution in combination with sophisticated image processing techniques make our approach sensitive for global and regional tissue growths, changes in laminar patterns and myelination in white and gray matter.

MRI parameter patterns of brain maturation

The combination of T2 and DTI contrasts has proven in the past to be highly sensitive for late developmental changes in the brain (Mengler et al., 2014). With increasing myelination and tightening of the myelin sheaths, T2 has been reported to decrease rapidly during the early postnatal phase, in rats as long as postnatal week eight (Wozniak and Lim, 2006). The T2 relaxation time continuously decreases from three weeks to twelve weeks, as observed in the present study, and is in agreement with earlier reports on T2 decrease (Hüppi and Dubois, 2006; Mengler et al., 2014; Samorajski and Rosten, 1973), caused predominantly by a reduction of tissue water content — further confirmed by decreasing proton density (Fig. 1) — and tissue reorganization processes. The increase of T2 between twelve and 24 weeks of age may indicate further late reorganization processes in the various anatomical ROIs (cf. Fig. 1) while in the case of the whole brain (Fig. 1) this only reflects the growing relative amount of free liquid in larger ventricles. Myelination and increasing cell density also contribute to the decrease of free water in the brain (Anderson et al., 2000; Chabert and Scifo, 2007) thus influencing T2 relaxation, as discussed in details in our earlier study on rat brain maturation (Mengler et al., 2014).

Fig. 3. Cortical thickness. A: the upper panel shows a lateral view onto the mouse brain, with the mean cortical thickness color coded on the surface, from left to right: three, eight, twelve and twenty-four weeks. The white line depicts the lateral thickness profile plotted in the diagram beneath. The mean cortical thickness is plotted from anterior to posterior for each of the four ages: three weeks (blue), eight weeks (red), twelve weeks (green), and twenty-four weeks (purple). B: mean cortical thickness from the anterior to posterior aspect of M1 and S1, respectively. The profile plotted, is showcased in the upper right corner of each graph. Instead of the standard deviation, the individual cortical thickness plots for M1 are illustrated in Supplementary Fig. 3 (Inline Supplementary Fig. S3).

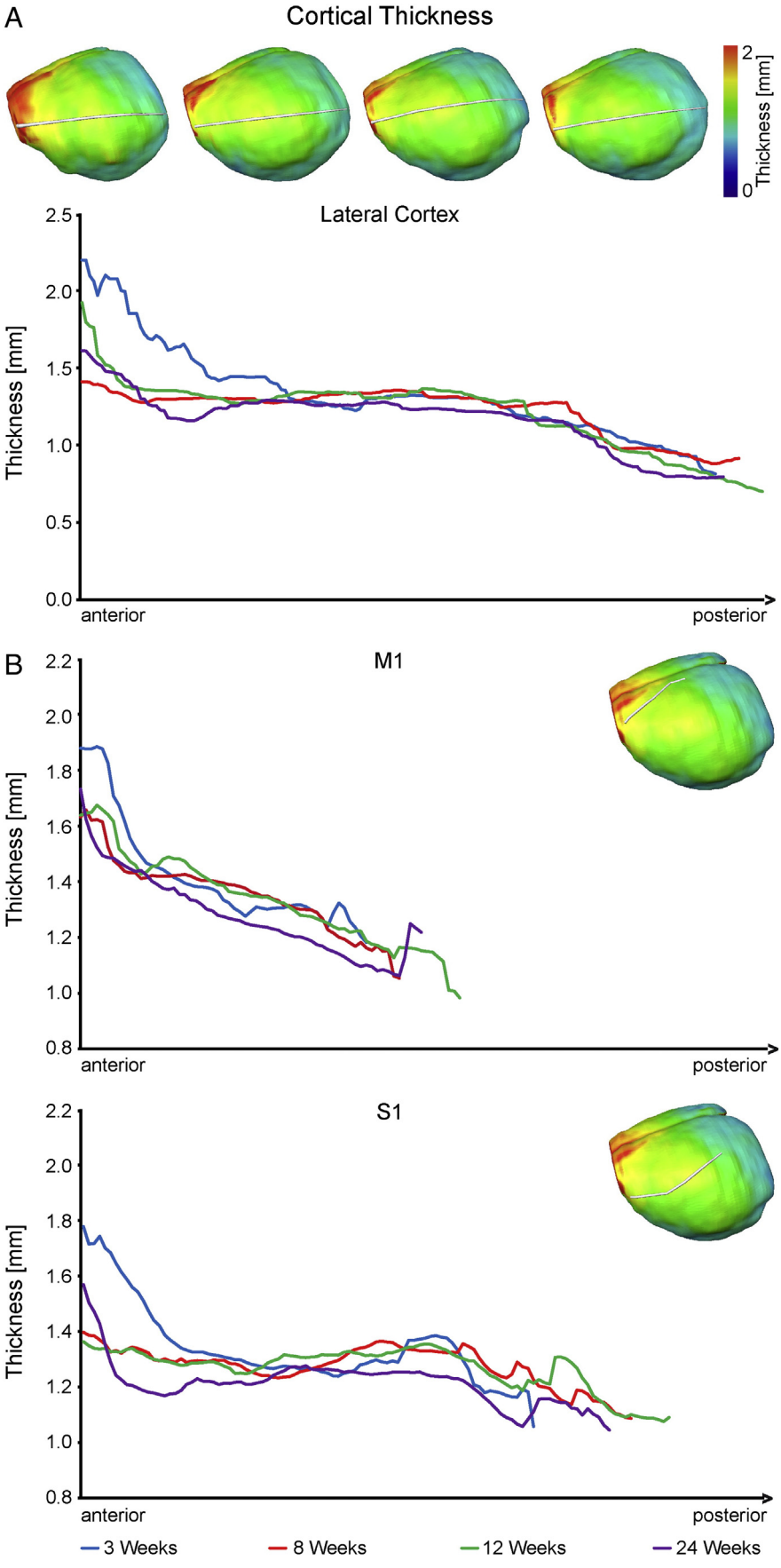
A
Cortical Thickness
2
0
Thickness [mm]
Lateral Cortex
Thickness [mm]
2.5
2.0
1.5
1.0
0.5
0.0
anterior
posterior
B
M1
Thickness [mm]
2.2
2.0
1.8
1.6
1.4
1.2
1.0
0.8
anterior
posterior
S1
Thickness [mm]
2.2
2.0
1.8
1.6
1.4
1.2
1.0
0.8
anterior
posterior
3 Weeks
8 Weeks
12 Weeks
24 Weeks

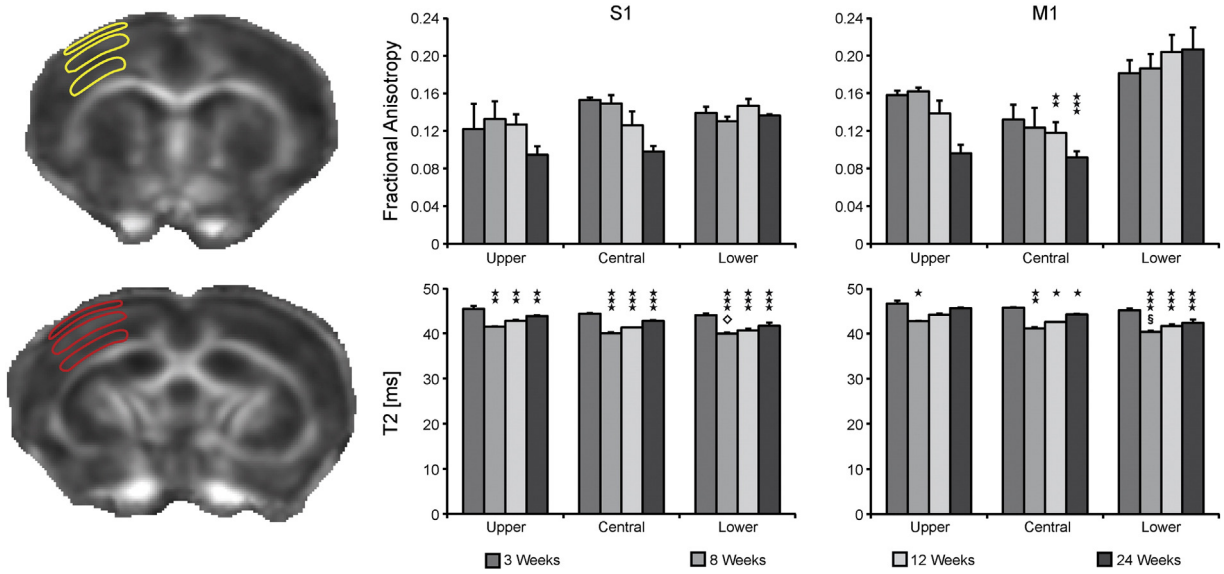

Fig. 4. MRI parameters in cortex layers. Left: FA maps of an eight week old mouse, superimposed with layer ROIs. For the sake of visibility, the ROIs do not represent the S1 or M1 ROIs but showcase the tangential position of the ROIs and their boundaries. Right: graphs show mean T2 and fractional anisotropy (FA) in S1 and M1 for the different age groups in the upper, central and lower cortex ROIs, as defined in the left panel. Error bars and significance levels are corresponding to Fig. 1.

Myelination changes are well reflected in diffusion tensor parameters (Mengler et al., 2014). As the axial diffusivity values are not changing over age for most anatomical ROIs in our results, changes of fractional anisotropy (FA) are due to changes in radial diffusivity values. Although our present findings are different from results on dysmyelination in the shiverer mouse (Tyszka et al., 2006), they are conclusive and in line with earlier reports on FA and RD development (Deo et al., 2006; Mengler et al., 2014; Song et al., 2002). FA therefore can be used as surrogate reflecting the preferential orientation of myelin structures in a tissue volume. In most white matter ROIs (all except fimbrium), FA continuously increased in agreement with growing intensity on the Black and Gold II staining of myelin (Fig. 5). Gray matter ROIs show a slight decrease of FA with age indicating that ongoing tissue organization processes of network formation in gray matter reduce structural preferential orientations with time. Of all gray matter ROIs, this effect is most pronounced in the cortex (Fig. 1), continuing still between twelve and 24 weeks.

Cortical changes during maturation

The histological staining clearly shows for the cortex a layer-dependent and region dependent pattern that must be distinguished in the discussion of age dependent myelination. In an earlier study, Sizonenko et al. (2007) had divided the cortex into upper and lower cortex regions and reported a drop in FA and an initial drop in T2 followed by a gradual increase. Here, we subdivided the sensorimotor cortex into upper, middle and lower cortex sections, thus adding more detail to the region-specific evaluation. The upper two of the three sections overlaid on the cortex in the MRI images show a continuous decrease of FA with age. The lowest section is closely age independent in the somatosensory cortex area (S1) but is continuously increasing in the motor cortex (M1) (Fig. 4). While myelin staining shows an increasing staining intensity, FA decrease reflects the fact that the predominant radial cortical structure is increasingly challenged by growing horizontal layer organizations. The latter development results in reduction of preferential direction organization of diffusion. The different behaviors of the lowest section in the somatosensory and motor cortices, respectively, indicate that different time lines must be considered for this structural reorganization process in different anatomical cortex regions. A corresponding behavior is documented for barrel cortex and secondary somatosensory cortex (S2) in the supplement (Inline Supplementary Fig. S2). Furthermore, it shows the necessity to subdivide the cortex in layers for MRI analysis so that layer-dependent changes are not averaged out (Fig. 4 and Inline Supplementary Fig. S2) (Baloch et al., 2009). Summarizing these observations, the interlaminar differences in myelination, observed with histology, are matched by a radial gradient in T2 and FA values at the approximate position of the histological central layers II/III and lower layers IV–V. While quite low but stable with time in layers IV–VI, directionality decreases over time in layer II/III. As interlayer connections get stronger and myelination increases, the radial organization is superposed and the tangential layers of the neocortex are revealed.

The cortex volume changes only marginally over the period three to 24 weeks, in contrast to the situation in rats where cortical volume kept increasing during the first three months (Mengler et al., 2014). Cortical thickness in rats increases during the first month, but then stagnates. In mice, we have observed a gradual cortex thickness decrease from rostral to caudal (Fig. 3), independent of age. With growing age, this thickness is decreasing in all positions along the rostral–caudal line, but this age dependent decrease is most pronounced at the rostral end. In general, there is a global tendency to level out this thickness gradient along the rostral–caudal line with increasing age. Thus, the cortex volume of mice remains closely constant from three weeks as the continuing thickness decrease compensates for the brain volume increase with age. In rats, the continuing cortex volume increase is explained by brain expansion paralleled by thickness stabilization after four weeks of age.

Consequences for age determination of a fully matured mouse brain

From the present findings, it becomes clear that one needs to carefully choose the desired variable to define a stable condition, which is no longer varied by increasing age. Cortex volume appears not to be a sensitive parameter, while cortical thickness is more suitable: the most drastic decrease occurs during the first eight to twelve weeks, after which time only slight changes are noted. Also, the MRI parameters, T2 and FA, generally show their most pronounced changes during the first two to three months. When using myelination as maturation criteria, very pronounced increases were observed till twelve weeks of age, with only minor changes thereafter.

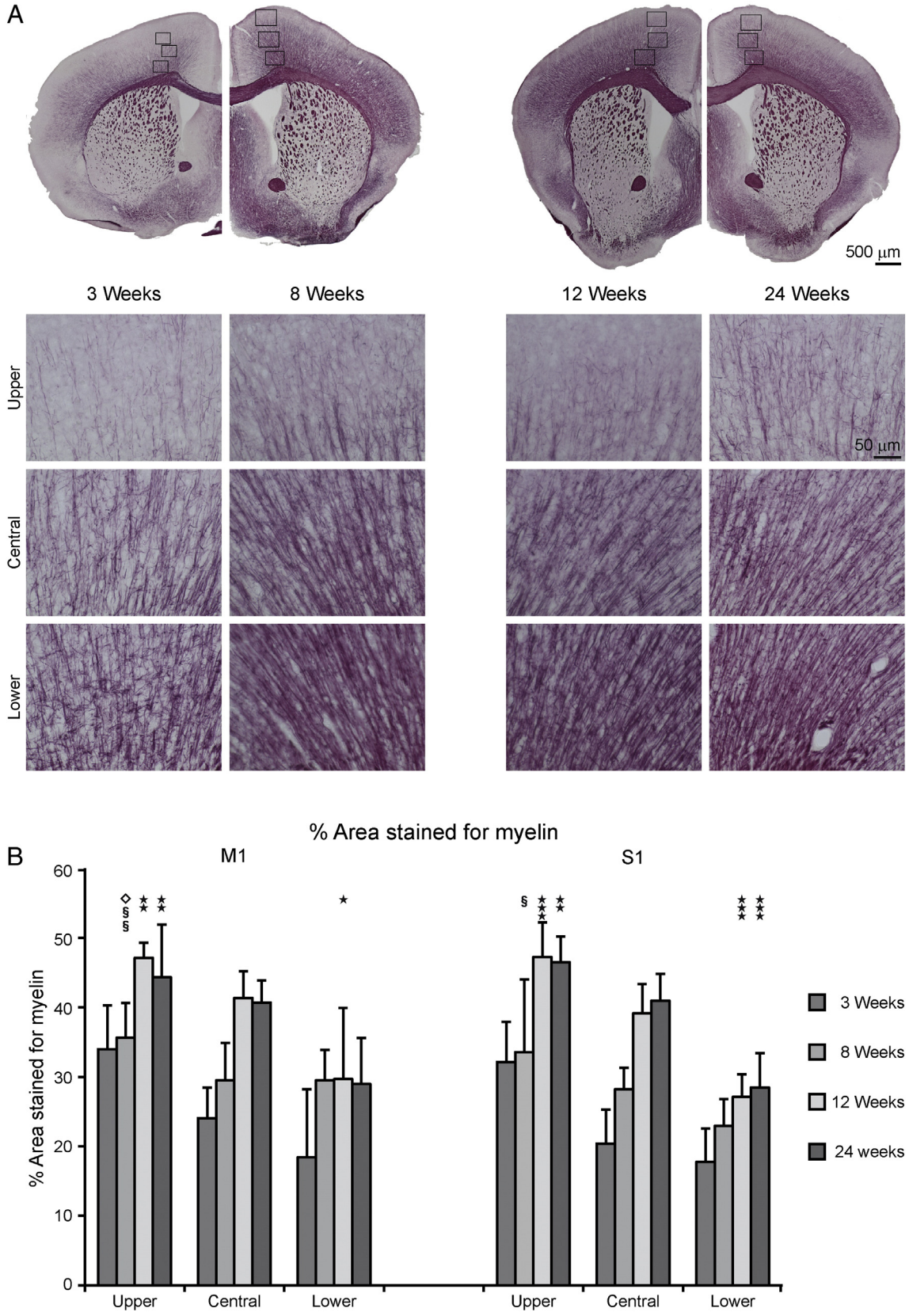

Fig. 5. Myelin content in cortex layers. A: representative myelin staining from a three, eight, twelve and twenty-four week old mouse. The upper row shows an overview of one hemisphere (4× magnification) for every age. Close-ups from the indicated positions were taken with 40× magnification in the upper, central and lower cortices. Shown here are ROIs in M1. B: quantification of myelin content in upper, central and lower M1 and S1, given by the percentage of myelin stained area. Error bars and significance levels are corresponding to Fig. 1.

Taken these different criteria together, it appears best to define the period up to month three as adolescent with clear maturation dependent alterations. From three months of age, with only very small further changes observed, beginning adulthood of the mouse brain may be considered. This distinction is of importance as many studies on cerebral diseases are based on the assumption of dealing with adult animals as analysis of disease development should not be modulated by ongoing maturation processes. From our present results, it appears advisable to prefer mice of three months of age or even older when stable, adult brains as baseline must be demanded.

Conclusions

We have followed various anatomic changes and tissue characterization by MRI parameters as well as myelination as a function of brain age in the mouse. Our results clearly indicate that the adolescent phase with ongoing changes in the brain lasts at least till three months of age. For the large number of studies involving mouse brains for genetic investigations with transgenic animals or for neurological disease studies, mice should be used at the age of three months or later when adult animals are required. However, it must be cautioned that our various applied metrics show different behaviors with some reaching stabilization earlier than others. Thus, the relevance of the chosen metric in future studies will influence the choice of age window for stable brain conditions.

Acknowledgments

We thank Melanie Nelles and Michael Diedenhofen from the Max Planck Institute for Metabolism Research for technical support and Ulla Uhlenküken for the professional preparation of figures. This research was supported by grants from the FP7 European Union program TargetBraIn (LH: HEALTH-F2-2012-279017), BrainPath (AK; MH: PIAPP-GA-2013-612360), and GlowBrain (SS: REGPOT-2012-CT2012-316120).

References

Adamczak, J., Schneider, G., Nelles, M., Que, I., Suidgeest, E., van der Weerd, L., Löwik, C., Hoehn, M., 2014. In vivo bioluminescence imaging of vascular remodeling after stroke. Front. Cell. Neurosci. 8 (Article 274).

Andersen, S.L., 2003. Trajectories of brain development: point of vulnerability or window of opportunity? Neurosci. Biobehav. Rev. 27, 3–18.

Anderson, A.W., Xie, J., Pizzonia, J., Bronen, R.A., Spencer, D.D., Gore, J.C., 2000. Effects of cell volume fraction changes on apparent diffusion in human cells. Magn. Reson. Imaging 18, 689–695.

Baloch, S., Verma, R., Huang, H., Khurd, P., Clark, S., Yarowsky, P., Abel, T., Mori, S., Davatzikos, C., 2009. Quantification of brain maturation and growth patterns in C57BL/6J mice via computational neuroanatomy of diffusion tensor images. Cereb. Cortex 19, 675–687.

Basser, P.J., Mattiello, J., Lebihan, D., 1994. Estimation of the effective self-diffusion tensor from the NMR spin-echo. J. Magn. Reson. Ser. B 103, 247–254.

Bockhorst, K.H., Narayana, P.A., Liu, R., Vijjula, P.A., Ramu, J., Kamel, M., Wosik, J., Bockhorst, T., Hahn, K., Hasan, K.M., Perez-Polo, J.R., 2008. Early postnatal development of rat brain: in vivo diffusion tensor imaging. J. Neurosci. Res. 86, 1520–1528.

Chabert, S., Scifo, P., 2007. Diffusion signal in magnetic resonance imaging: origin and interpretation in neurosciences. Biol. Res. 40, 385–400.

Deo, A.A., Grill, R.J., Hasan, K.M., Narayama, P.A., 2006. In vivo serial diffusion tensor imaging of experimental spinal cord injury. J. Neurosci. Res. 83, 801–810.

Franklin, K.B.L.P.G. (Ed.), 2007. The Mouse Brain in Stereotaxic Coordinates, 3rd ed. Elsevier Academic Press, San Diego, CA.

Hüppi, P.S., Dubois, J., 2006. Diffusion tensor imaging of brain development. Semin. Fetal Neonatal Med. 11, 489–497.

Jones, D.K., Horsfield, M.A., Simmons, A., 1999. Optimal strategies for measuring diffusion in anisotropic systems by magnetic resonance imaging. Magn. Reson. Med. 42, 515–525.

Khmelinskii, A., Mengler, L., Kitslaar, P., Staring, M., Hoehn, M., Lelieveldt, B.P.F., 2013. A visualization platform for high-throughput, follow-up, co-registered multi-contrast MRI rat brain data. Medical Imaging 2013: Biomedical Applications in Molecular, Structural, and Functional Imagingp. 8672.

Klein, S., Staring, M., Murphy, K., Viergever, M.A., Pluim, J.P.W., 2010. elastix: a toolbox for intensity-based medical image registration. IEEE Trans. Med. Imaging 29, 196–205.

Leow, A.D., Klunder, A.D., Jack, C.R., Toga, A.W., Dale, A.M., Bernstein, M.A., Britson, P.J., Gunter, J.L., Ward, C.P., Whitwell, J.L., Borowski, B.J., Fleisher, A.S., Fox, N.C., Harvey, D., Kornak, J., Schuff, N., Studholme, C., Alexander, G.E., Weiner, M.W., Thompson, P.M., 2006. Longitudinal stability of MRI for mapping brain change using tensor-based morphometry. NeuroImage 31, 627–640.

Meaney, M.J., Stewart, J., 1981. A descriptive study of social development in the rat (*Rattus norvegicus*). Anim. Behav. 29, 34–45.

Mengler, L., Khmelinskii, A., Diedenhofen, M., Po, C., Staring, M., Lelieveldt, B.P., Hoehn, M., 2014. Brain maturation of the adolescent rat cortex and striatum: changes in volume and myelination. NeuroImage 84, 35–44.

Mori, S., Itoh, R., Zhang, J.Y., Kaufmann, W.E., van Zijl, P.C.M., Solaiyappan, M., Yarowsky, P., 2001. Diffusion tensor imaging of the developing mouse brain. Magn. Reson. Med. 46, 18–23.

Paxinos, G., Franklin, K.B., 2001. The Mouse Brain in Stereotaxic Coordinates. Academic Press.

Samorajski, T., Rosten, C., 1973. Age and regional differences in the chemical composition of brains of mice, monkeys and humans. Progress in Brain Research: Neurobiological Aspects of Maturation and Aging. Elsevier, pp. 253–265.

Schmued, L., Bowyer, J., Cozart, M., Heard, D., Binienda, Z., Paule, M., 2008. Introducing Black-Gold II, a highly soluble gold phosphate complex with several unique advantages for the histochemical localization of myelin. Brain Res. 1229, 210–217.

Sizonenko, S.P.V., Camm, E.J., Garbow, J.R., Maier, S.E., Inder, T.E., Williams, C.E., Neil, J.J., Huppi, P.S., 2007. Developmental changes and injury induced disruption of the radial organization of the cortex in the immature rat brain revealed by in vivo diffusion tensor MRI. Cereb. Cortex 17, 2609–2617.

Skare, S., Hedehus, M., Moseley, M.E., Li, T.Q., 2000. Condition number as a measure of noise performance of diffusion tensor data acquisition schemes with MRI. J. Magn. Reson. 147, 340–352.

Smith, S.M., 2002. Fast robust automated brain extraction. Hum. Brain Mapp. 17, 143–155.

Song, S.K., Sun, S.W., Ramsbottom, M.J., Chang, C., Russell, J., Cross, A.H., 2002. Dysmyelination revealed through MRI as increased radial (but unchanged axial) diffusion of water. NeuroImage 17, 1429–1436.

Spear, L.P., Brake, S.C., 1983. Periadolescence: age-dependent behavior and psychopharmacological responsivity in rats. Dev. Psychobiol. 16, 83–109.

Tissir, F., Goffinet, A.M., 2003. Reelin and brain development. Nat. Rev. Neurosci. 4, 496–505.

Tyszka, J.M., Readhead, C., Bearer, E.L., Pautler, R.G., Jacobs, R.E., 2006. Statistical diffusion tensor histology reveals regional dysmyelination effects in the shiverer mouse mutant. NeuroImage 29, 1058–1065.

van Dorsten, F.A., Hata, R., Maeda, K., Franke, C., Eis, M., Hossmann, K.-A., Hoehn, M., 1999. Diffusion- and perfusion-weighted MR imaging of transient focal cerebral ischaemia in mice. NMR Biomed. 12, 525–534.

Webster, S.J., Van Eldik, L.J., Watterson, D.M., Bachstetter, A.D., 2015. Closed head injury in an age-related Alzheimer mouse model leads to an altered neuroinflammatory response and persistent cognitive impairment. J. Neurosci. 35, 6554–6569.

Wozniak, J.R., Lim, K.O., 2006. Advances in white matter imaging: a review of in vivo magnetic resonance methodologies and their applicability to the study of development and aging. Neurosci. Biobehav. Rev. 30, 762–774.

Yanovsky, I., Thompson, P.M., Osher, S., Leow, A.D., 2008. Asymmetric and symmetric unbiased image registration: statistical assessment of performance. 2008 IEEE Computer Society Conference on Computer Vision and Pattern Recognition Workshops, pp. 1–3.

Zempel, H., Mandelkow, E., 2014. Lost after translation: missorting of tau protein and consequences for Alzheimer disease. Trends Neurosci. 37, 721–732.

Zhang, J.Y., Richards, L.J., Yarowsky, P., Huang, H., van Zijl, P.C.M., Mori, S., 2003. Three-dimensional anatomical characterization of the developing mouse brain by diffusion tensor microimaging. NeuroImage 20, 1639–1648.

Zhang, J.Y., Miller, M.I., Plachez, C., Richards, L.J., Yarowsky, P., van Zijl, P., Mori, S., 2005. Mapping postnatal mouse brain development with diffusion tensor microimaging. NeuroImage 26, 1042–1051.

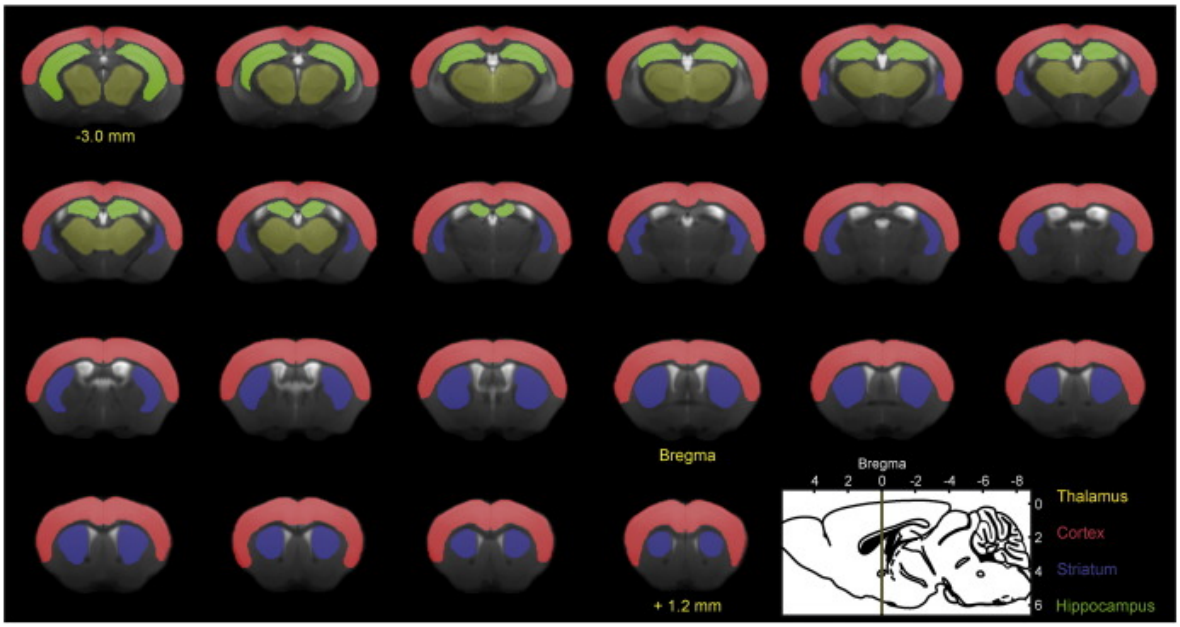

Inline Supplementary Figure S1

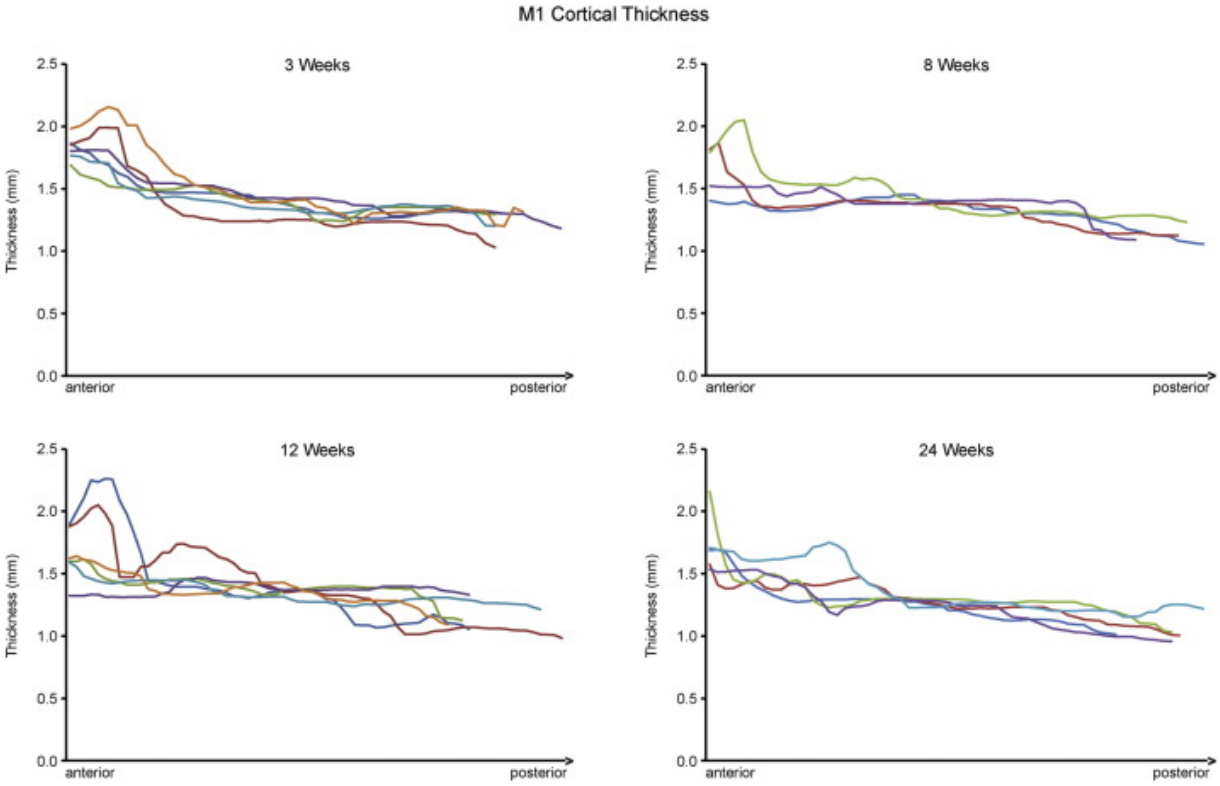

Inline Supplementary Figure S2

-

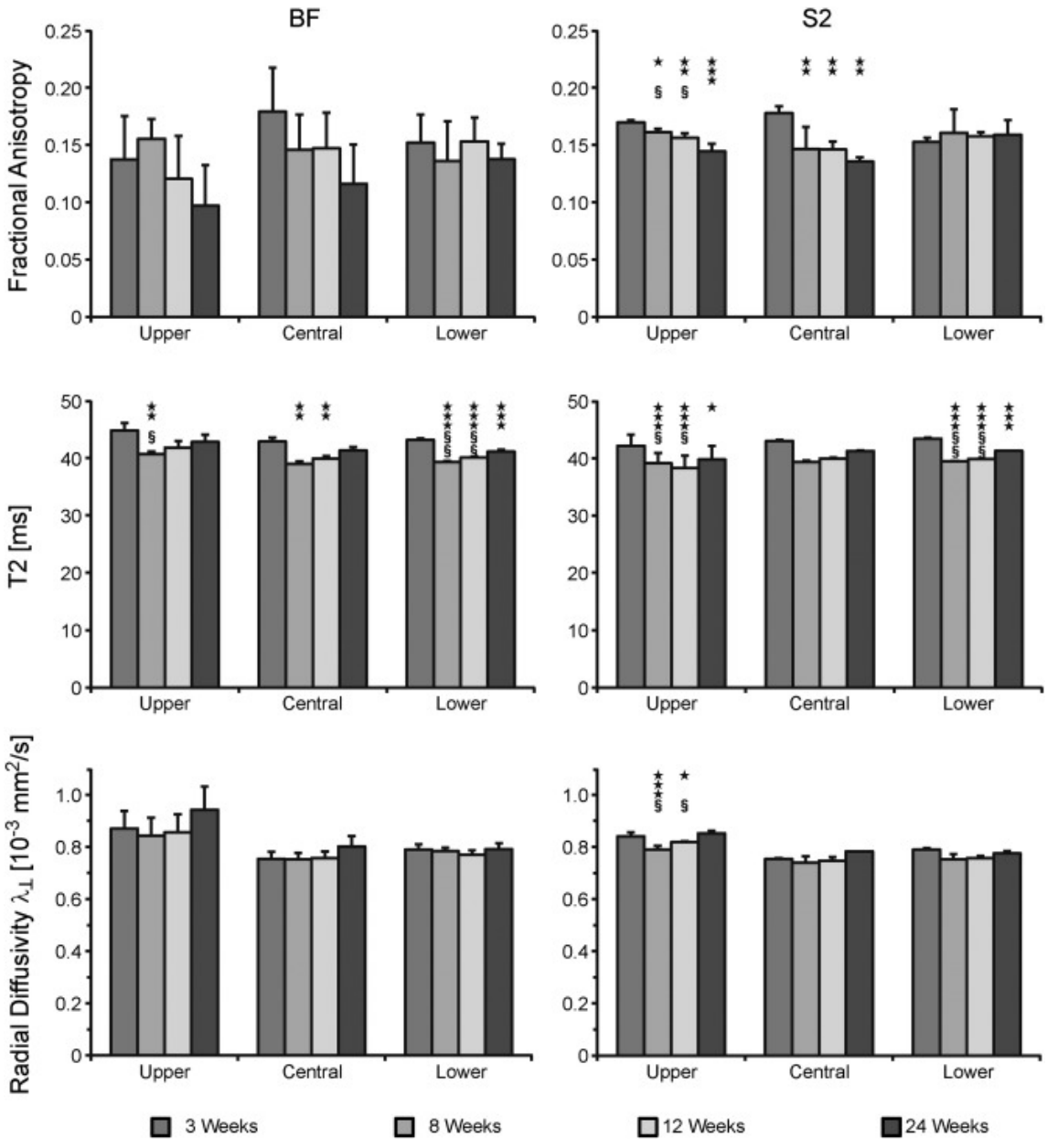

Inline Supplementary Figure S3

Publication IV – Brain Ageing in Rat

Healthy ageing: a functional and structural profile of the rat brain

Luam Hammelrath, Artem Khmelinskii, Chrystelle Po, Eberhardt Pracht, Dirk Wiedermann, Heike Endepols, Cordula Schäfer, Marius Staring, Boudewijn P.F. Lelieveldt, Mathias Hoehn

in preparation

Healthy ageing: a functional and structural profile of the rat brain

Luam Hammelrath[a], Artem Khmelinskii[c,d], Chrystelle Po[a] *, Eberhard Pracht[a,e], Dirk Wiedermann[a], Heike Endepols[b,f], Cordula Schäfer[a], Marius Staring[c], B.F Lelieveldt[c,g] and Mathias Hoehn[a,c,d]

Max Planck Institute for Neurological Research, [a]In-vivo-NMR Laboratory and [b]Multimodal Imaging, Cologne, Germany

[c] Division of Image Processing, Dept. of Radiology, Leiden University Medical Center, Leiden, The Netherlands

[d] Percuros B.V., Enschede, the Netherlands

[e] DZNE German Centre for Neurodegenerative Diseases, Bonn, Germany

[f] Institute of Radiochemistry and Experimental Molecular Imaging, University Hospital of Cologne, Cologne, Germany

[g] Dept. of Intelligent Systems, Delft University of Technology, Delft, the Netherlands

[*] FMTS, ICube, CNRS, Université de Strasbourg, France

Keywords: MRI, age, development, fMRI, rat, DTI, DBM, lifespan, vessel density

to be submitted to: Neurobiology of ageing

Correspondence to:

Prof. Dr. Mathias Hoehn
In-vivo-NMR Laboratory
Max Planck Institute for Metabolism Research
Gleuelerstrasse 50
D-50931 Köln, Germany
Phone: +49-221-4726-315
Fax: +49-221-4726-337
Email: mathias@sf.mpg.de

Abstract

We conducted a lifespan study on rats monitoring healthy ageing of the brain. Calorie restricted rats were employed repetitively up to the age of 24 months using non-invasive imaging techniques. We investigated the effect of age on structural (Diffusion Tensor Imaging, T2) as well as functional (fMRI) and vascular (angiographies) integrity. This explorative study like this benefits from an automated evaluation technique that is based on individual structural changes rather than manual ROI analysis. For this purpose, we used deformation-based morphometry to address volumetric changes in the brain.

We found a rather gradual change with different pacing in the MR parameters and between the major grey matter structures of the brain. While general and regional volume decrease appears to happen consistently between 18 and 20 months. The fMRI signal as well as the angioarchitecture strengthened until the age of 12 month and showed signal decrease and vascular deterioration, but stable vessel density until 24 months. Dependent on the study purpose, the different time frames for ageing onset should be considered. A study on vascular or functional changes needs to anticipate age-related changes already with 12 months, while focussing on the structural and volumetric changes in the brain, will reveal an ageing phenotype not before an age of 20 months.

1. Introduction

Demographic change is challenging economic and medical systems as well as science. A lot has been done in the last decades to understand ageing processes, from telomeres to oxidative stress damage, from *C. elegans* to transgenic mice strains. And many of the insights hold therapeutic potential for a prolonged health span. Especially therapies intervening with the IGF-1 pathway and the somatotropic axis are promising candidates, modulating the insulin metabolism and prolonging both life and health span [1].

Extensive cross-sectional and follow-up studies in humans have and still are building up a standard, including biomarkers for neurodegenerative diseases. A comparable ageing reference is not established in rodents. In particular a temporal profile of translational relevant parameters is needed, in order to judge the true clinical potential of tested therapies (compare [2]). A highly translational tool is Magnetic resonance imaging (MRI). MRI has become an indispensible tool for clinical neurodiagnostics and with higher field strengths, stronger gradients and increasing resolution also for translational research. MRI is non-invasive, provides high resolution and lacks histological artifacts, like shearing or shrinking, allowing for longitudinal anatomical studies.

Until now, MR studies on ageing rats are sparse and limited to longitudinal studies on pathological phenotypes (alcohol-preferring rat [3]) or mice [4].

We conducted a lifespan study on Wistar rats in order to establish an age reference for the most widely used imaging techniques. Based on structural MRI and histological validation, we could already show brain development to continue well after three months of age [5]. Here we investigated the effect of age on structural (Diffusion Tensor Imaging, T2) and volumetric measures (deformation based morphometry (DBM)) as well as functional and vascular integrity.

2. Materials and Methods

2.1 Animal husbandry

All animal experiments were conducted in accordance with the German Animal Welfare Act and approved by the local authorities (Landesamt für Naturschutz, Umwelt und Verbraucherschutz NRW). From postnatal day 21 on (weaning age) twelve male Wistar rats (Harlan-Winkelmann GmbH, Borchen, Germany) were kept in an environment with controlled temperature (21+/- 1°C), humidity (55%+/-10%), and light (12/12h dark/light cycle). Animals were housed in groups of four until the age of two months, and in pairs afterwards; in cages equipped with bedding, nesting material, paper, wooden blocks, a tunnel, a hideout with exploration platform and unlimited access to water. From the age of eight weeks, rats were

calorie restricted to 80% of their ad libitum consumption. Somatosensory performance was assessed every eight weeks, to ensure the health of the animals. Tests included a neurological score for general reflexes and outer appearance (Table 1), motor performance (Rotarod) and somatosensory tests for asymmetry in forepaw use (cylinder).

2.2 Animal groups

Animals were divided into three separate groups, with ages different for study entry (2 and 8 months) and survival (12, 18 and 24 months, see Fig. 1). This interleaved study design can exclude effects of repetitive anaesthesia (different entry ages) and allows histological evaluation of the tissue (survival time). Three animals had to be excluded in the course of the study due to spontaneous tumour formation (n=2 at the age of 12m and 20m), one died under anaesthesia (22m, n=1). All animals underwent structural MRI scans on a bimonthly basis, fMRI with 2 months, as a young adult control time point, and at 10, 16 and 24months.

2.3 Magnetic Resonance Imaging

MRI experiments were conducted on an 11.7T Bruker BioSpec horizontal bore dedicated animal scanner (Bruker Biospin, Ettlingen, Germany). RF transmission was achieved with a quadrature volume resonator (inner diameter 72mm), while a quadrature rat brain surface coil (~30mm x 30mm) was used for signal reception. Rats were placed in an MRI compatible cradle, and the head was fixed with earbars and a support ring for the upper incisors in order to reduce movement artefacts.

Animals were anesthetized with 2% isoflurane (Forane, Baxter, Deerfield, IL, USA) in a 70/30 mixture of N_2O and O_2, and vital functions were monitored during the whole anesthesia period using DASYLab (version 9.0, Measurement Computing Cooperation, Norton, MA, USA). The breathing rate was assessed via a pressure pad, placed under the thorax, and kept at 70-80 breaths/minute by adjusting the isoflurane concentration. Body temperature was recorded with a rectal temperature probe, and regulated by a feedback system (set value: 37°C) controlling a heating blanket with warm circulating water (MedRes, Cologne, Germany).

Both scan protocols, T2WI and DTI, were set to cover the volume between the rhinal fissure (rostrally) and the anterior part of the cerebellum (caudally) and were acquired with identical geometry (field of view: 28mm x 28mm, matrix 192 x 192, 0.5 mm slice thickness, no interslice gaps). The number of slices was adjusted individually in every session.

Quantitative T2 maps were acquired using a Multi Slice Multi Echo sequence (MSME; TR/TE=5,000ms/10ms; 10 echoes). For every voxel a monoexponential decay curve was extrapolated from the ten multi-echo trains of the MSME (IDL version 6.4, Boulder, CO,

USA), the resulting spin-spin relaxation curve yields the quantitative T2 map (t until 37% decay) and the proton density (S at TE=0ms).

Diffusion Tensor Imaging was recorded with an 8-shot spin echo EPI sequence (30 directions; b-value=670 s/mm^2, and five supplementary A0 images), with a gradient scheme according to Jones 30 [6, 7]. DTI data, in general is prone to distortions due to eddy currents, induced when strong gradient pulses are switched on and off, and to motion artefacts, originating from the subject. Prior to tensor calculation (DTI Studio 3.0.3, Baltimore, MD, USA), we therefore applied an eddy current correction (FSL version 4.1.7, FMRIB Centre, Oxford, UK) and visually inspected the single frames, discarding the corrupted ones. The occurrence of other distortions and artefacts was limited during image acquisition by applying an automatic ghost correction (ghostings), the use of a fat suppression module (1.9ms Gaussian pulse, 1400Hz bandwidth, 2ms spoiler) (off resonance artefacts) and navigator echoes.

2.3 Data post processing

A study-specific template brain was created from datasets of fourteen months old Wistar rats (n=12). We chose an "aged" template brain, reflecting the actual data better than a young "standard" template brain (usually three months). By reducing the necessary transformation of the data, possible registration mistakes are minimised. The TurboRARE sequence, used for the generation of the rat brain template, used a TR/TEeff = 4,000ms/32.5ms and a RARE factor of eight. Two averages were recorded with a field of view 28mm × 28mm (matrix 192 × 192) and 0.5mm slice thickness. Volumes of interest (VOI) were manually created for key grey matter structures: hippocampus, striatum, cortex and thalamus.

Registration was conducted in a coarse-to-fine manner, using normalized cross-correlation as similarity measure. Three discrete registration steps, with increasing degrees of freedom were implemented (rigid, affine, non linear B-spline), in order to normalize the images to a common space. The first echo of the MSME served as source; the template brain as target volume. Registration followed a hierarchical scheme, employing a Gaussian pyramid on every level (four in the rigid and affine, two in the B-spline part), in order to avoid local minima traps. The resulting deformation fields were applied to the corresponding T2- and DTI-maps.

Datasets were registered between ages of a subject, as well as individually to the template. The latter allowed the evaluation of the VOIs individually for every age and subject, both in terms of MR parameters and volume. The step-by-step registration yields incremental volumetric information, for each age-step can be assigned to a deformation field. The

logarithmic transform of the deformation fields (the determinant of the Jacobian matrix) was employed in order to examine local volume changes [8, 9].

2.4 Angiography

MR angiographies visualize the architecture of the major blood vessels and can reveal anomalies, clotting or injuries. One angiography sequence was implemented in order to image all major vessels (FLASH 2-D TOF TE=2ms, TR=15 ms, FOV 40mm x40mm, matrix 256 x 256, slice thickness of 0.4mm, flip angle of 80°). By adding a saturation band over the neck of the animals, all signal flowing into the brain, i.e. the arterial contribution to the signal, is deleted. This second sequence was used in order to image mainly the cerebral veins. The combination of the two sequences allows the non-invasive assessment of both arteries and veins longitudinally without the use of contrast agents.

2.5 Functional MRI

After an initial anaesthesia with isoflurane, the animals were positioned in the scanner, as stated above. Additionally, two pairs of needle electrodes were inserted into both forepaws and a subcutaneous infusion was placed for anaesthesia delivery.

The detailed anaesthesia protocol was described previously and shall only briefly be repeated here [10, 11]. A bolus of medetomidine (0.05ml/kg bodyweight; Domitor®, Pfizer, Berlin, Germany) was administered subcutaneously. Isoflurane was slowly reduced and discontinued while N2O was exchanged for N2. To allow for stabilization of the physiological conditions, fMRI acquisition and continuous infusion of medetomidine solution (0.1 ml/kg bodyweight/h in saline solution) were not started until 20 min after bolus injection. After completion of the fMRI experiments, atipamezol (1 ml/kg body weight; Antisedan®, Pfizer, Berlin, Germany) was injected subcutaneously with 2 ml of saline solution to reverse the sedative effect and to substitute for fluid loss during the experiment.

BOLD fMRI was recorded using a spin-echo EPI sequence (TE= 17.5ms; TR=3,000ms; FOV 28.8x28.8 mm, Matrix 96x96, with 1.2mm slice thickness). Electrical forepaw stimulation was achieved with rectangular pulses (3mA, 6Hz, 0.3ms, in house built stimulation unit), the paradigm consisted of five blocks (45s resting and 15s stimulation period) with a supplementary 45s resting period at the end, adding up to 115 repetitions and an acquisition time of 5min and 45s. A set of three fMRI scans was collected for the right and left paw, respectively, and for anatomical reference a supplementary structural sequence (TurboRARE) was acquired.

The fast fMRI sequences are prone to motion artefacts. Therefore all datasets were therefore motion corrected (FSL) prior to statistical evaluation. Motion correction was applied

separately for each slice and was restricted to in-plane translations and rotations. The BOLD percent change was calculated voxel-wise, using a Student's t-test (details see [11, 12]).
The anatomical reference was registered to the template brain. The relative position of the fMRI sequence to the anatomical template combined with the transformation matrix resulting from the registration procedure, allows assigning fMRI cluster to predefined brain regions (s. VOIs above). A cluster was defined as a group of at least fifteen adjacent voxels in any dimension (stretching in-plane and contiguous MR image slides) with a p-value of 0.01 or better. Thus, a conservative and robust selection of the correct activated region was assured. All functional postprocessing was automated in a Python pipeline, guaranteeing an unbiased ROI selection.

2.6 Histology

At designated ages, brains were perfused with PBS and 4% PFA. The brains were extracted and postfixed overnight in PFA, followed by incubation in 30% sucrose solution. Tissue sections of 40µm were cut (Microtome, Leica Microsystems, Wetzlar, Germany) and preserved at -20°C. Sections at four selected levels were stained for blood vessels and astrocytes using RECA (Serotec Rat Endothelial Cell Antibody + biotinylated secondary + streptavidin conjured Alexa488) and GFAP antibodies. Vessel density was calculated for different anatomical structures, according to the procedure described by Wu et al. [13]. ROIs for cortex, striatum and thalamus were positioned both in the left and right hemisphere and on four, two and two consecutive sections respectively (Keyence BZ-9000, Keyence Corp., Neu-Isenburg, Germany). ROI analysis was performed using ImageJ software (version 1.46r, NIH, Bethesda, MD, USA).

2.7 Statistics

Due to the interleaved study design, statistical evaluation of the MRI data was performed with a mixed models approach using the maximum likelihood model (SPSS version 22, IBM Corp. Armonk, NY, USA). The different group sizes (heterogeneous variances) were accounted for by a heterogeneous, autoregressive covariate structure. Post-hoc pairwise comparisons were Bonferroni corrected. Histological quantification was statistically evaluated using a univariate analysis of variances (ANOVA). Regression maps of brain volume changes were calculated using SPM 8 (UCL, London; UK) with Matlab 2011b (Mathworks Inc, Natick, MA, USA).

3. Results

3.1 Health status

Over the course of the study the bodyweight stayed in a healthy range, not exceeding 450g (see Fig2) and the behavioural and neurological scoring did not reveal any sensorimotor deficits (Table 2). We can therefore assume the rats in this study to be healthy.

3.2 Structural and volumetric ageing profiles

Structural MR datasets were evaluated for quantitative MR parameters as well as volume changes.

ROI analysis revealed a significant effect of age upon the volume of cortex ($F(8, 46) = 5.8$, $p<0.001$), striatum ($F(8, 43) = 2.9$, $p<0.011$), hippocampus ($F(8, 37) = 3.22$, $p<0.01$) and whole brain ($F(8, 31)= 2.85$, $p<0.05$) (Fig.3). Post-hoc pair-wise comparisons however, could only show the cortical volume at 24 months to be significantly reduced compared to the other ages. In the whole brain, a trend is visible separating the ages from 8m to 14m and from 16m to 24m. Deformation-based morphometry detected the volume decrease to localize at the lateral cortex in level with the ear canals. A volume increase can be in the thalamus and next to the lateral ventricles (Fig. 4).

T2 values are decreasing with age all over the brain; this effect reaches statistical significance in the cortex ($F(8, 15) = 20.1$, $p<0.001$), striatum ($F(8, 17) = 20.1$, $p<0.001$) and thalamus ($F(8, 19) = 9.7$, $p<0.001$) (Fig. 5). Fractional anisotropy shows a gradual increase over time, which is statistically significant in all grey matter regions analysed (ctx: $F(8, 19)= 5.9$, $p<0.001$; cpu: $F(8, 18) = 3.1$, $p<0.05$; hip: $F(8, 19) = 2.7$, $p< 0.05$, thal: $F(8, 18) = 4.2$, $p<0.01$) (for Hippocampus see Suppl. Fig 1, thalamus Suppl. Fig. 2 and whole brain Suppl. Fig. 3).

Other diffusion derived parameters, like radial diffusivity (RD) and Tensor Trace (TT) show a decline with age only in the cortex (RD: $F(8, 19)= 2.9$, $p<0.05$; TT: $F(8, 21) = 3.14$, $p<0.05$) and across the whole brain (RD: $F(8, 14) = 3.14$, $p>0.028$; TT: $F(8, 15) = 3.46$, $p<0.05$).

Additionally, a significant difference between the age of 24m and the younger ages was apparent in the post-hoc pairwise analysis of T2 and FA in the cortex.

3.3 Functional ageing profiles

The BOLD fMRI signal intensity in the contralateral S1 somatosensory cortex is increasing between the ages of two and ten months and is decreasing slowly with further ageing of the animals. Simultaneously the activated area of the representation field becomes increasingly focussed with time, with the cluster size reducing from about 1,000 pixels to a mere 500 pixel

in two year old animals ($F(3, 8) = 4.91$, $p > 0.05$, Fig 6b). The negative BOLD signal of the ipsi- and contralateral striatum exhibits a corresponding pattern over time, with the strongest negative BOLD at 10 months. Simultaneously, the spatial extent of the signal is increasing in the young ($F(3, 5) = 6.18$, $p<0.05$). Additionally, we could observe a difference in negative BOLD incidence, while a strong negative BOLD is always found in the young, we found the cluster size as well as its occurrence strongly reduced after 10m, with many sessions not revealing any striatal BOLD signal (Fig.6b).

3.4 Blood supply

Cerebral blood vessels were assessed longitudinally via MR angiography as well as *ex vivo* in histological sections. MR angiography yields a qualitative measure for the state of cerebral arteries and veins. Close inspection of the datasets in a 3D-representation did not reveal changes in the major blood vessels (Fig. 7).

The histological evaluation of vessels with RECA cannot distinguish between arterial and venous contribution, however it allows for both a quantitative and a qualitative judgement. Qualitative analysis of the vessels indicated an impact of age. With 18 and 24 months vessels showed signs of degeneration. They appeared thinner and the incidence of string vessels increased (Fig. 8 close up). At the same time the staining intensity increased indicating an increased access to the antigen. Quantification of vessel density suggested an increase in striatal blood vessels after 3m, but no age dependent changes in cortical vessel density (Fig 8b).

4. Discussion

We conducted a longitudinal imaging study in rats, characterizing the ageing process in the healthy brain via structural MRI and functional imaging. Here we want to discuss the data and compare it to human ageing biomarkers.

4.1 Health status

When studying “normal” ageing the first concern must be directed to the health state of the animals. Regular laboratory rats are far from being normal rats. Standard laboratory conditions include a perpetual supply of food, little sensory stimulation and no motivation for exercise, letting the control rats for disease models and pharmacological interventions rapidly grow obese, insulin resistant and hypertensive [14]. This detrimental health state is confounding ageing studies, superposing the actual ageing effect by age-related but not age-determining diseases. An established method to prolong life and health span is a chronic

calorie restricted diet [15]. However, calorie restriction is not primarily a means to prolong life but it mainly prevents, delays or reduces the incidence of obesity associated diseases and tumours. Calorie restriction by only 20% of the *ad libitum* consumption stabilizes the body weight and increases the life and health span [16-18]. The beneficial effects of calorie restriction were shown in the last decades for numerous systems and different physiological levels: from DNA-repair mechanisms and neurogenesis rate to the cerebrovascular system and sensorimotor performance [19-21]. Additionally to dietary restriction, sensory enrichment was reported to be highly beneficial in a number of behavioural, anatomical and molecular studies. Or rather, the artificial sensory deprivation in standard laboratory housing is harming brain development, decreases the expression level of neurotrophins and alters the behaviour, among other things (for reviews see: [22, 23]). Environmental enrichment was shown to not disturb standardization or reproducibility [24, 25]. . In the study presented here, rats were kept under calorie restriction by 20%, housed in groups and their cages were equipped to allow rat specific behaviour. The laboratory housing was modified to serve the innate physiological and behavioural needs of rats, such as climbing, hiding, gnawing, nest building, rearing and social interaction to ensure a healthy and species-specific behavioural repertoire. Under such conditions, our rats were ageing without growing obese with a low incidence of spontaneous tumours and without somatosensory deficits.

4.2 Structural MRI

The different grey matter (GM) structures exhibit different structural consistency over time. The diffusion-derived parameters in the thalamus and hippocampus show the most dramatic changes before the age of 14m, while T2 is decreasing continuously throughout life. The cortex and striatum don't show a demonstrative change in the rate of de-/ or increase over life, with a steady increase in Fractional Anisotropy and a steady decrease in the other quantitative parameters.

The MR parameters presented in this study indicate that the hippocampal and thalamic parenchyma are getting denser with age, as indicated by a reduction of free water (T2). In parallel, Fractional Anisotropy (FA), a marker for the directionality of tissue structure, is increasing throughout life in cortex, striatum, thalamus and hippocampus. Its counterpart, Radial Diffusivity (RD), is reflecting the diffusivity perpendicular to the main diffusion direction and is decreasing. The detected FA increase and RD decrease in the grey matter structures are an indicator for on-going myelination. We reported previously that myelination is detectable until month three and beyond in Wistar rats [5]. In human studies, myelination was repetitively shown to continue well after adolescence, showing an inverted U-shaped development [26]. DTI studies showed an increase in FA in the human caudate nuclei and putamen and other deep brain GM into the third decade of life and stagnation thereafter [27,

28]. In the whole brain, FA remains unchanged. However, it must be considered, that this particular ROI includes the cerebral ventricles. The ventricles are known to enlarge with age, both in humans and in rodents [4, 29, 30], affecting in particular the DTI parameters. The DTI measures reflecting directionality will tend to decrease, while mean diffusivity will increase with increasing CSF contribution unless counteracted by a strong reduction of diffusion in the brain parenchyma.

The continuous volume increase of the whole brain levels out at the age of 20m. In the grey matter structures an age-related volume change found in the cortex alone. The detected cortical volume loss after 22m is comparable both in extent and SD to findings described in 14 month old, ad libitum fed mice [4]. This delay can be attributed to the longer life span of rats as well as to the benefit of fasting. Cortical volume loss is a well-characterized biomarker for human brain ageing, where the frontal and temporal cortices seem to be most vulnerable [31]. The cortical thinning during human ageing is not attributed to neuronal loss, but rather to shrinkage of big neurons and a decrease of synaptic density ([32], for review see: [29]). Hippocampal volume is showing an age-related decline in humans [33, 34] that comes along with memory impairment. Age, however, is in cortex and hippocampus not linked to a loss in pyramidal cells, both in humans [35, 36] and in rats [37].

4.3 Functional ageing profile

Forepaw fMRI revealed an effect in age in the activation area (cluster size) as well as in the signal intensity (BOLD %). BOLD fMRI signal is a complex signal and is not only dependent on the neuronal activity but also on the somatosensory sensitivity and cortical representation field, the conduction latency, the mechanism of neurovascular coupling and the hemodynamic response (the cerebrovascular architecture and cerebral blood flow/ volume). This is challenging in an ageing study, as cortical plasticity, sclerotic vessels or alterations in neurotransmitter release can occur with age and change the BOLD signal.

The positive BOLD signal got stronger until the age of 10m. Electrophysiological studies, mapping the cortical representation fields, showed the representation field for the forepaw to be shifted in ageing rats: areas formerly excited by cutaneous stimulation, were activated by subcutaneous stimuli. This cortical reorganisation occurred until the age of eight months [38] and was sustained, both in extent and strength of neuronal response with progressing age (until 25 months) [39, 40].

The decrease of the cortical BOLD signal in rats older than ten months, whether due to reduced blood supply or attenuated neuronal activation, is supported by preliminary PET data indicating a reduction of ^{18}FDG accumulation in the cortex and striatum (not shown here). Our results are in line with an earlier human fMRI study reporting a decrease in spatial

extent and incidence of positive BOLD with age [41]. It is unlikely that elder patients did not have a neuronal response to a motor task, but rather that it did not evoke a detectable response. This observation supports the hypothesis that the reduction in positive BOLD signal and activation area is coupled to a reduced hemodynamic response.

The bilateral negative BOLD in the striatum seemed to be more affected by age, than the positive BOLD signal in the S1 of the contralateral forepaw. Negative BOLD is a well-known, but poorly understood phenomenon. So far, two explanations are discussed. Either negative BOLD is a result of a “vascular steal” mechanism, where the increased CBV in the activated areas would be compensated by a local decrease in CBV in other regions of the circuitry [42]. Or negative BOLD is reflecting an actual reduction of neuronal activity, thus an inhibition after the stimulus. Electrophysiological studies reported a decline in functional inhibition in aged rats (24m) compared to young ones (3m) [43]. The phenomenon was first described in human fMRI studies, reporting a conversion from negative to positive BOLD with age upon motor tasks. However, this pattern was matched with an increased area of positive BOLD, indicating a general over-activation with age [44, 45]. This, however, is in opposition to our results in rats, revealing a decreased activation area (cluster size) in the contralateral S1 with age.

4.4 Angioarchitectural changes

Angioarchitecture in the cortex and striatum showed age-related deteriorations. While the vessel density was unchanged with age, the vessels had a reduced diameter and the occasion of string vessels was increased. These first, qualitative changes could not be visualized with MR angiographies, as they concern mostly small vessels, undetected by MRI. It is notable, however, that vessel density increased between the ages of three and twelve months, supporting our previous findings that brain maturation proceeds after three months in rats.

The quantitative data of our study is supported by previous reports, stating that calorie restriction preserves cortical microvessel density in ageing rats, while reducing the vascular reactivity upon CO_2 challenge [46].

The described qualitative changes will have contributed to the reduced BOLD signal with age, as any angioarchitectural changes, whether a reduction of vessels or vascular damage, can lead to impaired vascular reactivity and reduced vascular recruitment. A reduction in vascular reactivity in turn affects the spatial extent and signal intensity of the BOLD signal, both of the positive and negative.

5. Conclusion

For the first time, we could show structural and functional age-changes in the rat brain in-vivo, based on a two year longitudinal study.

General expectation of a defined point of conversion from adulthood to beginning of ageing process was not fulfilled; instead we found a rather gradual change with different pacing in the analysed structures and parameters. However, general and regional volume decrease appears to happen consistently between 18 and 20 months.

Function and angioarchitecture show strengthening during the first year of life with a following decrease to the level of early adulthood (2/3 months). Although the functional result is similar, age-related deterioration is probably based on different mechanisms, rather than a mere reversal of maturation processes. While cortical reorganisation and myelination help increasing the BOLD signal during early adulthood, neurovascular coupling and vascular deterioration are supposed to cause the reduction of the BOLD signal with age. In the paradigm used here, the weaker negative BOLD signal in the striatum is more affected by age-related changes than the rather robust positive BOLD signal in the cortical representation fields of the forepaws.

6. Acknowledgements

We thank Claudia Hafeneger, Melanie Nelles and Michael Diedenhofen of the Max Planck Institute for Metabolism Research for technical support. This work was financially supported by BMBF (0314104) and ENCITE EU-FP7 (HEALTH-F5-2008-201842) program.

7. References

1. Holzenberger, M., et al., *IGF-1 receptor regulates lifespan and resistance to oxidative stress in mice.* Nature, 2003. **421**(6919): p. 182-7.
2. Fontana, L., et al., *Medical research: treat ageing.* Nature, 2014. **511**(7510): p. 405-7.
3. Adolf, P., et al., *Longitudinal Brain Magnetic Resonance Imaging Study of the Alcohol-Preferring Rat. Part II: Effects of Voluntary Chronic Alcohol Consumption.* Alcoholism: Clinical and Experimental Research, 2006. **30**(7): p. 1248-1261.
4. Maheswaran, S., et al., *Longitudinal regional brain volume changes quantified in normal aging and Alzheimer's APP x PS1 mice using MRI.* Brain Res, 2009. **1270**: p. 19-32.
5. Mengler, L., et al., *Brain maturation of the adolescent rat cortex and striatum: changes in volume and myelination.* Neuroimage, 2014. **84**: p. 35-44.
6. Skare, S., et al., *Condition number as a measure of noise performance of diffusion tensor data acquisition schemes with MRI.* Journal of Magnetic Resonance, 2000. **147**(2): p. 340-352.
7. Jones, D.K., M.A. Horsfield, and A. Simmons, *Optimal strategies for measuring diffusion in anisotropic systems by magnetic resonance imaging.* Magnetic Resonance in Medicine, 1999. **42**(3): p. 515-525.
8. Leow, A.D., et al., *Longitudinal stability of MRI for mapping brain change using tensor-based morphometry.* Neuroimage, 2006. **31**(2): p. 627-640.
9. Yanovsky, I., et al., *Asymmetric and Symmetric Unbiased Image Registration: Statistical Assessment of Performance.* 2008 Ieee Computer Society Conference on Computer Vision and Pattern Recognition Workshops, Vols 1-3, 2008: p. 280-287.
10. Weber, R., et al., *A fully noninvasive and robust experimental protocol for longitudinal fMRI studies in the rat.* NeuroImage, 2006. **29**(4): p. 1303-1310.
11. Kalthoff, D., et al., *Functional connectivity in the rat at 11.7T: Impact of physiological noise in resting state fMRI.* Neuroimage, 2011. **54**(4): p. 2828-39.
12. Seehafer, J.U., et al., *No Increase of the Blood Oxygenation Level-Dependent Functional Magnetic Resonance Imaging Signal with Higher Field Strength: Implications for Brain Activation Studies.* Journal of Neuroscience, 2010. **30**(15): p. 5234-5241.
13. Wu, E.X., H.Y. Tang, and J.H. Jensen, *High-resolution MR imaging of mouse brain microvasculature using the relaxation rate shift index Q.* Nmr in Biomedicine, 2004. **17**(7): p. 507-512.
14. Martin, B., et al., *â€œControlâ€ laboratory rodents are metabolically morbid: Why it matters.* Proceedings of the National Academy of Sciences: p. -.
15. McCay, C.M., M.F. Crowell, and L.A. Maynard, *The Effect of Retarded Growth Upon the Length of Life Span and Upon the Ultimate Body Size: One Figure.* J. Nutr., 1935. **10**(1): p. 63-79.
16. Wang, C., et al., *Caloric restriction and body weight independently affect longevity in Wistar rats.* International Journal of Obesity, 2004. **28**(3): p. 357-362.
17. Masoro, E.J., *Mortality and growth - characteristics of rat strains commonly used in aging research.* Experimental Aging Research, 1980. **6**(3): p. 219-233.
18. Masoro, E.J., *Caloric restriction-induced life extension of rats and mice: A critique of proposed mechanisms.* Biochimica Et Biophysica Acta-General Subjects, 2009. **1790**(10): p. 1040-1048.
19. Mattson, M.P. and R.Q. Wan, *Beneficial effects of intermittent fasting and caloric restriction on the cardiovascular and cerebrovascular systems.* Journal of Nutritional Biochemistry, 2005. **16**(3): p. 129-137.
20. Kumar, S., et al., *Interactive effect of excitotoxic injury and dietary restriction on neurogenesis and neurotrophic factors in adult male rat brain.* Neuroscience Research, 2009. **65**(4): p. 367-374.

21. Bruce-Keller, A.J., et al., *Food restriction reduces brain damage and improves behavioral outcome following excitotoxic and metabolic insults.* Annals of Neurology, 1999. **45**(1): p. 8-15.
22. Nithianantharajah, J. and A.J. Hannan, *Enriched environments, experience-dependent plasticity and disorders of the nervous system.* Nat Rev Neurosci, 2006. **7**(9): p. 697-709.
23. van Praag, H., G. Kempermann, and F.H. Gage, *Neural consequences of enviromental enrichment.* Nat Rev Neurosci, 2000. **1**(3): p. 191-198.
24. Wolfer, D.P., et al., *Laboratory animal welfare: cage enrichment and mouse behaviour.* Nature, 2004. **432**(7019): p. 821-2.
25. Richter, S.H., J.P. Garner, and H. Wurbel, *Environmental standardization: cure or cause of poor reproducibility in animal experiments?* Nat Methods, 2009. **6**(4): p. 257-61.
26. Raz, N., et al., *Regional brain changes in aging healthy adults: General trends, individual differences and modifiers.* Cerebral Cortex, 2005. **15**(11): p. 1676-1689.
27. Pal, D., et al., *Quantification of age- and gender-related changes in diffusion tensor imaging indices in deep grey matter of the normal human brain.* Journal of Clinical Neuroscience, 2011. **18**(2): p. 193-196.
28. Munivenkatappa, A., et al., *In vivo Age-related Changes in Cortical, Subcortical Nuclei, and Subventricular Zone: A Diffusion Tensor Imaging Study.* Aging and Disease, 2013. **4**(2): p. 65-75.
29. Fjell, A.M. and K.B. Walhovd, *Structural Brain Changes in Aging: Courses, Causes and Cognitive Consequences.* Reviews in the Neurosciences, 2010. **21**(3): p. 187-221.
30. Chen, C.C.V., Y.Y. Tung, and C. Chang, *A lifespan MRI evaluation of ventricular enlargement in normal aging mice.* Neurobiology of Aging, 2011. **32**(12): p. 2299-2307.
31. Tisserand, D.J., et al., *Regional frontal cortical volumes decrease differentially in aging: An MRI study to compare volumetric approaches and voxel-based morphometry.* Neuroimage, 2002. **17**(2): p. 657-669.
32. Terry, R.D., R. Deteresa, and L.A. Hansen, *Neocortical Cell Counts in Normal Human Adult Aging.* Annals of Neurology, 1987. **21**(6): p. 530-539.
33. Schuff, N., et al., *Age-related metabolite changes and volume loss in the hippocampus by magnetic resonance spectroscopy and imaging.* Neurobiol Aging, 1999. **20**(3): p. 279-85.
34. Jack, C.R., Jr., et al., *Rate of medial temporal lobe atrophy in typical aging and Alzheimer's disease.* Neurology, 1998. **51**(4): p. 993-9.
35. West, M.J., et al., *Differences in the Pattern of Hippocampal Neuronal Loss in Normal Aging and Alzheimers-Disease.* Lancet, 1994. **344**(8925): p. 769-772.
36. West, M.J., *Regionally Specific Loss of Neurons in the Aging Human Hippocampus.* Neurobiology of Aging, 1993. **14**(4): p. 287-293.
37. Rasmussen, T., et al., *Memory impaired aged rats: No loss of principal hippocampal and subicular neurons.* Neurobiology of Aging, 1996. **17**(1): p. 143-147.
38. Coq, J.O. and C. Xerri, *Age-related alteration of the forepaw representation in the rat primary somatosensory cortex.* Neuroscience, 2000. **99**(3): p. 403-411.
39. Godde, B., et al., *Age-related changes in primary somatosensory cortex of rats: evidence for parallel degenerative and plastic-adaptive processes.* Neuroscience and Biobehavioral Reviews, 2002. **26**(7): p. 743-752.
40. Spengler, F., B. Godde, and H.R. Dinse, *Effects of aging on topographic organization of somatosensory cortex.* Neuroreport, 1995. **6**(3): p. 469-473.
41. D'Esposito, M., et al., *The Effect of Normal Aging on the Coupling of Neural Activity to the Bold Hemodynamic Response.* NeuroImage, 1999. **10**(1): p. 6-14.
42. Harel, N., et al., *Origin of negative blood oxygenation level-dependent fMRI signals.* J Cereb Blood Flow Metab, 2002. **22**(8): p. 908-17.
43. Schmidt, S., et al., *Age-related decline of functional inhibition in rat cortex.* Neurobiology of Aging, 2010. **31**(3): p. 504-511.

44. Riecker, A., et al., *Functional significance of age-related differences in motor activation patterns.* Neuroimage, 2006. **32**(3): p. 1345-1354.
45. Mattay, V.S., et al., *Neurophysiological correlates of age-related changes in human motor function.* Neurology, 2002. **58**(4): p. 630-635.
46. Lynch, C.D., et al., *Effects of moderate caloric restriction on cortical microvascular density and local cerebral blood flow in aged rats[small star, filled].* Neurobiology of Aging, 1999. **20**(2): p. 191-200.
47. Schallert, T., et al., *CNS plasticity and assessment of forelimb sensorimotor outcome in unilateral rat models of stroke, cortical ablation, parkinsonism and spinal cord injury.* Neuropharmacology, 2000. **39**(5): p. 777-787.
48. Rozas, G., M.J. Guerra, and J.L. Labandeira-Garcia, *An automated rotarod method for quantitative drug-free evaluation of overall motor deficits in rat models of parkinsonism.* Brain Research Protocols, 1997. **2**(1): p. 75-84.

Figure legends

Figure 1: Study design. Three groups of Wistar rats were included, differing in survival time and age at study entry. This interleaved design allowed for histological evaluation and accounted for possible effects of repetitive anaesthesia and testing. Solid bars indicate the period in the study, with the ages for MRI and behavioural testing, hatched bars indicate only housing within the animal facility. The n numbers give the final group sizes, respecting losses due to tumours and anaesthesia.

Figure 2: Bodyweight as a function of age. Bodyweight of individual animals is given by grey-scale symbols, the general trend is depicted in red and characterized by a log(mean)R^2= 0.8615. Calorie Restriction (CR) was introduced at an age of 8 weeks (P56), as indicated by the dashed line. Consequently, bodyweight increase is slowing down, reaching a rather stable state around 400g.

Figure 3: Volume changes of grey matter structures. Grey lines indicate the mean volume at a certain age, the shaded area gives the respective standard deviation. Volume is decreasing significantly in cortex, striatum and hippocampus over time (ctx: $F(8,46)=5.78$ $p<0.001$; cpu: $F(8,43)=2.9$ $p<0.01$; hip: $F(8,37)=3.22$ $p<0.01$).

Figure 4: Deformation based morphometry. Selected sections from the template brain superimposed with positive (red) and negative (blue) cluster. Cluster represent pixels that showed a significance of at least $p<0.05$ in a regression of the logarithmic transform of the determinant of the Jacobians from 14 to 24 months.

Figure 5: MR parameters of striatum and cortex. Fractional anisotropy (FA), radial diffusivity (RD), T2 and tensor trace (TT) profiles from striatum (blue) and cortex (red). Mixed models analysis revealed an effect of age in FA in striatum and cortex, in RD in cortex, in T2 in striatum ($F(8,17)=20.1$ $p<0.001$) and cortex ($F(8,15)=8.7$ $p<0.001$) and in TT in the cortex. Results of post-hoc pairwise comparison is indicated by red or blue asterisks, indicating a significant difference to the age of 24m, with a p-value >0.05 (*) or <0.001 (***).

Figure 6: Evolution of signal intensity and cluster size of BOLD fMRI signal with age: data from the primary sensory cortex (S1) in red and striatal changes in blue. Error bars represent the standard deviation. A: Mean BOLD change over time in S1 and striatum show a mirror profile, with the strongest signal at 10m. B: Mean cluster size is decreasing continuously in S1 and peaks at 10m in striatum. C: Representative BOLD fMRI maps at two, ten and 24 months were superimposed onto original EPI images.

Figure 7: Angiography reconstruction prepared in Paravision 5.0 using a 3D representation tool (MIP). All scans were taken from the same subject and are oriented in a rostro-caudal direction. In the left column unsaturated angiographies are depicted, representing all bigger vessels, in the right column the saturated angiographies, visualising the venous contribution alone.

Figure 8: Vessel density. Panel is showing representative RECA staining (40X magnification, scale bar represents 50µm) in the cortex (left) and striatum (right). Qualitative assessment of the vessels shows signs of degeneration, like string vessels (white arrow in the far right image) and thinning of the vessels. Quantitative analysis of vessel density in the cortex (red) and striatum) did not reveal any major changes in the number of vessels.

Tables and Table legends

somatosensory test		scoring	
Neurological score:			
appearance	secretion	no – yes	1 – 0
	colour and state of fur	White/sleek - scrubby	1 – 0
activity	exploring and rearing at cage walls	# walls approached in homecage	4 – 3 – 2 – 1 – 0
		# walls approached in labcage	4 – 3 – 2 – 1 – 0
sensory reflexes	whiskers: left and right	yes – no	1 – 0
	forelimbs: left and right	yes – no	1 – 0
			Max. 14 points
Cylinder test:	forelimb use asymmetry	Percentage use while exploring the walls Percentage use under strain (rearing, returning) [47]	
RotaRod:	Motor performance	Overall Rod performance in a fixed speed protocol with 5-40 rpm in 5rpm increments, according to [48]	

Table 1: Overview of neurological scoring and behavioural tests. Neurological score included three major categories with several subscores, summing up to a maximal score of 14 points in a healthy and well-groomed rat. The somatosensory tests were evaluated separately, based on video recordings (forelimb use asymmetry) and automated recording of "time on the rod" (RotaRod).

age	Neurological score	Cylinder: contact left / right paw	Rotarod (mean ORP)
8 months	14 +/-0	50/50 +/- 5%	2920.42 +/- 51%
10 months	14 +/-0	49/51 +/- 2.3%	2652.08 +/- 57%
12 months	14 +/-0	50/50 +/- 4.3%	3725.36 +/- 53%
14 months	13.85 +/- 0.24	48/52 +/- 3.8%	2881.79 +/- 63%
16 months	13.75 +/- 0.26	49/51 +/- 1.9%	2542.31 +/- 69%
18 months	13.8 +/- 0.23	50/50 +/- 9.4%	1946.25 +/- 89%
20 months	13.75 +/- 0.26	50/50 +/- 4%	4433.13 +/- 50%
22 months	13.75 +/- 0.28	49/51 +/- 3.2%	4669.38 +/- 50%
24 months	13.9 +/- 0.23	47/53 +/- 2.1%	3942.5 +/- 20%

Table 2: Neurological scoring and behavioural results for different ages. Given are the mean scores and the standard deviation per age. The neurological score contains information on outer appearance, activity and sensory reflexes and peaks with a value of 14. The Cylinder test, scores the independent use of the left and right forepaw, in order to uncover asymmetries in forepaw use. The Rotarod performance is rated with the Overall Rod Performance (ORP), calculated as the total area under the curve in a plot of "time on the rod" against rotation speed (according to [48]). In this setup included rotations between 5 and 40 rotations per minute (rpm) with 5rpm increments, each for max. 300s.

Figure 1

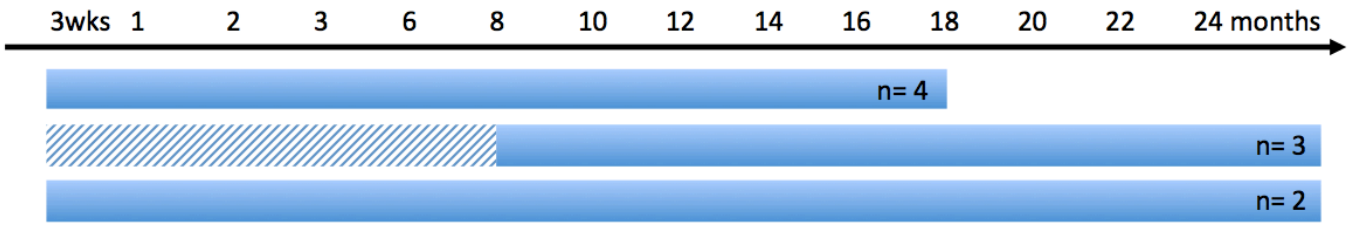

Figure 2

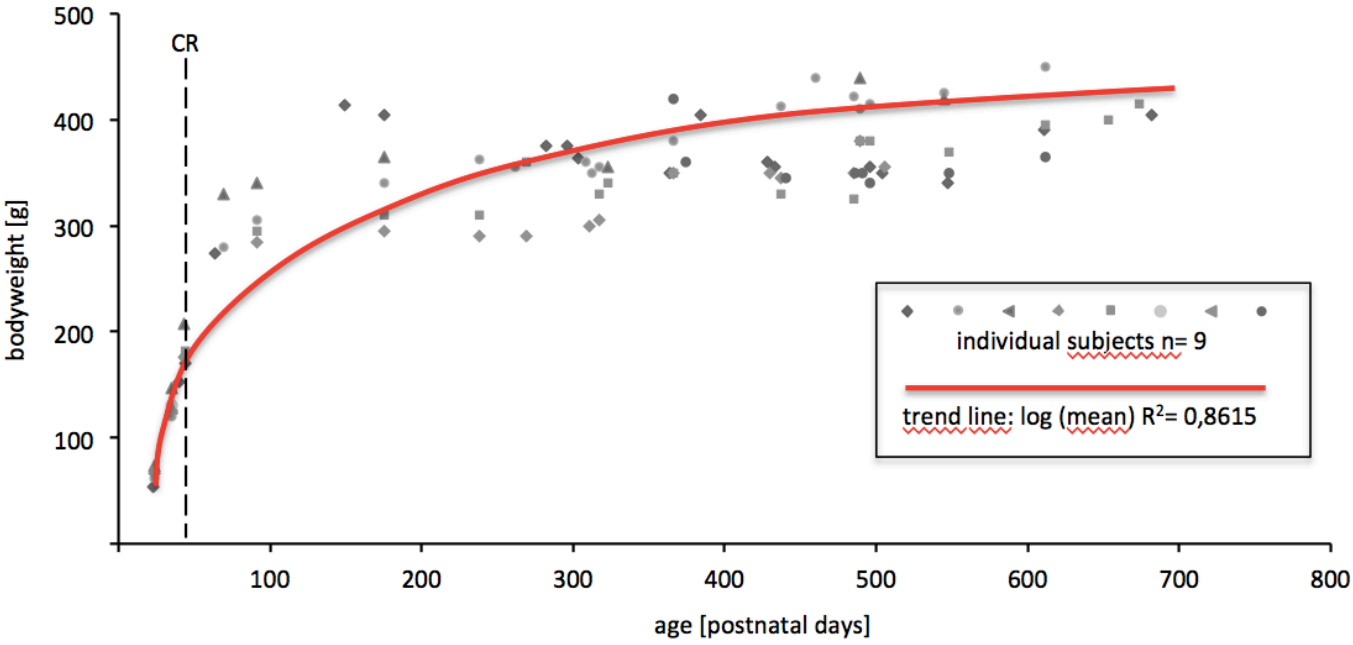

Figure 3

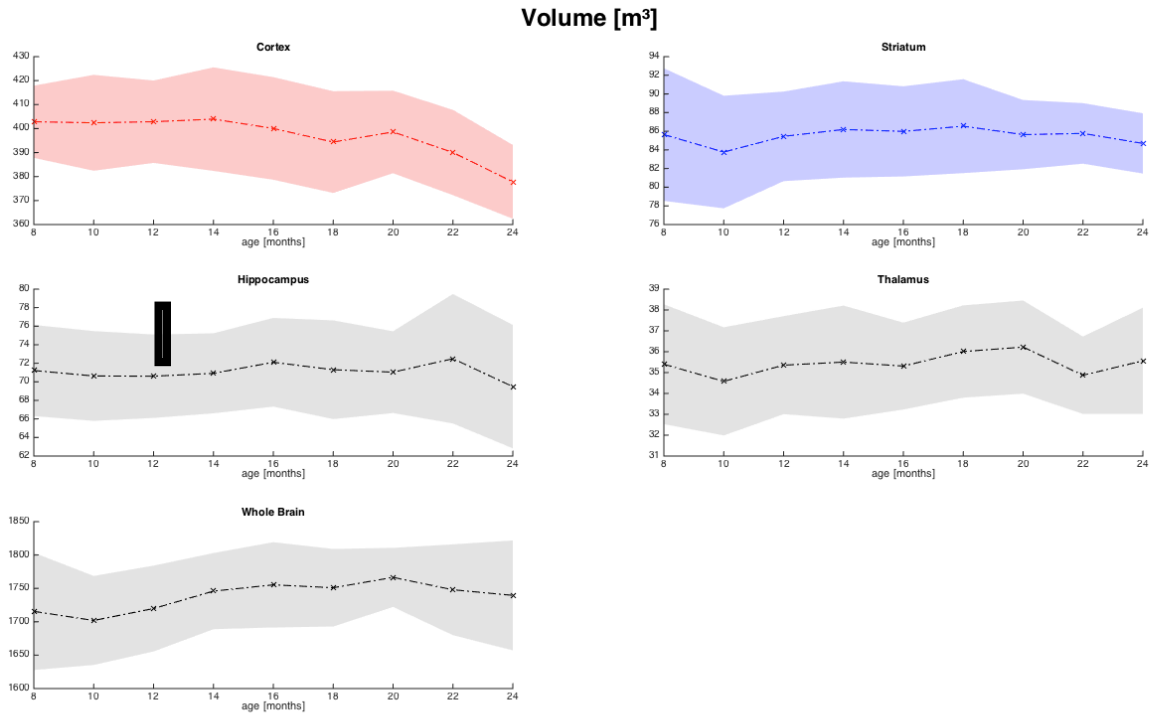

Figure 4

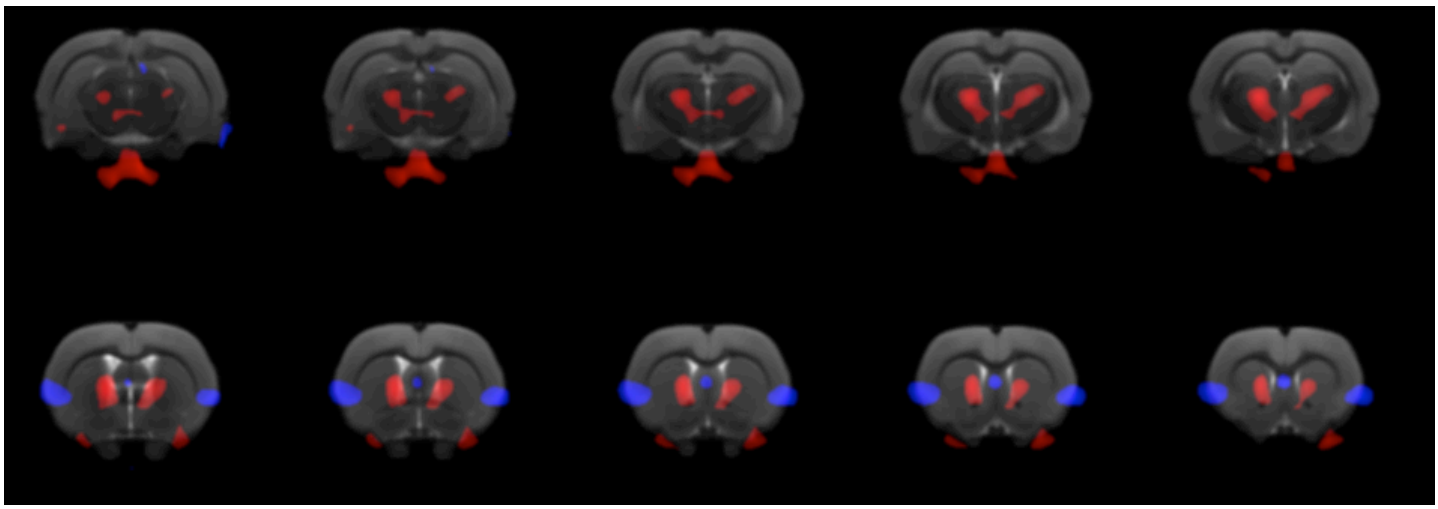

Figure 5

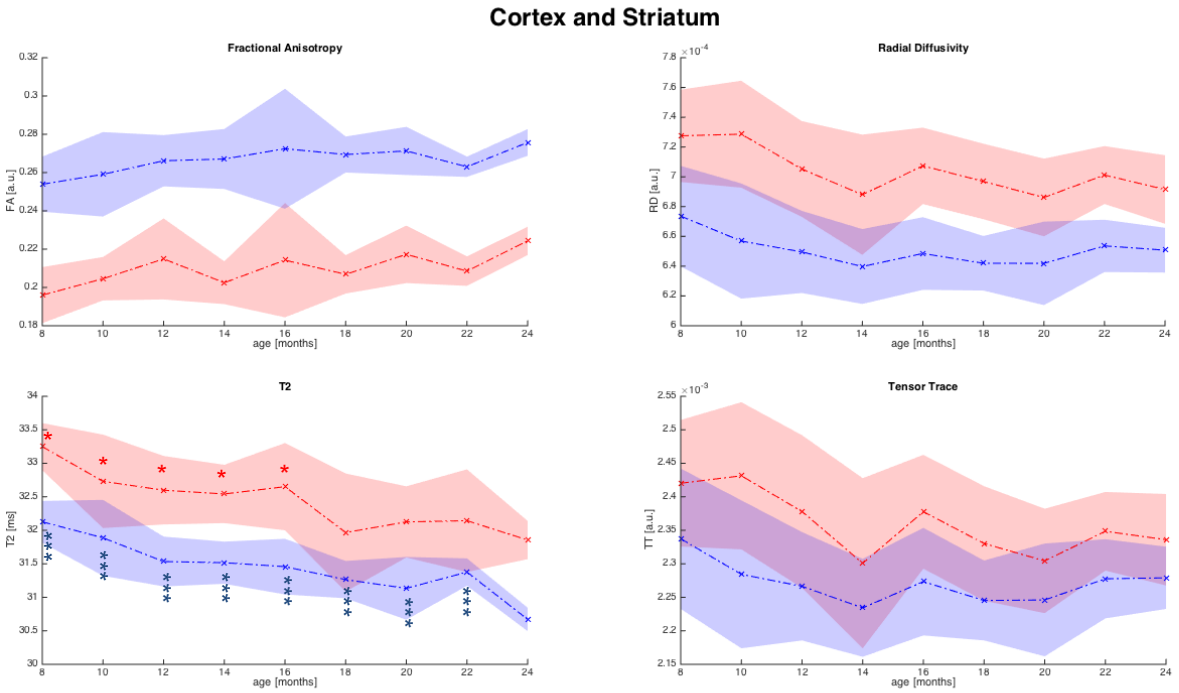

Figure 6

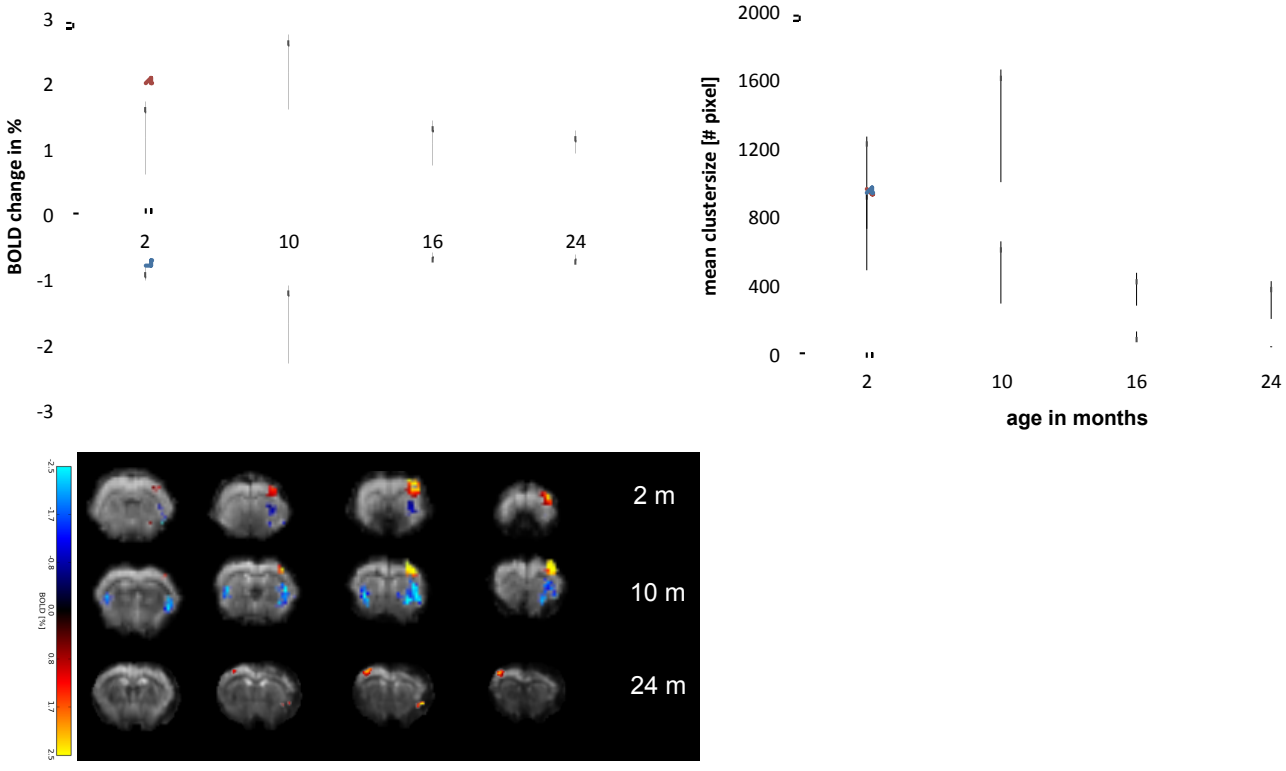

Figure 7

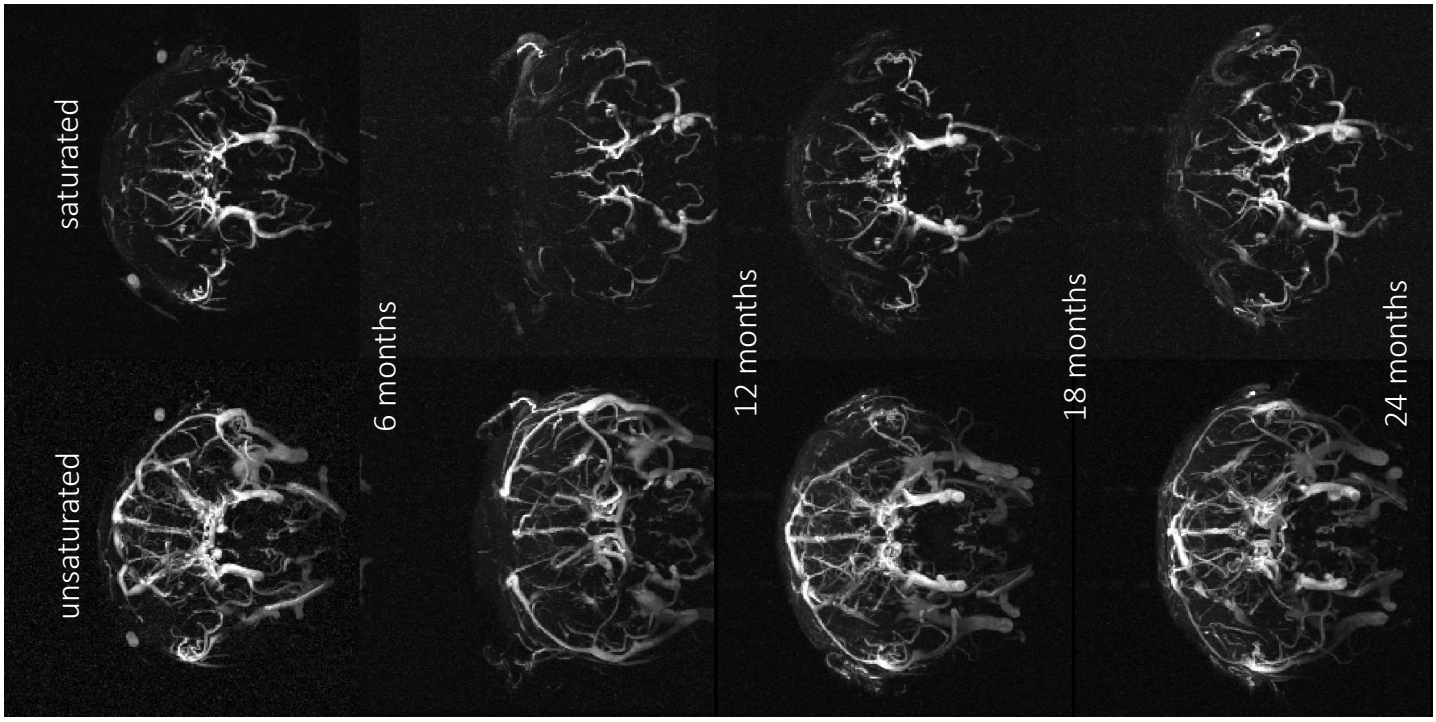

Figure 8

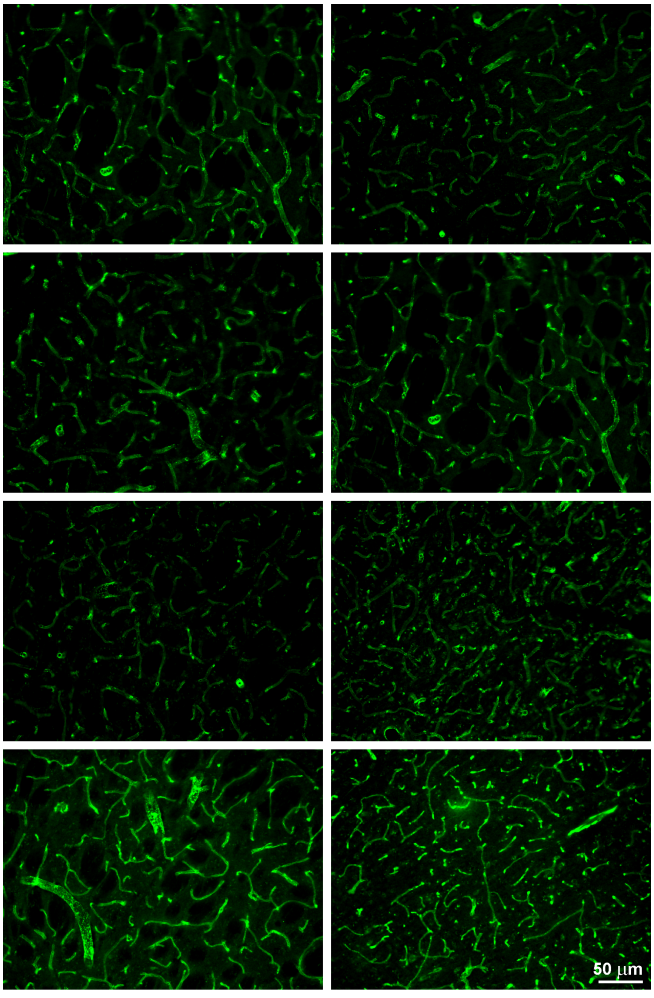

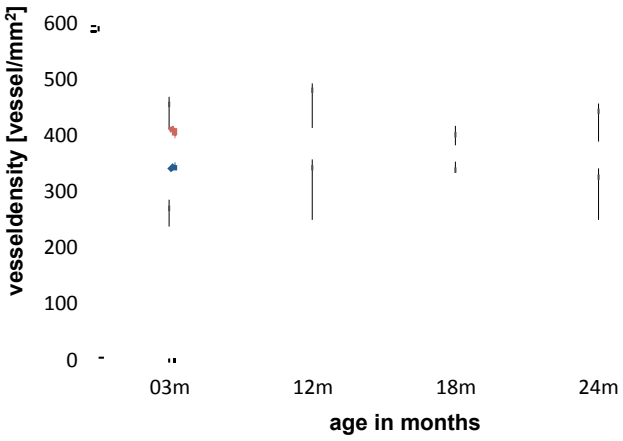

close up: cortex 24m

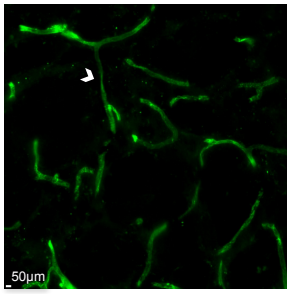

Supplentary Figure 1

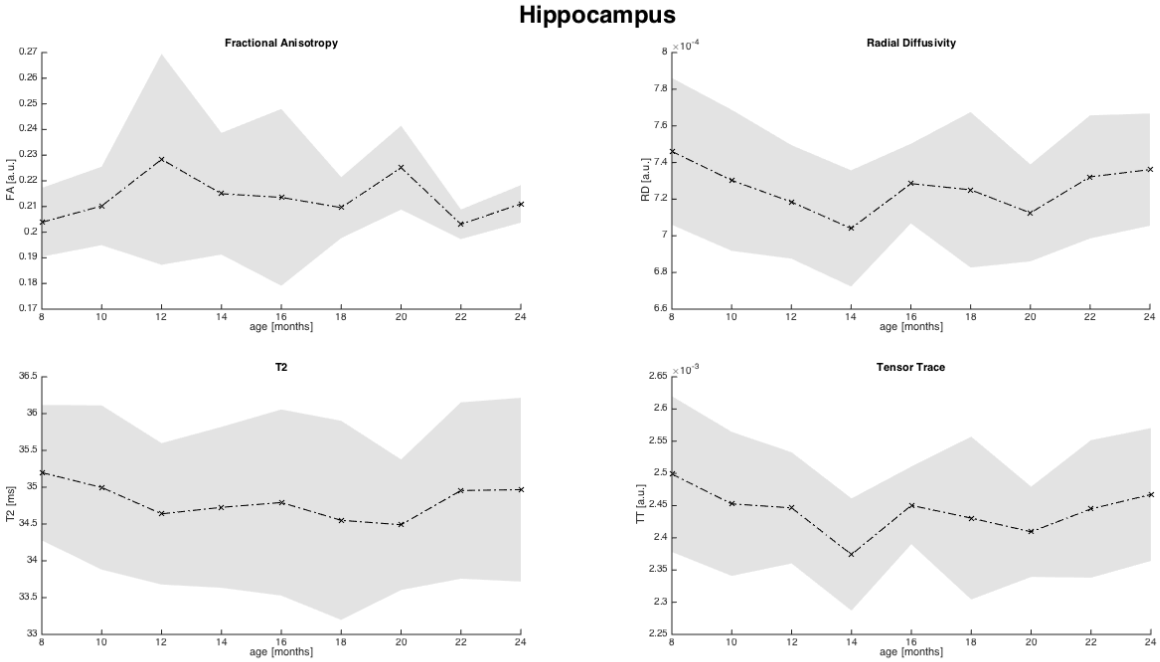

Supplementary Figure 2

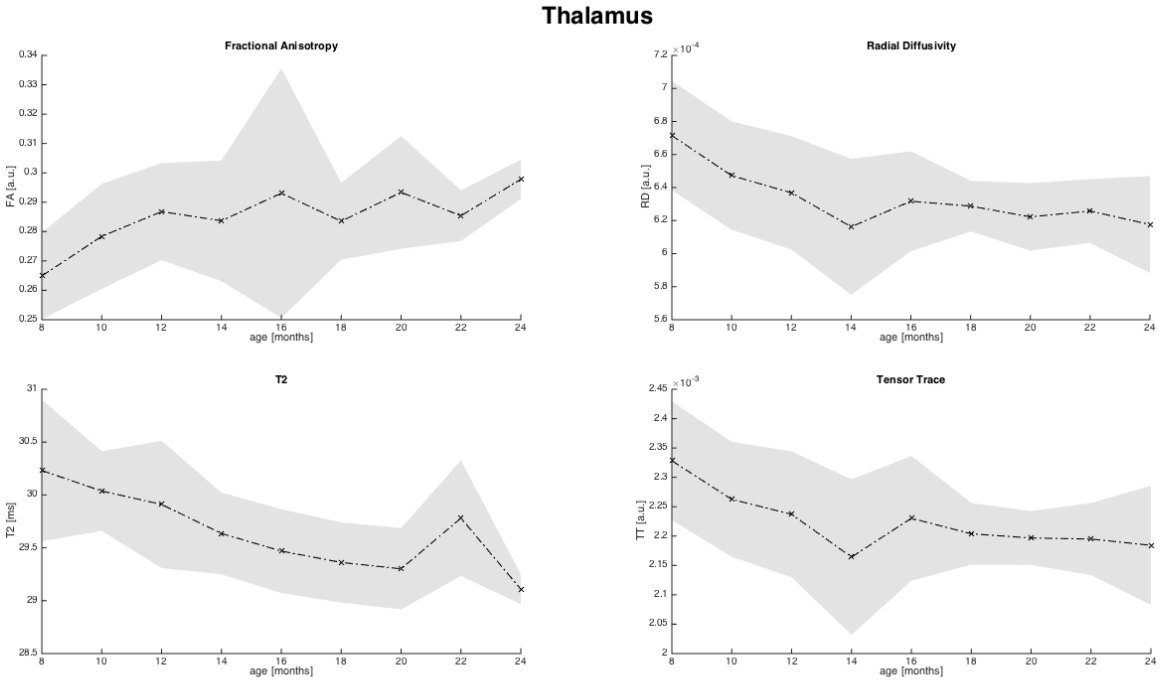

Supplementary Figure 3

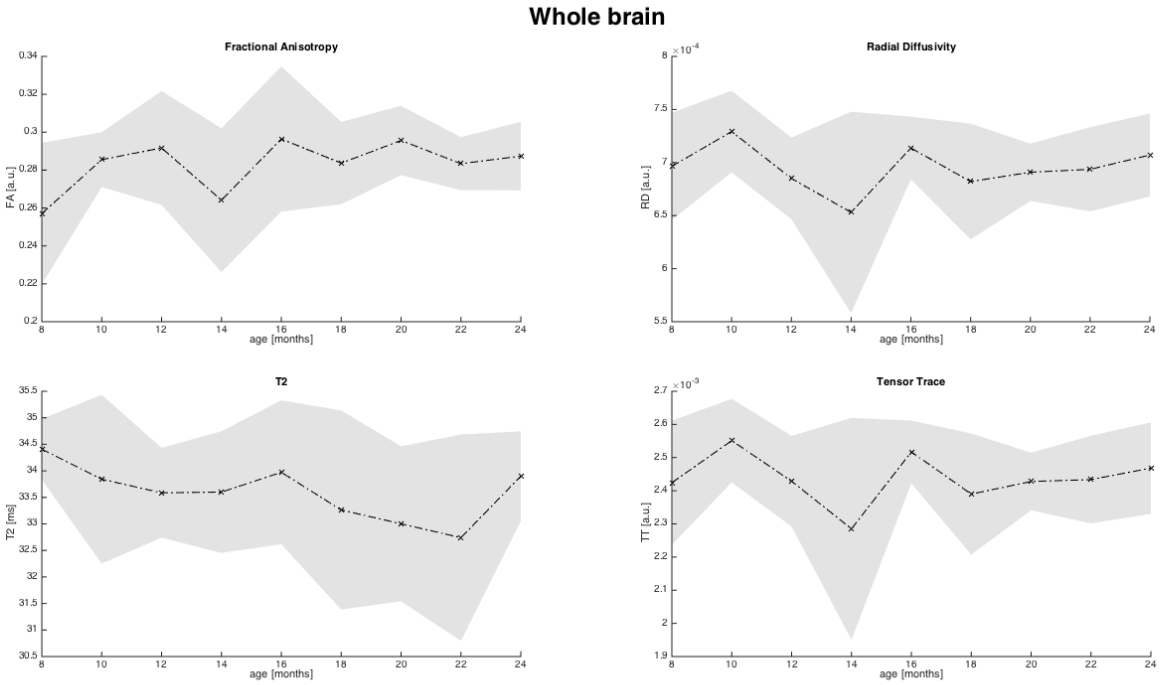

Discussion

The aim of the presented work was to investigate maturation and ageing processes in the rodent brain. For the first time, we present a life-span study in rats, monitoring MR parameters in the same subjects over the course of 24 months. MRI has become an indispensible tool in neurodiagnostics as it allows for repetitive imaging, without compromising tissue integrity or developmental processes. The highly translational nature of MRI facilitates the use of the same methods in the clinic and in animal models. This applies both for image acquisition and post-processing strategy. Here, structural MRI revealed cerebral maturation processes, until the third postnatal month both in mice and rats. The results will help future neuropathological studies, choosing an appropriate age for a given intervention in order to avoid confounding developmental processes. The life span study in rats showed for the first time longitudinal changes during healthy cerebral ageing, attributed to age alone rather than age-related diseases. In the following paragraphs, the different results shall be discussed with a special emphasis on translational analogies.

Registration: Parameters and Success Rate

Registration of different data to a common space is a crucial step in an imaging study, guaranteeing reliable and reproducible results, independent of rater experience. Differences in tissue contrast and brain size challenge registration paradigms in a longitudinal study. In order to minimize registration artefacts, compromising the data integrity, we acquired study-specific or study-relevant template brains with the same MR scanner hardware. Similar data in terms of SNR, resolution, brain size and age reduces the warping necessary to match the source data (subjects) to the target (template). Reducing the extent of necessary deformation or warping results in fewer registration mistakes and makes the registration process more reliable and robust. For the presented studies we established a protocol for MR image registration based on a hierarchical scheme using normalized cross-correlation as a similarity measure. The hierarchy included different, discrete registrations with increasing degrees of freedom. Each registration included a Gaussian pyramid (a method of reducing the risk of local minima traps, see from page 17) where each registration is run repetitively with increasing resolution/ reduced Gaussian filtering. The registration was first conducted in a rigid scheme (DOF=6), employing a Gaussian pyramid of four steps, followed by an affine registration (DOF=12) with a Gaussian pyramid of four steps and finally a non-linear B-spline registration (DOF of

about 1000) with a Gaussian pyramid of two steps. The details of the registration procedure were adapted to the individual studies and template brains. All registration paradigms can be reviewed online:

Mouse maturation: http://elastix.bigr.nl/wiki/index.php/Par0025

Rat maturation: http://elastix.bigr.nl/wiki/index.php/Par0020^

Rat ageing: http://elastix.bigr.nl/wiki/index.php/Par0026

Quality assurance of the registration process cannot be done automatically but relies on the interaction of the researcher. Therefore, we created a graphical user interface, providing a fast and reliable tool to judge the registration success by side-by-side comparison. The GUI allows evaluation of the registration accuracy between the template, the corresponding ROIs and the quantitative MRI maps of a subject.

By creating study-specific templates, an elaborated and adaptable registration procedure and a platform to evaluate the registration accuracy, we established a sound basis for the extensive data analysis necessary in a longitudinal imaging study.

Brain Maturation

Comparison from rat and mouse maturation

Our developmental studies in rat and mouse revealed species differences, concerning time scaling and maturation strategy. In rats the cortex reaches its maximal thickness within the first month and is stable with further brain growth until the final volume is reached with two months. We showed the cortical cell density to remain stable in this transition phase; a finding supported by stereological reports quantifying the number of neurons [48]. Murine maturation is faster concerning the volumetric parameters: the cortical and cerebral volume are stable already after three weeks. The cortical thickness however, is thinning over the following months; an effect visualised by the colour coded brain surfaces in publication III: *Morphological maturation of the mouse brain: An in vivo MRI and histology investigation* (from page 45).

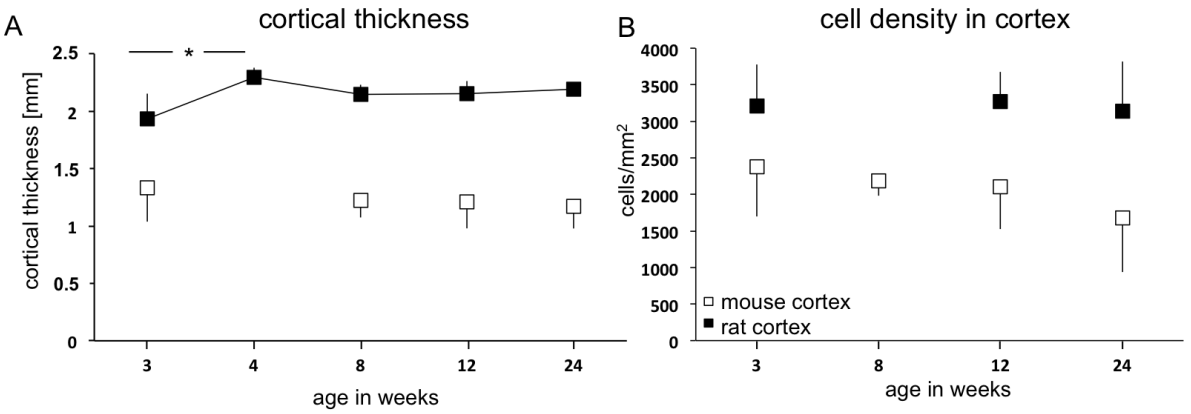

Figure 4: Mouse vs. Rat: cortical thickness and cell density
A: Cortical thickness assessed longitudinally in rats (closed squares) and in a cross-section MRI study in mice (open squares), error bars represent the standard deviation. In rats cortical thickness is peaking in the first month and stabilizes further on. The asterisk indicates a statistically significant difference in a pairwise comparison between ages ($p<0.05$). In mice cortical thickness is slowly, but steadily decreasing after three weeks. B: Cortical cell density, as assessed by quantification of Nissl-staining is unchanged in rats and mice. For mice however no statistical anaylsis was performed, due to a low number of examined specimen (n=2 per age). For more detailed information on the methods, see from page 21, publication II and III.

Apart from the volumetric measures however, the MR parameters indicated a maturation process in the brain parenchyma and particularly in the cortex of both species. The two studies show a rather long maturation phase between the adolescent and the adult brain. Especially the process of myelination within the grey matter (GM) structures can be traced with MRI until the age of three months, both in rats and mice. Earlier reports by Song et al. reported the Radial Diffusivity (RD) to be the most sensitive parameter to myelination changes in white matter [49; 50]. Our comparison to histology showed that neither RD nor Fractional Anisotropy (FA) are sensitive enough for the myelination state in GM. The effects on FA and RD are presumably superimposed by the strong morphological changes in the brain parenchyma. Especially in the cortex, the elaboration of the tangential laminae is counteracting the effect of the myelinated radial fibres. Strengthening of intralaminar connections, by synaptogenesis, dendritic arborisation, disturb the preferential, radial diffusion along the fibres. During the maturation of GM T2 and Mean Diffusivity (MD) indicate a denser tissue, a development corresponding better to myelination than the direction-sensitive parameters FA and RD. Both MD and T2 are a measure for the portion of free water, reflecting a reduction of extracellular space during development, attributed to myelination as well as changes in cellular architecture. In the end MD and T2 decrease profit from the simultaneous maturation of local networks, while the directional parameters are masked.

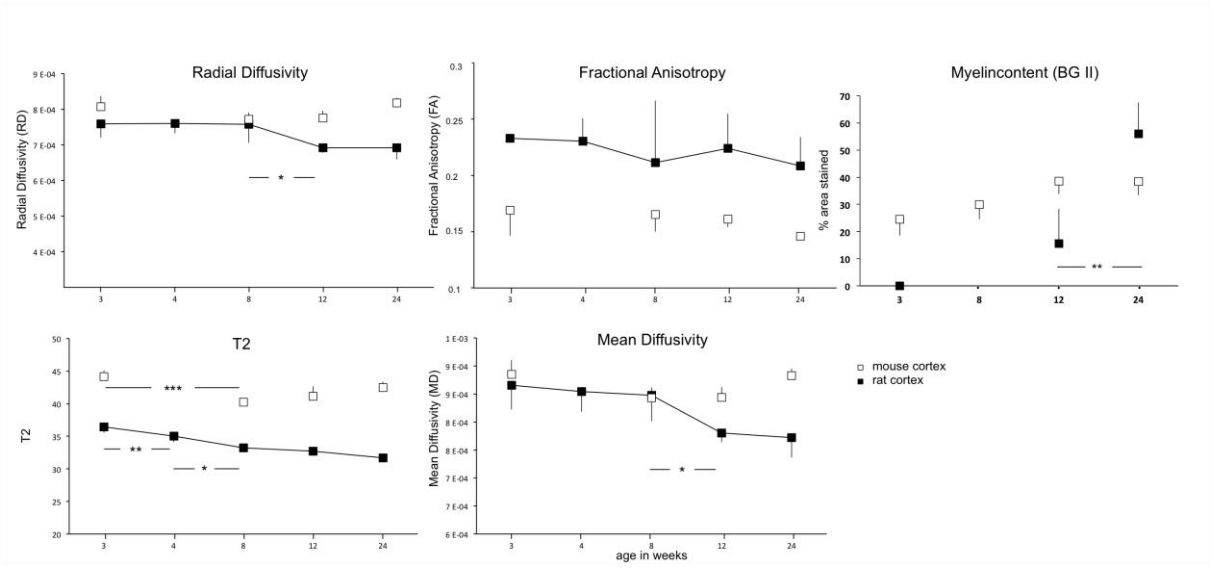

Figure 5: Mouse vs rat: MR and myelin content in the cortex
In rats (closed squares) all MR parameters show a decrease within the first six months. The effect is not significant in the main diffusion direction (FA), but in the perpendicular diffusivity (RD) and even more pronounced in the mean diffusivity (MD). T2 shows highly reproducible values with a small standard deviation (represented by the error bars) and seems to be sensitive for structural changes in the first two months. The MR parameters are believed to reflect the myelination only in the first months, as tangential interlayer connections conceal the on-going myelination of the radial fibres. In mice (open squares) the differences are subtle, but the trend relates to the change in myelination observed by Black and Gold II (BG II) staining.

Comparison to human maturation

Cortical thinning is a well-known phenomenon and has been shown to be a marker both of development and ageing in humans. However, the similar morphometric change does not necessarily reflect comparable neurobiological processes. In the contrary it is likely that fundamentally different reasons are leading to similar symptoms. Cortical atrophy of different cortical areas has long been established as an imaging marker for ageing. Some cortical regions were reported to be preferentially vulnerable to age-associated degeneration, with the prefrontal association cortex being most affected and most temporal areas being spared. This patchwork pattern was repetitively shown both in *in vivo* MRI studies as well as in *post mortem* histology [33; 51]. This age-related cortical thinning is attributed to atrophy rather than selective apoptosis, to demyelination and the degeneration of synapses and shrinkage of neuronal cell bodies [52-55]. Continuous cortical thinning after adolescence is fairly well described in humans and reported in cross-sectional as well as longitudinal MRI studies [56; 57]. This late maturation is characterized in humans and rats by selective synapse elimination, pruning of axons and dendritic spines and even selective cell death [58-60]. These processes support systematically local network connectivity and regional specificity and are thus regarded a maturational marker.

Cerebral Ageing

Structural changes

During maturation the development appears to be rather synchronized between cerebral structures. The evolution of the different MR parameters and the regional volume changes show a common pace during maturation (within a subject and species). The age-related changes in different structures and parameters in the brain, however, follow an individual timeline. The key GM structures for instance display a very heterogeneous evolution of the T2 values: in the thalamus T2 is decreasing continuously with age. In cortex and striatum the decrease is subtle but accelerating after 16 or 22 months respectively, while in the hippocampus values are stable throughout the observed age period. In those structures exhibiting a decrease in T2, although slow, it is accompanied by a faster decrease of the Tensor Trace (TT or TT/3= Mean Diffusivity). This combination indicates a reduction of free water in the ECM, a shift of extracellular to intracellular water and thus an increasingly denser tissue. A previous report on the Apparent Diffusion Coefficient (ADC) and T2 supports the result of a reduced diffusivity and a rather stable T2 in the cortex and no changes in the hippocampus of twelve months old rats compared to three months old rats [61]. The observed MR characteristics are opposing the anticipated age-related deteriorations such as increasing perivascular space, gliosis and demyelination. The reason might be a delayed onset in calorie restricted (CR) animals and supports the conclusion of healthy ageing. In human studies a change in ADC and other DTI-derived parameters is reported for WM but not for GM [62-64], single studies, however, show an increase of anisotropy with age in striatal structures [65].

Somatosensory changes

Our test battery could not detect any sensorimotor deficits with age. Earlier behavioural studies reported an age-related decline starting at the age of 22 months in CR rats, using a detailed walking track analysis [66]. *Ad libitum* fed (AL) rats were shown to improve within the first six months in an inclined plane test and display a nearly linear deterioration thereafter [67]. The chosen version of this test is based mainly on grip strength and reaction time and less on somatosensory skills. The stable performance might be due to the choice of tests used in our study, all designed for lesion assessment and focussing mainly on forepaw skills. Electrophysiological studies reported that the representation field in S1 of the forepaws varies only slightly with age and only after 24 months. The changes in the representation field of the hindpaws, however, were stronger and gait analysis supported the earlier

deterioration of skilled walking in the hindpaws [68]. This asymmetric ageing process can be attributed to the constant use and high dependency of rats on skilled reaching during eating, foraging and climbing, while the hindpaws are trained in tasks asking for strength rather than skill.

Functional and metabolic changes

BOLD fMRI is not only dependent on the neuronal activity but also the mechanism of neurovascular coupling and the cerebrovascular architecture and cerebral blood flow. Although the different contributions cannot be separated non-invasively, fMRI was shown to correlate with sensorimotor function both in humans and rodents [69; 70], making it worthwhile to investigate it as a potential readout or biomarker. Our results showed an increase of the BOLD fMRI signal in rats between a young age (2m) and adulthood (10m) followed by a decrease back to the level of early adulthood. Meanwhile the spatial extent of the BOLD fMRI signal is decreasing continuously over life. Age-related changes in the shape and amplitude of the fMRI signal following simple motor tasks were also described in human studies [71; 72], where both the amplitude and the spatial extent were found to be reduced. Furthermore a decreased SNR (median SNR_{old}= 5.9, median SNR_{young}= 7.6) and increasing physiological noise was reported in the elder subjects [71]. Resulting in less voxel above set activation threshold, reducing the spatial extent even further.

In order to elucidate possible mechanisms behind the an age-related BOLD signal change, we acquired MR angiographies, quantified the vessel density ex vivo and complemented the information on neuronal activity with metabolic PET. Histological evaluation of the cortex and striatum demonstrated stable vessel density, detailed inspection, however, showed the vessels to become thinner with progressing age. An age-related deterioration of cerebral blood vessels would attribute to the decreasing spatial extent and signal intensity. Nevertheless, MRI angiographies could not resolve this change, reflecting only the major blood arteries and veins of the brain. A subset of animals was employed repetitively in metabolic PET experiments, a measure for neural glucose consumption in resting state under anaesthesia. The ^{18}FDG PET data revealed an age-dependent decrease in glucose consumption, both in the striatum as well an in the primary somatosensory cortex (Figure 6). Visual assessment of the quantitative datasets confirms, that this holds true for the whole brain, not only the selected ROIs.

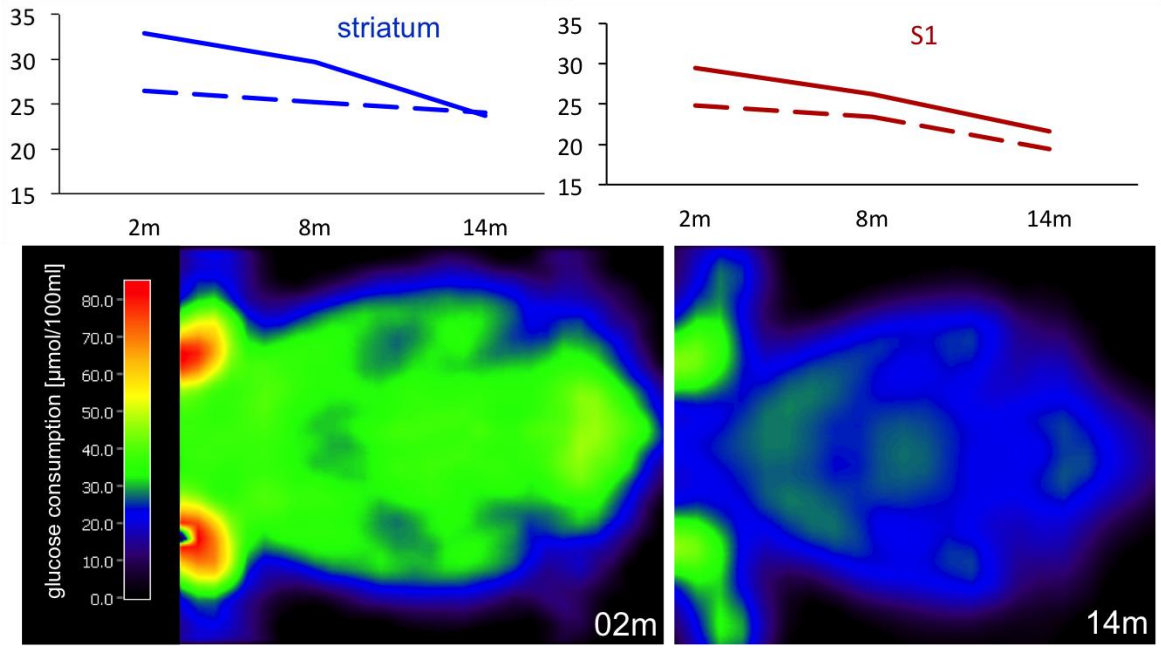

Figure 6: Metabolic PET in ageing rats
Dynamic metabolic PET data was acquired on a dedicated small animal µPET scanner (Siemens, Focus 220). Shown here are two subjects (dashed and solid line) and a representative axial view of the brain of one of the rats (dashed line). Animals were injected with 2mCi 18Fluoro-deoxy-D-glucose intravenously; simultaneously data collection was started and continued for 60 min. Blood glucose levels were determined with a glucometer. PET data is at first qualitative and needs kinetic modelling in order to extract the quantitative measure of glucose consumption. Here we employed the 2-tissue-compartment model with four rate constants, using an input function derived from the whiskers area, as described previously [43]. The local glucose consumption is given by: glucose consumption rate constant * blood glucose level (Kglc*CP, glc).

The result of a reduced BOLD cluster and signal intensity during forepaw fMRI as well as the reduced glucose consumption during resting state PET could be attributed to deficient local blood supply. The extent of vessel deterioration or better vessel maintenance, revealed by MRI and histology, is insufficient to cause such dramatic changes. On the other hand it seems highly unlikely that neuronal activation (fMRI) and activity (PET) is affected that strongly during healthy ageing, particularly in absence of any somatosensory deterioration or strong structural changes. Ageing presumably shows a much greater impact on the mechanism of neurovascular coupling than expected, reducing the BOLD signal upon activation in the fMRI experiments. The reduction in the PET data might be assigned to age-related reactions to fasting (before PET acquisition) or isoflurane anaesthesia.

Conclusion

The presented maturation studies on rat and mouse brain suggest that both species should not be considered adult before the age of three months. Future studies on neuropathological diseases or lesion models should consider this age threshold in order to avoid on-going developmental changes confounding the study outcome.

The age-related morphological changes of the brain, reflected in MRI do not manifest themselves before the age of 20 months and the neurological and sensorimotor scoring could not reveal any behavioural deficits in the aged rats. The functional and metabolic results suggest the start of age-related deterioration, presumably due to vascular damage. The changes are, however, still in a healthy range and data suffers from high standard deviation (fMRI) and low n-numbers (PET). Based on the imaging and behavioural data we conclude that the ageing effect is not yet pathological at the age of 24 months and agree with the nomenclature proposed by Altun [66], classifying rats between 21 and 24 months to be at the conversion from adult to ageing (middle aged). Considering the complete life span in rats, it appears that grey matter is becoming increasingly dense with age, slowing down with adulthood (from 3 months on) and accelerating again in the middle age (20m).

A future study should monitor rats at least until the age of 30 months and include an *ad libitum* (AL) control group. As AL animals are rapidly growing obese, such a study design would ask for a new MRI setup with a scanner suited for bigger subjects (scanner access and probe tuning and matching). The rigid planning of a longitudinal study is challenging and needs to counteract unexpected and unavoidable confounds, such as changes in experimental setup, staff or even facilities. With increasing lifetime the incidence of animals sacrificed due to spontaneous tumour formation, disease or sudden death rises and it becomes more difficult to avoid changes in infrastructure.

For translational use, we suggest to use memory tests in combination with task-related PET, skilled motor tasks and fMRI. Despite the complexity of the signal, BOLD fMRI is the most commonly used fMRI technique and a strong tool in the evaluation of the functional state of the somatosensory system. Combined with sensorimotor tests, fMRI gives a sound feedback on the functional impact of an intervention or therapeutic treatment. Complex interpretation of the BOLD signal is challenging in an ageing study, as sclerotic vessels or alterations in neurotransmitter release can occur with age and change the BOLD signal. We propose to use hindpaw fMRI in an ageing study, employing a very high

temporal resolution in order to detect changes in the hemodynamic response, for example a prolonged latency with age.

Deformation based morphometry is beginning to prevail in clinical research, especially in exploratory studies. We have set up an elaborated post-processing pipeline for data registration and analysis, helping to transfer results between translational and clinical research. Optimizing a post-processing strategy that reliably segments white matter, grey matter and cerebrospinal fluid in rodent MRI data, would allow analysis of white matter tracts in the rodent brain and volume changes of the ventricles. Both are established markers for ageing in the human brain.

For the first time we presented longitudinal and non-invasive imaging data in healthy rats, following the same subjects for up to two years. The studies presented in this thesis established a baseline for the most frequently used MR parameters and offered histological support for the interpretation. The focus on maturation and ageing allows an appropriate age choice in future neuropathological studies on rat and mouse models.

Glossary

AL	ad libitum, diet with unlimited access to food
ANOVA	analysis of variance
B	magnetic field
BG II	Black and Gold II staining
BF	barrel field cortex
BOLD	blood oxygen level dependent
CBF	cerebral blood flow
CBV	cerebral blood volume
CMR	cerebral metabolic rate
$CMRO_2$	cerebral metabolic rate of oxygen
CNS	central nervous system
CPu	caudate putamen
CR	calorie restricted
CSF	cerebrospinal fluid
DOF	degrees of freedom
DHb	deoxygenated haemoglobin
DTI	diffusion tensor imaging
DWI	diffusion weighted imaging
EPI	echo planar imaging
FA	fractional anisotropy
^{18}FDG	^{18}Fluoro-deoxy-D-glucose
fMRI	functional magnetic resonance imaging
FSL	FMRIB software Library
FOV	field of view
FID	free induction decay
GM	grey matter
glucose-6-P	glucose-6-Phophate

i.p.	intraperitoneal (injection)
MD	Mean Diffusivity (= Tensor Trace/ 3)
MGE	multi gradient echo
MRI	magnetic resonance imaging
MSME	multislice multiecho
M1	primary motor cortex
N_2	nitrogen
N_2O	nitric oxide
O_2	oxygen
OHb	oxygenated haemoglobin
PD	proton density
PFA	paraform aldehyde
PET	positron emission tomography
pixel	picture element
RARE	rapid acquisition with refocused echoes
RECA	rat endothelial cell antigen
RF	radio frequency
RD	Radial Diffusivity
ROI	region of interest
S1	primary somatosensory cortex
S2	secondary somatosensory cortex
s.c.	subcutaneous (injection)
SEM	standard error of the mean
SNR	signal-to-noise ratio
T	Tesla, SI unit for the strength of a magnetic field (B)
T1	longitudinal relaxation time (s.page 8)
T2/ T2*	transversal relaxation time (s. page 8)
TA	acquisition time
TE	echo time
TR	repetition time

TT	tensor trace
VOI	volume of interest
voxel	volume element
WM	white matter

References

1. Weismann A. Essays upon Heredity. Oxford1889.

2. Cournil A, Kirkwood TBL. If you would live long, choose your parents well. Trends Genet. 2001 May;17(5):233-5. PubMed PMID: WOS:000168718500001. English.

3. Sternberg PW, Horvitz HR. Post-Embryonic Non-Gonadal Cell Lineages of the Nematode Panagrellus-Redivivus - Description and Comparison with Those of Caenorhabditis Elegans. Dev Biol. 1982;93(1):181-205. PubMed PMID: WOS:A1982PG95300020. English.

4. Medawar. An unsolved problem of biology. The Medical journal of Australia. 1953 Jun 13;1(24):854-5. PubMed PMID: 13062953.

5. Williams GC. Pleiotropy, Natural-Selection, and the Evolution of Senescence. Evolution. 1957;11(4):398-411. PubMed PMID: WOS:A1957XE15100002. English.

6. McCay CM, Crowell MF, Maynard LA. The Effect of Retarded Growth Upon the Length of Life Span and Upon the Ultimate Body Size: One Figure. J Nutr. 1935 July 1, 1935;10(1):63-79.

7. McCay CM, Maynard LA, Sperling G, Barnes LL. Retarded Growth, Life Span, Ultimate Body Size and Age Changes in the Albino Rat after Feeding Diets Restricted in Calories: Four Figures. J Nutr. 1939 July 1, 1939;18(1):1-13.

8. Heilbronn LK, Ravussin E. Calorie restriction and aging: review of the literature and implications for studies in humans. American Journal of Clinical Nutrition. 2003;78(3):361-9. PubMed PMID: WOS:000184904900003.

9. Masoro EJ. Caloric restriction and aging: an update. Experimental Gerontology. 2000;35(3):299-305.

10. Masoro EJ. Caloric restriction-induced life extension of rats and mice: A critique of proposed mechanisms. Biochimica Et Biophysica Acta-General Subjects. 2009;1790(10):1040-8. PubMed PMID: WOS:000270516100011.

11. Nisoli E, Tonello C, Cardile A, Cozzi V, Bracale R, Tedesco L, et al. Calorie restriction promotes mitochondrial biogenesis by inducing the expression of eNOS. Science. 2005 Oct 14;310(5746):314-7. PubMed PMID: 16224023.

12. Squier TC. Oxidative stress and protein aggregation during biological aging. Experimental Gerontology. 2001 Sep;36(9):1539-50. PubMed PMID: WOS:000171580700010. English.

13. Kirkwood TB. Immortality of the germ-line versus disposability of the soma. Basic life sciences. 1987;42:209-18. PubMed PMID: 3435387.

14. Kenyon C, Chang J, Gensch E, Rudner A, Tabtiang R. A C-Elegans Mutant That Lives Twice as Long as Wild-Type. Nature. 1993 Dec 2;366(6454):461-4. PubMed PMID: WOS:A1993MK09800063. English.

15. van Heemst D. Insulin, IGF-1 and longevity. Aging and disease. 2010 Oct;1(2):147-57. PubMed PMID: 22396862. Pubmed Central PMCID: 3295030.

16. Sherlock M, Toogood AA. Aging and the growth hormone/insulin like growth factor-I axis. Pituitary. 2007;10(2):189-203. PubMed PMID: 17492509.

17. Holzenberger M, Dupont J, Ducos B, Leneuve P, Geloen A, Even PC, et al. IGF-1 receptor regulates lifespan and resistance to oxidative stress in mice. Nature. 2003 Jan 9;421(6919):182-7. PubMed PMID: 12483226.

18. Fontana L, Kennedy BK, Longo VD, Seals D, Melov S. Medical research: treat ageing. Nature. 2014 Jul 24;511(7510):405-7. PubMed PMID: 25056047.

19. Hossmann KA. Experimental models for the investigation of brain ischemia. Cardiovascular Research. 1998;39(1):106-20. PubMed PMID: WOS:000074921300009.

20. Blandini F, Armentero M-T, Martignoni E. The 6-hydroxydopamine model: news from the past. Parkinsonism Relat Disord. 2008;14 Suppl 2:S124-9. PubMed PMID: MEDLINE:18595767.

21. Janus C, Westaway D. Transgenic mouse models of Alzheimer's disease. Physiology & Behavior. 2001;73(5):873-86.

22. Brown AW, Marlowe KJ, Bjelke B. Age effect on motor recovery in a post-acute animal stroke model. Neurobiology of Aging. 2003;24(4):607-14. PubMed PMID: WOS:000182799900010.

23. Chen Y, Sun FY. Age-related decrease of striatal neurogenesis is associated with apoptosis of neural precursors and newborn neurons in rat brain after ischemia. Brain Research. 2007;1166:9-19. PubMed PMID: WOS:000249463400002.

24. Wasserman JK, Yang H, Schlichter LC. Glial responses, neuron death and lesion resolution after intracerebral hemorrhage in young vs. aged rats. European Journal of Neuroscience. 2008;28(7):1316-28. PubMed PMID: WOS:000259941100008.

25. Sutherland GR, Dix GA, Auer RN. Effect of age in rodent models of focal and forebrain ischemia. Stroke. 1996;27(9):1663-7. PubMed PMID: WOS:A1996VF03200047.

26. Sullivan EV, Adalsteinsson E, Hedehus M, Ju C, Moseley M, Lim KO, et al. Equivalent disruption of regional white matter microstructure in ageing healthy men and women. Neuroreport. 2001 Jan 22;12(1):99-104. PubMed PMID: 11201100. Epub 2001/02/24. eng.

27. Sullivan EV, Pfefferbaum A. Diffusion tensor imaging in normal aging and neuropsychiatric disorders. Eur J Radiol. 2003 Mar;45(3):244-55. PubMed PMID: 12595109. Epub 2003/02/22. eng.

28. Hardy SE, Perera S, Roumani YF, Chandler JM, Studenski SA. Improvement in usual gait speed predicts better survival in older adults. J Am Geriatr Soc. 2007 Nov;55(11):1727-34. PubMed PMID: WOS:000250553100004. English.

29. de Brito LBB, Ricardo DR, de Araujo DSMS, Ramos PS, Myers J, de Araujo CGS. Ability to sit and rise from the floor as a predictor of all-cause mortality. Eur J Prev Cardiol. 2014 Jul;21(7):892-8. PubMed PMID: WOS:000337571700012. English.

30. Evans AC, Brain Development Cooperative G. The NIH MRI study of normal brain development. Neuroimage. 2006 Mar;30(1):184-202. PubMed PMID: 16376577.

31. Jernigan TL, Archibald SL, Berhow MT, Sowell ER, Foster DS, Hesselink JR. Cerebral structure on MRI, Part I: Localization of age-related changes. Biological psychiatry. 1991 Jan 1;29(1):55-67. PubMed PMID: 2001446.

32. Voineskos AN, Rajji TK, Lobaugh NJ, Miranda D, Shenton ME, Kennedy JL, et al. Age-related decline in white matter tract integrity and cognitive performance: a DTI tractography and structural equation modeling study. Neurobiol Aging. 2012 Jan;33(1):21-34. PubMed PMID: 20363050. Pubmed Central PMCID: 2945445.

33. Walhovd KB, Fjell AM, Reinvang I, Lundervold A, Dale AM, Eilertsen DE, et al. Effects of age on volumes of cortex, white matter and subcortical structures. Neurobiol Aging. 2005 Oct;26(9):1261-70; discussion 75-8. PubMed PMID: 16005549.

34. Kalthoff D. Functional Connectivity of the Rat Brain in Magnetic Resonance Imaging. Cologne, Germany: RWTH Aachen; 2011.

35. Stejskal EO, Tanner JE. Spin Diffusion Measurements: Spin Echoes in the Presence of a Time-Dependent Field Gradient. The Journal of Chemical Physics. 1965;42(1):288-92.

36. Zonta M, Angulo MC, Gobbo S, Rosengarten B, Hossmann K-A, Pozzan T, et al. Neuron-to-astrocyte signaling is central to the dynamic control of brain microcirculation. Nat Neurosci. 2003;6(1):43-50.

37. Quayle JM, Nelson MT, Standen NB. ATP-sensitive and inwardly rectifying potassium channels in smooth muscle. Physiol Rev. 1997 October 1, 1997;77(4):1165-232.

38. Lindauer U, Megow D, Matsuda H, Dirnagl U. Nitric oxide: a modulator, but not a mediator, of neurovascular coupling in rat somatosensory cortex. Am J Physiol Heart Circ Physiol. 1999 August 1, 1999;277(2):H799-811.

39. Heeger DJ, Ress D. What does fMRI tell us about neuronal activity? Nature Reviews Neuroscience. 2002 Feb;3(2):142-51. PubMed PMID: WOS:000173726300021. English.

40. Weber R, Ramos-Cabrer P, Wiedermann D, van Camp N, Hoehn M. A fully noninvasive and robust experimental protocol for longitudinal fMRI studies in the rat. NeuroImage. 2006;29(4):1303-10.

41. Hyder F, Behar KL, Martin MA, Blamire AM, Shulman RG. DYNAMIC MAGNETIC-RESONANCE-IMAGING OF THE RAT-BRAIN DURING FOREPAW STIMULATION. Journal of Cerebral Blood Flow and Metabolism. 1994;14(4):649-55. PubMed PMID: WOS:A1994NT49900015.

42. . Available from: http://www.hamamatsu.com.

43. Backes H, Walberer M, Endepols H, Neumaier B, Graf R, Wienhard K, et al. Whiskers area as extracerebral reference tissue for quantification of rat brain metabolism using 18F-FDG PET: application to focal cerebral ischemia. The Journal of Nuclear Medicine. 2011;52(8):1252.

44. J. Michael Fitzpatrick DLGH, and Calvin R. Maurer, Jr. Handbook of Medical Imaging - Volume 2, Medical Image Processing and Analysis, Chapter 9. Bellingham, Washington, USA: SPIE PRESS; 2000.

45. Maintz JB, Viergever MA. A survey of medical image registration. Medical image analysis. 1998 Mar;2(1):1-36. PubMed PMID: 10638851.

46. Sotiras A, Davatzikos C, Paragios N. Deformable medical image registration: a survey. IEEE Trans Med Imaging. 2013 Jul;32(7):1153-90. PubMed PMID: 23739795. Pubmed Central PMCID: 3745275.

47. Lester H, Arridge SR. A survey of hierarchical non-linear medical image registration. Pattern Recogn. 1999 Jan;32(1):129-49. PubMed PMID: WOS:000078298000010. English.

48. Markham JA, Morris JR, Juraska JM. Neuron number decreases in the rat ventral, but not dorsal, medial prefrontal cortex between adolescence and adulthood. Neuroscience. 2007 Feb 9;144(3):961-8. PubMed PMID: WOS:000243912600019. English.

49. Song SK, Sun SW, Ramsbottom MJ, Chang C, Russell J, Cross AH. Dysmyelination revealed through MRI as increased radial (but unchanged axial) diffusion of water. Neuroimage. 2002 Nov;17(3):1429-36. PubMed PMID: WOS:000179012800031.

50. Song SK, Yoshino J, Le TQ, Lin SJ, Sun SW, Cross AH, et al. Demyelination increases radial diffusivity in corpus callosum of mouse brain. Neuroimage. 2005 May 15;26(1):132-40. PubMed PMID: 15862213.

51. Fjell AM, Walhovd KB. Structural Brain Changes in Aging: Courses, Causes and Cognitive Consequences. Reviews in the neurosciences. 2010;21(3):187-221. PubMed PMID: WOS:000280984200003. English.

52. Jacobs B, Driscoll L, Schall M. Life-span dendritic and spine changes in areas 10 and 18 of human cortex: a quantitative Golgi study. J Comp Neurol. 1997 Oct 6;386(4):661-80. PubMed PMID: 9378859.

53. Esiri MM. Ageing and the brain. The Journal of pathology. 2007 Jan;211(2):181-7. PubMed PMID: 17200950.

54. Morrison JH, Hof PR. Life and death of neurons in the aging cerebral cortex. International review of neurobiology. 2007;81:41-57. PubMed PMID: 17433917.

55. Dickstein DL, Kabaso D, Rocher AB, Luebke JI, Wearne SL, Hof PR. Changes in the structural complexity of the aged brain. Aging Cell. 2007 Jun;6(3):275-84. PubMed PMID: WOS:000247315100004. English.

56. Tamnes CK, Ostby Y, Fjell AM, Westlye LT, Due-Tonnessen P, Walhovd KB. Brain Maturation in Adolescence and Young Adulthood: Regional Age-Related Changes in Cortical Thickness and White Matter Volume and Microstructure. Cerebral cortex. 2010 Mar;20(3):534-48. PubMed PMID: WOS:000274488600004. English.

57. Pfefferbaum A, Mathalon DH, Sullivan EV, Rawles JM, Zipursky RB, Lim KO. A quantitative magnetic resonance imaging study of changes in brain morphology from infancy to late adulthood. Arch Neurol. 1994 Sep;51(9):874-87. PubMed PMID: 8080387.

58. Shaw P, Kabani NJ, Lerch JP, Eckstrand K, Lenroot R, Gogtay N, et al. Neurodevelopmental trajectories of the human cerebral cortex. Journal of Neuroscience. 2008 Apr 2;28(14):3586-94. PubMed PMID: WOS:000254623500008. English.

59. Huttenlocher PR, Dabholkar AS. Regional differences in synaptogenesis in human cerebral cortex. Journal of Comparative Neurology. 1997 Oct 20;387(2):167-78. PubMed PMID: WOS:A1997XZ20500001. English.

60. Koss WA, Belden CE, Hristov AD, Juraska JM. Dendritic Remodeling in the Adolescent Medial Prefrontal Cortex and the Basolateral Amygdala of Male and Female Rats. Synapse. 2014 Feb;68(2):61-72. PubMed PMID: WOS:000328395000002. English.

61. Heiland S, Sartor K, Martin E, Bardenheuer HJ, Plaschke K. In vivo monitoring of age-related changes in rat brain using quantitative diffusion magnetic resonance imaging and magnetic resonance relaxometry. Neuroscience Letters. 2002;334(3):157-60. PubMed PMID: WOS:000179763300004.

62. Bhagat YA, Beaulieu C. Diffusion anisotropy in subcortical white matter and cortical gray matter: Changes with aging and the role of CSF-suppression. Journal of Magnetic Resonance Imaging. 2004 Aug;20(2):216-27. PubMed PMID: WOS:000222927600012. English.

63. Abe O, Aoki S, Hayashi N, Yamada H, Kunimatsu A, Mori H, et al. Normal aging in the central nervous system: quantitative MR diffusion-tensor analysis. Neurobiology of Aging. 2002 May-Jun;23(3):433-41. PubMed PMID: WOS:000175175600013. English.

64. Helenius J, Soinne L, Perkio J, Salonen O, Kangasmaki A, Kaste M, et al. Diffusion-weighted MR imaging in normal human brains in various age groups. American Journal of Neuroradiology. 2002 Feb;23(2):194-9. PubMed PMID: WOS:000174472300005. English.

65. Camara E, Bodammer N, Rodriguez-Fornells A, Tempelmann C. Age-related water diffusion changes in human brain: a voxel-based approach. Neuroimage. 2007 Feb 15;34(4):1588-99. PubMed PMID: 17188516.

66. Altun M, Bergman E, Edstrom E, Johnson H, Ulfhake B. Behavioral impairments of the aging rat. Physiology & Behavior. 2007;92(5):911-23. PubMed PMID: WOS:000251698400018.

67. Murphy MP, Rick JT, Milgram NW, Ivy GO. A simple and rapid test of sensorimotor function in the aged rat. Neurobiol Learn Mem. 1995 Sep;64(2):181-6. PubMed PMID: 7582826.

68. David-Jurgens M, Churs L, Berkefeld T, Zepka RF, Dinse HR. Differential Effects of Aging on Fore- and Hindpaw Maps of Rat Somatosensory Cortex. Plos One. 2008;3(10). PubMed PMID: WOS:000265121700007.

69. Johansen-Berg H, Dawes H, Guy C, Smith SM, Wade DT, Matthews PM. Correlation between motor improvements and altered fMRI activity after rehabilitative therapy. Brain. 2002 Dec;125:2731-42. PubMed PMID: WOS:000179250400013. English.

70. Weber R, Ramos-Cabrer P, Justicia C, Wiedermann D, Strecker C, Sprenger C, et al. Early prediction of functional recovery after experimental stroke: Functional magnetic resonance imaging, electrophysiology, and behavioral testing in rats. Journal of Neuroscience. 2008 Jan 30;28(5):1022-9. PubMed PMID: WOS:000252778000002. English.

71. D'Esposito M, Zarahn E, Aguirre GK, Rypma B. The Effect of Normal Aging on the Coupling of Neural Activity to the Bold Hemodynamic Response. NeuroImage. 1999;10(1):6-14.

72. Hesselmann V, Zaro Weber O, Wedekind C, Krings T, Schulte O, Kugel H, et al. Age related signal decrease in functional magnetic resonance imaging during motor stimulation in humans. Neuroscience Letters. 2001;308(3):141-4.

Curriculum vitae

Luam Kidane Hammelrath (née Mengler)

Academic Background:

Poster and Presentations during PhD

03/2015	European Molecular Imaging Meeting (EMIM), Tübingen, D
01/2015	Glowbrain Conference: Visualization of molecular markers, Zagreb, HR
06/2014	European Molecular Imaging Meeting (EMIM), Antwerp, B
06/2013	European Molecular Imaging Meeting (EMIM), Torino, I
11/2011	Neuroscience Conference, Washington D.C, US
06/2011	European Molecular Imaging Meeting (EMIM), Leiden, NL

Publication list

Mengler, L., A. Khmelinskii, M. Diedenhofen, C. Po, M. Staring, B. P. Lelieveldt and M. Hoehn (2014). "Brain maturation of the adolescent rat cortex and striatum: changes in volume and myelination." Neuroimage 84: 35-44.

Hammelrath, L., S. Skokic, A. Khmelinskii, A. Hess, N. van der Knaap, M. Staring, B. P. Lelieveldt, D. Wiedermann and M. Hoehn. "Morphological maturation of the mouse brain: An in vivo MRI and histology investigation" NeuroImage 125: 144-152

Hammelrath, L., C. Po, A. Khmelinskii, E. Pracht, M. Staring, C. Schäfer, B. P. Lelieveldt, and M. Hoehn. „Healthy ageing: a functional and strucutral profile of the rat brain“ *In preparation*

Boehm-Sturm, P., M. Aswendt, A. Minassian, S. Michalk, **L. Mengler**, J. Adamczak, L. Mezzanotte, C. Lowik and M. Hoehn (2014). "A multi-modality platform to image stem cell graft survival in the naive and stroke-damaged mouse brain." Biomaterials 35(7): 2218-2226.

Khmelinskii, A., **L. Mengler**, P. Kitslaar, M. Staring, M. Hoehn and B. P. F. Lelieveldt (2013). "A visualization platform for high-throughput, follow-up, co-registered multi-contrast MRI rat brain data." Medical Imaging 2013: Biomedical Applications in Molecular, Structural, and Functional Imaging 8672

Boehm-Sturm, P., T. D. Farr, J. Adamczak, J. F. Jikeli, **L. Mengler**, D. Wiedermann, T. Kallur, V. Kiselev and M. Hoehn (2013). "Vascular changes after stroke in the rat: a longitudinal study using optimized magnetic resonance imaging." Contrast Media Mol Imaging 8(5): 383-392.

Boehm-Sturm, P., **L. Mengler**, S. Wecker, M. Hoehn and T. Kallur (2011). "In Vivo Tracking of Human Neural Stem Cells with F-19 Magnetic Resonance Imaging." Plos One 6(12).

Danksagung

An dieser Stelle möchte ich allen Personen danken, die mich unterstützt haben, ob wissenschaftlich, emotional, organisatorisch oder kulinarisch.

Prof. Dr. Mathias Hoehn, für sein Vertrauen einer Diplomandin dieses Mammutprojekt zu geben und für seine langjährige Unterstützung während all der kleinen und großen Rückschläge und Durchbrüche.

Prof. Dr. Michael Hofmann, der mich als Doktorandin angenommen hat obwohl er gerade selber so frisch an der Uni Bonn war.

Meinen Mitstreitern und Kollegen der ivNMR Gruppe am MPI, allen voran Daniel, Therèse, Tracy, Chrystelle, Joanna, Philipp, Jan, Marion, Claudia, Annette, Lisa und Nadine für mehr oder weniger wissenschaftliche Unterstützung. Alle langen Abende, Wochenenden und Nachtschichten, alle kleinen Triumpfe und größeren Wutausbrüche wären ohne Euch nicht halb so erträglich und sind mit euch schon fast schön gewesen. So vielen am MPI, die immer ein offenes Ohr und eine freie Telefonleitung hatten und mir bereitwillig geholfen haben. Danke, Dirk Wiedermann und Heike Endepols.

Meinen Freunden, die mir einen anderen Blickwinkel, viel Lachen und großartige Pausen gebracht haben.

Vor allem aber danke ich meiner Familie für ihre grenzenlose Unterstützung. Allen voran danke ich meinen Männern zu Hause (dem Großen wie dem Kleinen wie dem Kleinsten), die mich jeden Tag daran erinnern, dass es Wichtigeres gibt als missglückte Färbungen und aussichtslose Statistikergebnisse. Zum Beispiel Kitzelattacken und Schürfwunden.

Danke.